UNIVERSITY OF CALIFORNIA, SAN DIEGO

Dynamic Modulated Brachytherapy (DMBT) and Intensity Modulated Brachytherapy (IMBT) for Treatment of Rectal and Breast Carcinomas

A dissertation submitted in partial satisfaction of the requirements
for the degree Doctor of Philosophy

in

Physics

by

Matthew Julian Webster

Committee in charge

Professor Henry Abarbanel, Chair
Professor William Y. Song, Co-Chair
Professor Michael Anderson
Professor Eva Maria Collins
Professor Thomas Liu

2014

The dissertation of Matthew Webster is approved, and it is acceptable in quality and form for publication on microfilm and electronically:

_____

_____

_____

_____

Co-Chair

_____

Chair

University of California, San Diego

2014

Dedication

To my supervisors, family, friends, and colleagues,

I would like to take this opportunity to express my sincere gratitude to all those who have supported me to complete this thesis. This thesis could not have been accomplished without the help of you all.

Table of Contents

List of Abbreviations

APBI – Accelerated partial breast irradiation

BED – Biological effective dose

CRT – Chemo-radiotherapy

CT – Computed tomography

DSB – Double-strand breaks

DHI – Dose heterogeneity index

DMBT – Dynamic modulated brachytherapy

EBRT – External beam

EUD – Equivalent uniform dose

HDR – High-dose rate

HR – High risk

ICMA – Intracavitary mold applicator

LDR – Low-dose rate

LQ – Linear quadratic

MC – Monte Carlo

MDR – Medium-dose rate

MRI – Magnetic resonance imaging

OAR – Organs at risk

PET – Positron emission tomography

PTV – Planning target volume

SAVI – Strut-Adjusted Volume Implant

TPS – Treatment planning software

VMAT – Volumetric modulated arc therapy

WBI – Whole breast irradiation

List of Figures

List of Tables

Acknowledgements

First of all, I feel tremendously fortunate to have had the opportunity to work with my supervisor, Dr. William Y. Song. I am deeply indebted and thankful for his help, guidance and encouragement during my five years of research.

Special thanks also go to my colleagues, Chun Joo Park, Kevin Kauweloa, and Daeyup Han at University of California, San Diego, Center for Advanced Radiotherapy Technologies. I am so fortunate to have worked together with you all who enriched my life and have given me so much fun during my time working here.

Last but not least, I want to thank all of my family members. You have made countless sacrifice for me, and have provided me with steady guidance and encouragement.

The text of Chapter 2, in part or in full, is a reprint of the material as it appears in the following publication: Webster M.J., Devic S, Vuong T, Han D, Park JC, Scanderbeg D, Lawson J, Song B, Watkins WT, Pawlicki T, Song WY. Dynamic modulated brachytherapy (DMBT) for rectal cancer. Med Phys 2013;40(1):011718-1-011718-12. The dissertation author was the primary researcher and author, and the co-authors listed in this publication directed and supervised the research which forms the basis for this chapter.

The text of Chapter 3, in part or in full, is a reprint of the material as it appears in the following publication: Webster M.J., Devic S, Vuong T, Han D, Scanderbeg D, Choi D, Song B, Song WY . HDR Brachytherapy of Rectal Cancer Using a Novel Grooved-Shielding Applicator Design. Med Phys 2013;40(9):091704-1-091704-10. The

dissertation author was the primary researcher and author, and the co-authors listed in this publication directed and supervised the research which forms the basis for this chapter.

The text of Chapter 4, in part or in full, is being prepared for submission to the Journal of Medical Physics. The dissertation author was the primary researcher and author, and the co-authors listed in this publication directed and supervised the research which forms the basis for this chapter.

Vita

2005-2009 Bachelor of Arts, Macalester College, St. Paul

2009-2011 Master of Science, University of California, San Diego

2011-2014 Doctor of Philosophy, University of California, San Diego

Publications

Han D, Webster M.J., Scanderbeg D, Mell L, Yashar C, Mundt AJ, Choi D, Song B, Devic S, Song WY . Dynamic Modulated Brachytherapy (DMBT) for Cervical Cancer (I): A Multi-Groove Tandem Design. *Int J Radiat Oncol Biol Phys* 2013 Submitted

Bergamo A, Sandhu A, Rahn D, Moiseenko V, Hoisak J, Webster M.J., Han DY, Park SH, Pawlicki T, Mundt AJ, Song WY . Utility of 4DPETCT for ITV definition. *Radiother Oncol* 2013 Submitted.

Webster M.J., Devic S, Vuong T, Han D, Scanderbeg D, Choi D, Song B, Song WY . HDR Brachytherapy of Rectal Cancer Using a Novel Grooved-Shielding Applicator Design. Med Phys 2013;40(9):091704-1-091704-10.

Webster M.J., Devic S, Vuong T, Han D, Park JC, Scanderbeg D, Lawson J, Song B, Watkins WT, Pawlicki T, Song WY. Dynamic modulated brachytherapy (DMBT) for rectal cancer. Med Phys 2013;40(1):011718-1-011718-12.

Park, J.C., Park, S.H., Kim, J.H., Yoon, S.M., Song, S.Y., Liu, Z., Song, B., Kauweloa, K., Webster, M.J., Sandhu, A., Mell, L.K., Jiang, S.B., Mundt, A.J., and Song, W.Y. Liver motion during cone beam computed tomography guided stereotactic body radiation therapy. Med Phys 2012; 39

Fields of Study

Major Field: Physics
Studies in Biophysics
Professor Henry Abarbanel

ABSTRACT OF THE DISSERTATION

Dynamic Modulated Brachytherapy (DMBT) and Intensity Modulated Brachytherapy (IMBT) for Treatment of Rectal and Breast Carcinomas

by

Matthew Julian Webster

Doctor of Philosophy in Physics
University of California, San Diego, 2014

Professor Henry Abarbanel, Chair
Professor William Y. Song, Co-Chair

The ultimate goal of any treatment of cancer is to maximize the likelihood of killing the tumor while minimizing the chance of damaging healthy tissues. One of the most effective ways to accomplish this is through radiation therapy, which must be able to target the tumor volume with a high accuracy while minimizing the dose delivered to healthy tissues. A successful method of accomplishing this is brachytherapy which works by placing the radiation source in very close proximity to the tumor. However, most current applications of brachytherapy rely mostly on the geometric manipulation of

isotropic sources, which limits the ability to specifically target the tumor. The purpose of this work is to introduce several types of shielded brachytherapy applicators which are capable of targeting tumors with much greater accuracy than existing technologies. These applicators rely on the modulation of the dose profile through a high-density tungsten alloy shields to create anisotropic dose distributions.

Two classes of applicators have been developed in this work. The first relies on the active motion of the shield, to aim a highly directional radiation profile. This allows for very precise control of the dose distribution for treatment, achieving unparalleled dose coverage to the tumor while sparing healthy tissues. This technique has been given the moniker of *Dynamic Modulated Brachytherapy* (DMBT). The second class of applicators, designed to reduce treatment complexity uses static applicators. These applicators retain the use of the tungsten shield, but the shield is motionless during treatment. By intelligently designing the shield, significant improvements over current methods have been demonstrated. Although these static applicators fail to match the dosimetric quality of DMBT applicators the simplified setup and treatment procedure gives them significant appeal.

The focus of this work has been to optimize these shield designs, specifically for the treatment of rectal and breast carcinomas. The use of Monte Carlo methods and development of optimization algorithms have played a prominent role in accomplishing this. The use of shielded applicators, such as the ones described here, is the next logical step in the rapidly evolving field of brachytherapy.

Chapter 1 Introduction

1.1 Radiation Therapy

Cancer is one of the most deadly diseases in the world, affecting almost all people's lives either directly or indirectly. There are over 200 types of recognized cancers, each with its own unique cause and form of manifestation. As a result, treatment is a difficult and complicated process. There are a number of treatment modalities available to treat cancer, either as stand-alone treatments or as synergetic combinations. The three main treatment techniques that are frequently used in current clinical settings are surgery, radiation therapy, and chemotherapy. Radiation therapy, or radiotherapy, utilizes high energy, penetrating waves or particles such as X-rays, gamma rays, proton rays, or neutron rays to destroy tumor cells or keep them from reproducing. It utilizes ionizing radiation in a strictly controlled environment to treat cancer. Ionizing radiation can be administered using external beam therapy or by placing a radioactive material directly into a body tissue or cavity. Radiation therapy works by damaging the DNA within cancer cells thus interfering with the cell's ability to grow and reproduce. Currently, most common cancer types are treated with radiation therapy in some way and it can be used as the primary therapy or combined with surgery, chemotherapy, hormone therapy or some mixture of them. Over past decades, radiation therapy has become the most common way to treat cancer with nearly 2/3rd of all cancers treated with some form of radiation therapy.

Radiation therapy primarily kills tumors by compromising the reproductive ability of each cell's DNA, which, depending on the form of damage, can stop the cell from reproducing, kill the cell or mutate the cell. In order to successfully eradicate a tumor, every cell in it must be killed or stopped from reproducing. Otherwise, there will be local recurrence. Therefore, relatively high amounts of radiation are necessary to fully treat a tumor. Unfortunately, radiation is indiscriminate about which cells it kills. As a result, damage and mutation of healthy tissues are a critical issue in radiation delivery. Too much damage to healthy tissues can lead to serious detrimental side-effects or even cause secondary cancers. Therefore, it is the aim of all radiotherapy treatments to very specifically target the tumor while avoiding damage to all other tissues. The ultimate goal of radiation therapy is to deliver maximum radiation dose to the tumor volume while minimizing excessive dose to surrounding healthy tissues or organs surrounding the tumor.

1.2 Brachytherapy

A. History

Brachytherapy derives its name from the Greek word 'brachy' meaning 'short,' which refers to the distance between the therapeutic agent and the target lesion. This typically involves the placement of a radioactive gamma-emitter on or inside of a patient to treat tumors. The basis of brachytherapy was proposed in 1901, five years after radiation was discovered by Henri Becquerel in 1896. The first known suggestion of this modality was from Pierre Curie, who had the idea of placing radioactive sources inside of tumors as a method of treatment. It was quickly confirmed that this was an effective

method of reducing the tumor size. In the following decades, this method of inserting a radioactive source inside of the tumor itself gained considerable popularity as a treatment modality. During these early days of brachytherapy, radium was used as the primary source of radiation. In the 1940's and 50's radium was replaced by cobalt and gold-encapsulated radon. The gold was used as a method to block the high-energy electrons coming from the source. By 1958, applicators had started using Iridium-192 as the main radioactive source, which is still the predominant nucleotide used for modern day brachytherapy treatments.

During the course of the early- and mid-twentieth century, the rapidly increasing understanding of radiation led to more and more concerns regarding the use of radiotherapy, especially brachytherapy. While many side-effects for the patients were viewed as unavoidable, brachytherapy lost much of its support in the medical community due to the greatly undesired high dosages of radiation the therapists and operators were receiving during treatment regimens. However, in the 1950's remote afterloaders were developed to eliminate this problem. Remote afterloaders are specially designed machines which are capable of precisely controlling the location of the radioactive source. This allows the source to be safely shielded within the afterloader while it is not in use. The therapist can control the afterloader from a safe location to deliver the desired dose during treatment. By 1970, afterloaders had become an integral part in brachytherapy, creating a renewed interest in the technique, which has grown ever since.

Remote afterloaders have the added benefit of being able to more precisely control the position of the radioactive source than is allowed by manual control.

However, until the 1990's, this generally had no major impact on treatment capabilities. Until then, tumor localization was done primarily through 2D imaging techniques such as x-ray projections. As a result, dose planning was fairly simple and treatment plans were highly homogenous across most patients. However, the late twentieth century saw a revolution in 3D imaging techniques with the implementation of ultrasound, magnetic resonance imaging (MRI), computed tomography (CT), and positron emission tomography (PET). These allowed for more precise definitions of tumor volumes, which allowed for more precise, patient-specific, treatment plans.

Treatment planning did not reach its current level of precision and accuracy until the beginning of the twenty-first century when treatment planning software (TPS) became readily available. The development of 3D imaging techniques allowed for the accurate description of the where the dose needed to be delivered, but until TPS was advanced enough to quickly calculate dose distributions, it was difficult to determine what the optimal dose was and how to precisely deliver it. This method of computerized dosimetry integrates the imaged patient geometry with the brachytherapy applicators and the identified potential source locations. This allows the software to precisely calculate the optimal dwell times, how long the source delivers dose, at each dwell position, the locations the source can be at within the applicator. In addition to allowing for more precise dose delivery, TPS has also allowed for an increase in the complexity of radiotherapy applicators. Prior to the usage of TPS, most applicators had very simple designs with a relatively few dwell positions. Since then, applicators have become more complex with the number of dwell positions increasing by orders of magnitude. This has

marked a shift from covering the target volume with radiation with considerable excess dose to attempting to match the target volume precisely as possible. Better applicators are constantly being developed to help achieve this goal.

B. Applicator placement

With regards to the placement during treatment, there are two main types of brachytherapy treatments. These are known as interstitial and contact brachytherapy. Interstitial brachytherapy involves the placement of the source into the tumor lesion. This is most frequently done with hollow needles inserted into the patient. Depending on the type of treatment being delivered the needle is either used to deposit the source into the patient permanently or to act as a catheter for the source during treatment.

Contract brachytherapy involves placement of the radiation source adjacent to the target tissue. This can be carried out in a number of ways. The simplest method is surface brachytherapy where the applicator is typically placed on the outside of the body (e.g., skin or eyes). Additional techniques require placement of the applicator into the patient's body, but still externally of the target volume. Methods for doing this include placing the applicator directly within an existing body cavity (intracavitary), within a body lumen (intraluminal), or within blood vessels (intravascular).

Individually, interstitial brachytherapy is able to give superior dose distributions to any of the contact methods, but requires more highly trained staff, greater resources, and is far more invasive and unpleasant for the patient. It is common to combine contact techniques, especially intracavitary or intraluminal, with interstitial methods during a single treatment to maximize the degrees of freedom in dose optimization.

C. Dose rate

The dose rate for a brachytherapy applicator refers to the instantaneous intensity of the radiation, measured in grays (Gy), being delivered. The dose rate for a given radiation source can fall into one of three categories, low-dose rate (LDR), medium-dose rate (MDR) and high-dose rate (HDR). These refer to sources with dose rates up to 2Gy/hr, between 2 and 12 Gy/hr and over 12 Gy/hr, respectively. LDR treatments typically involve leaving the source in place for long periods of time, often permanently. For permanent LDR implants, commonly used to treat prostate cancer, the source must have a relatively short half-life, so that the radiation delivery has an endpoint. Currently, HDR brachytherapy is very widely used because it allows for very fast treatment times and typically allows for outpatient care.

For each dose rate, radiation can be delivered continuously, fractionated, or pulsed. LDR implants are an example of continuous delivery where the radiation is being delivered continuously for a long period of time. Conversely, HDR treatments are typically fractionated, which means a fraction of the total dose is delivered in short, distinct, periods many hours apart. As discussed later in 1.3 , continuous brachytherapy gives better outcomes. However, fractionated HDR treatments are far easier to deliver. Pulsed rate methods have been developed to make HDR treatments take on some characteristics of continuous treatment. This is done by delivering short pulses of radiation approximately once per hour. Due to the clinical difficulty in implementation, this is not a favored method of treatment.

1.3 Radiobiology of Brachytherapy

A. Role of brachytherapy

Brachytherapy, in all its forms is used primarily as a boost following EBRT with some instances of radical treatments. The underlying reason for this is uncertainty in carcinogenic cell locations due to microscopic nodal infiltration and nodal metastases.[3] To combat this, it is necessary to irradiate the entire region around the palpable tumor volume, regardless of how localized the dose could potentially be delivered. This is typically done using EBRT techniques. Due to the relative number of cells present in these regions versus the macroscopic region of the tumor, brachytherapy can be used to deliver a very high dose to the palpable regions, to increase the tumor control. In some cases, such as lumpectomies, there are no longer any macroscopic carcinogenic cells present, but brachytherapy is used to irradiate the tumor bed. This can be done either prior to or following EBRT treatments. Doing so afterwards often allows for tumor shrinkage to occur. As a result, the high dose region of the brachytherapy techniques will reach a larger percentage of the tumor volume making the treatment more effective. This is only true however, if the tumor cell doubling time is long relative to the regression rate.[4]

B. The linear quadratic formalism

When dealing with brachytherapy, it's important to consider prolonged exposures. For these situations, the LQ model gives the survival fraction, S, in terms of the dose, D.

The parameters α and β are constants for a given type of tissue, characterizing the probability of double strand breaks (DSB) forming from a single ionizing particle or two

independent ionizing particles, respectively. The final component, G, is related to the exposure time. It is there because as the exposure time increases, the chance of DSB repair grows and so the quadratic term becomes less prevalent. Therefore, the longer the exposure, relative to the half-time, $T_{1/2}$, repair of DSBs become more likely and the closer this variable goes to zero. Conversely, for short exposures, G approaches unity since the cells have not had a chance for DSB repair. For many cases, G can be calculated analytically. For example, for PLDR implants, $G = \lambda/(\lambda + \mu)$ where λ is the decay constant and $\mu = \ln 2 / T_{1/2}$. Solutions for G have been found for other specific and general cases.[5,6] An example of the effect of exposure time can be seen in Figure 1-1.[7]

C. Cell repopulation

The treatment time is the total time of treatment between the first delivered dose and the last. For permanent LDR seeds, this is the same as the exposure time, but for fractionated LDR or HDR treatments, it represents the time between the first and last fractions. When given time between fractions, cells have a chance to not only repair, as discussed above, but also repopulate as a function of T. After a treatment, an effective delay in the repopulation, T_D, can be accounted for by substituting in T-T_D for T. With this, the LQ model can be adjusted as

$$S = e^{-(\alpha D + G\beta D^2) + \gamma(T - T_d)}, \tag{1.1}$$

where γ is inversely proportional to the repopulation doubling time.

In order for two treatment regimens to be equivalent, it is easy to see that the exponentials for both regimens must be equal. This quantity, divided by -α, or $-\ln(S)/\alpha$, is referred to as the biological effective dose (BED). Therefore, when comparing different

brachytherapy treatment plans and treatment techniques, it is important to account for dose size, dose rate, exposure time, and total treatment time. It is worth noting that the LQ model can be further modified by accounting for resensitization and redistribution. However, the effect of these, while important, is beyond the scope of this review.

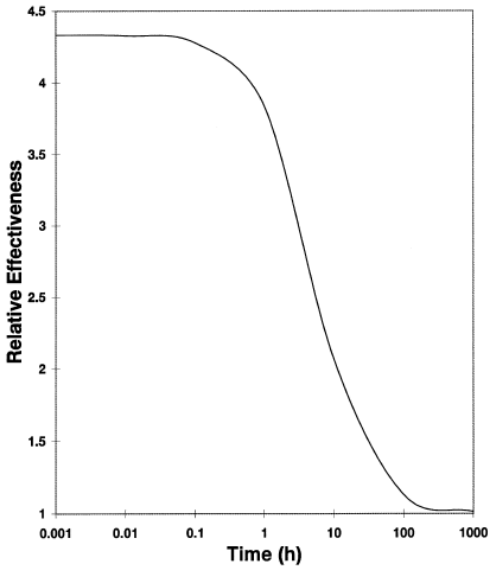

Figure 1-1. Variation of relative effectiveness of a single dose of 10 Gy with treatment time.

D. Non-uniform dose distributions

The LQ model implicitly assumes that the dose to a given volume is homogenous across the entire volume. However, for most brachytherapy applications, this does not hold. To apply the LQ model, it is therefore necessary to calculate the equivalent uniform dose (EUD) which is the dose that, if deposited to the entire volume homogeneously, would have the same biological effect. The easiest way to formulate its value is to add together the survival fractions of every dose value multiplied by the fractional volume receiving that dose, v_i, for the doses, D_i, in that cell. That is,

$$S(EUD) = \sum_i v_i S(D_i). \quad (1.2)$$

Therefore, for inhomogeneous brachytherapy dose distributions,

$$EUD_{BED} = -\frac{1}{\alpha}\ln\sum_i v_i S(D_i). \quad (1.3)$$

A more phenomenological generalized EUD (gEUD) has been developed.[9]

$$gEUD = (\sum_i v_i D_i^a)^{1/a}. \quad (1.4)$$

For this formula, *a* is a tissue-specific parameter that describes the volume effect. The parameter, *a*, can range from -∞, for when the gEUD is minimal, to +∞ for when the gEUD approaches the maximum dose. In practice, tumors, which have the least response have a negative value while serial organs have very high, positive, values. These values are purely empirical and lack any mechanistic explanation at the moment. Nonetheless, it is still used in treatment planning and comparison since it allows for the same functional form to be applied to both tumors and healthy organs.

E. Features of different treatment techniques

E.1 Continuous LDR brachytherapy and permanent seed implants

CLDR and permanent seed implant treatments have provided excellent therapeutic results. This is largely a result of the much shorter effective treatment times. This reduces the repopulation effect of the tumor. However, where the previously mentioned repopulation effects were considered discrete, it is now necessary to account for continuous ongoing biological processes.[5] Doing so requires changing the BED equation.

$$BED = RT\left[1 + \frac{2R}{\mu\left(\frac{\alpha}{\beta}\right)}\left(1 - \frac{1}{\mu T}(1 - e^{-\mu T})\right)\right]. \quad (1.5)$$

In this equation, the dose has been replaced with the dose rate, R. This equation works well for CLDR, but its application to permanent implants fails to account for cell repopulation and source decay. To accurately incorporate these effects, it is necessary to consider that the effective treatment time, T_{eff}, for a permanent implant is not infinite. Instead, once the tumor kill rate is surpassed by the tumor repopulation rate, the treatment is effectively finished and all excess radiation is wasted.[10] This occurs at

$$T_{eff} = -\frac{1}{\lambda}\ln\frac{\gamma}{\alpha D_0}. \tag{2.6}$$

As a result, the effective dose, D_{eff}, goes to zero after this point. That is, $D_{eff} = D\left(1 - e^{\lambda T_{eff}}\right)$. This model can be used in optimizing the choice of radionuclide for a given permanent implant. It should be clear that the efficacy of a source is strongly related to the α/β ratio, tumor growth rate, radiosensitivity and DSB repair rates. For any given permanent seed implant, it is possible to calculate the optimal dose rate of the seed.[11] The calculation is beyond the scope of this work, but some of the results can be found in Table 1-1.

Table 1-1. Optimum radionuclide half-life (h) for a tumor with α/β ratio of 10 Gy*

	BED_{nt} = 100 Gy_3			BED_{nt} = 250 Gy_3		
K ($Gyday^{-1}$)	RBE = 1	RBE = 1.5	RBE = 2	RBE = 1	RBE = 1.5	RBE = 2
0.01	926.0 (1080.0)	611.0 (708.0)	452.5 (524.0)	2322.0 (2704.5)	1530.0 (1772.5)	1137.5 (1311.0)
0.05	407.5 (484.0)	275.5 (324.0)	206.5 (241.0)	1020.5 (1212.5)	691.0 (811.0)	518.5 (605.0)
0.1	278.5 (335.5)	192.0 (227.5)	145.0 (171.0)	699.0 (841.0)	482.5 (571.0)	365.0 (429.5)
0.3	143.5 (179.0)	104.0 (126.5)	80.5 (96.5)	361.0 (450.0)	262.5 (318.0)	204.0 (244.0)
0.5	101.5 (129.5)	76.5 (94.0)	60.0 (73.0)	256.5 (327.5)	193.0 (238.0)	152.5 (185.0)
0.7	79.5 (103.5)	61.5 (76.5)	49.0 (60.0)	201.0 (261.5)	156.0 (194.5)	125.0 (153.0)
0.9	65.0 (86.5)	52.0 (65.5)	42.0 (51.5)	165.5 (219.0)	132.0 (166.5)	107.0 (132.0)
1.1	55.5 (74.5)	45.0 (57.5)	36.5 (45.5)	141.0 (189.5)	115.0 (146.5)	94.5 (117.0)

* Unbracketed figures correspond to the case where $\mu_{nt} = \mu_{tum} = 0.5\ h^{-1}$. For the bracketed figures, μ_{tum} is increased to $1.5\ h^{-1}$.

In general, faster growing tumors are better treated with shorter-lived radionuclides while slower growing tumors are more effectively managed with longer-

lived sources. However, shorter-lived sources have additional value since they are less sensitive to the tumor properties and LQ parameters. It has been determined that the greatest variation in the treatment effectiveness comes when the treatment time is on the same order as the half-life repair of sublethal damage. As a result, the effective treatment time must be suitably long to accomplish this.

When the length of treatment reaches the same order of magnitude as the half-life of the radioactive source, things become more complicated because dose rate is changing as the dose is being delivered. For the case of CLDR or non-permanent implants, with a source with an initial activity of R_0 and decay constant of λ,

$$BED = R_0\left(1 - e^{-\lambda T}\right)\left(1 + \frac{2R_0\lambda}{(\mu-\lambda)(\alpha/\beta)}\right)\left(\frac{A-B}{C}\right) \tag{1.6}$$

where:

$$A = \frac{1}{2\lambda}\left(1 - e^{-\lambda T}\right) \tag{1.7}$$

$$B = \frac{1}{\mu+\lambda}\left(1 - e^{-(\lambda+\mu)T}\right) \tag{1.8}$$

$$C = 1 - e^{-\lambda T}. \tag{1.9}$$

For the case of permanent implants where the time is effectively infinite, this simplifies to

$$BED = \frac{R_0}{\lambda}\left(1 + \frac{R_0}{(\mu+\lambda)(\alpha/\beta)}\right). \tag{1.10}$$

E.2 Fractionated high dose brachytherapy

In recent years, there has been a trend towards using more HDR brachytherapy treatments. This is largely influenced by the reduced cost and treatment time of these techniques. In general, HDR treatments use one to twelve fractions, depending on the

tumor and applicator. Regardless of the number of fractions, it can be assumed that there is sufficient time between fractions to allow for the complete repair of damage within the cells making it unnecessary to account for this in the LQ model.

The critical components of fractionated HDR therapies are the dose rates and number of fractions. The dose rate effect and the choice of nucleotide are discussed in a later section. It is well established that increasing the number of fractions helps increase the tumor control.[12] This arises from the biphasic nature of the LQ model and that dense fractionation can help keep the survival curve approximately in line with the linear response segment. This results in relatively small changes in acute effects, such as tumor control with large, beneficial contributions, on the late effects. The degree of this depends largely on the number of fractions used for a given dose.

This is important because, in general, LDR per fraction is more effective than HDR since high dose rates cause more relative damage and death to late responding tissues than acute responding tissues. Ideally, brachytherapy treatments would be done with fractionated LDR, but this is financially, logistically, and practically infeasible. Instead, fractionated HDR treatments are compared to single fraction LDR treatments.

This is done by comparing the BED. Now, instead of a single dose, D, there are now N fractions of dose d. From this,

$$BED = Nd\left(1 + \frac{d}{\alpha/\beta}\right). \tag{1.11}$$

An example case can be seen in Figure 1-2.[7] This figure compares a single 40Gy/48hr LDR treatment to HDR treatments with varying fraction quantities. The point at which the late and early effects match is considered the matching point for the LDR

and HDR treatments. In this case, α/β is 10Gy and 3Gy for early and late responding tissues, respectively. For this particular case, the equivalence point occurs around 11 fractions. This particular example assumes that, other than α/β, the biological responses of the different tissue types are identical. In reality, this is not the case. It is possible to show that the actual fractionation equivalence point could be as low as 3 fractions for similar cases.[13]

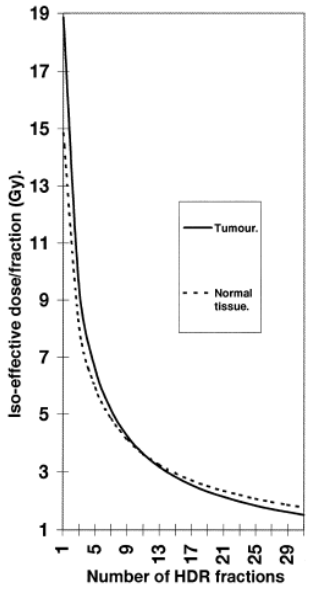

Figure 1-2. Variation of Iso-effective dose for tumor and late-reacting normal tissue with changing HDR fraction number.

The discussion above relates to the use of isotropic sources in both LDR and HDR regimens. However, advancements in many brachytherapy technologies have made this inaccurate. The most important improvement has been the sculpting of the radiation dose. New applicators utilize geometric modulation of the source and tissue positions as well as intensity modulation from the source itself to greatly improve the normal tissue sparing.

It has been shown that doing so can reduce the number of necessary fractions to match LDR to unity.[14,15]

With modern applicators and setup, additional fractions serve to improve the dose over LDR. However, it is important to determine the optimal dose per fraction for treatment. If it is assumed, on average, the normal tissue receives a fraction, g, of the dose to the tumor, then the optimal dose per fraction, z, is given by

$$\left(g - \frac{(\alpha/\beta)_{late}}{(\alpha/\beta)_{tum}}\right) z^2 - 2fgKz - (\alpha/\beta)_{late} fK = 0 \quad (1.12)$$

where f is the time between fractions and K is defined by the intrinsic radiosensitivity, α, and potential doubling time, T_{pot} as $K = \ln 2 / (\alpha T_{pot})$. Typically, this gives the optimal fraction dose size to be 3-8 Gy per fraction. In the case where tissue sparing cannot be achieved or smaller fraction sizes are required, the time between fractions should be reduced.

F. Radioisotope effectiveness

There are currently numerous radioactive sources that are used for different brachytherapy treatments. The most commonly used isotopes have mean energies ranging from 21 keV for ^{103}Pd to 662 keV for ^{137}Cs. In addition, there are electronic x-ray sources capable of delivering a wide range of energies.[16] Beyond the range of the different isotopes, each isotope has a complete spectrum of gamma-ray energies, in some cases reaching a few MeV. This is critically important because biological effectiveness varies with photon energy photons with different energies will deposit dose differently. This is different from the energy gradients associated with the overall dose distributions discussed above.

The relative biological effectiveness (RBE) of the different isotopes can be estimated directly from energy deposition patterns using mircodosimetry. In the applicable range, the biological response per unit dose, R_i, to a particular radiation, *i*, can be calculated as

$$R_i = \int w(y) d_i(y) dy \tag{1.13}$$

where *y* is the lineal energy, a stochastic quantity, defined as the energy deposited by a single photon track divided by the average path length in the cellular target. The microdosimetric single-event spectrum, denoted by d_i, is the dose-weighted probability that a photon will deposit lineal energy in the target volume of interest. Finally, *w*, describes the cellular response by an individual target to the lineal energy. For sparsely ionizing radiations, such as those used in brachytherapy it is reasonable to assume that this quantity is proportional to y. Therefore, for LDR sources,

$$RBE_i \propto \int y d_i(y) dy. \tag{1.14}$$

RBE values have been calculated for a number of brachytherapy sources. Using ^{60}Co as a reference point, ^{192}Ir, ^{241}Am, ^{125}I, and ^{103}Pd have RBI values of 1.3, 2.1, 2.1, and 2.3, respectively. The approach described is only applicable to LDR brachytherapy sources, but can be incorporated into HDR source calculations by simply modifying the BED.[17] That is,

$$BED = D\left(RBE + \frac{GD}{\alpha/\beta}\right). \tag{1.15}$$

G. Effects of tumor shrinkage

The general effects of the tumor volume have already been discussed, but it is important to consider what effect this has on the LQ model. In the case where the tumor

is growing, the dose in the BED calculations must be adjusted to represent a greater dose since now the average dose to the tumor is increasing. That is to say, when finding the BED the following adjustments must be made for a tumor that shrinks exponentially with rate constant *z*:

HDR: $d \to d(1 + (N-1)zt)$. (1.16)

CLRD: $R \to R(1 + zT)$.

For permanent seed implants, the equation becomes considerably more cumbersome. Throughout the BED equation, $\lambda \to \lambda - 2z,\ T \to T_{eff}$, and then the entire equation then gets scaled by a factor of $\left(1 - e^{-\lambda T_{eff}}\right)$. For this case,

$$T_{eff} = \frac{\ln K/R_0}{\lambda - 2z} \quad (1.17)$$

H. EBRT and brachytherapy

As previously discussed, brachytherapy is infrequently used as a radical treatment, but instead is usually used in conjunction with EBRT. The survival fraction for such a dual-modality treatment is simply $S = S_{EBRT}S_{BT}e^{\gamma T'}$. Again, γ is determined by the speed of repopulation. Here, T' is the time between the different treatment techniques, going to zero if the treatments overlap. It is useful to translate this information into an equivalent EBRT reference regimen made of 2Gy fractions. In this case,

$$EUD = -\frac{\ln S}{\alpha + \beta d - 1.4\gamma/d}. \quad (1.18)$$

Figure 1-3 shows some of the potential uses of this formulation. It shows both how the different modalities combine as well as how to calculate a specific component when given a desired goal.

Modalities	Prescribed Dose[a] (Gy)	EUD[b] (Gy)	TCP[b] (%)	EUD[c] (Gy)
EBRT alone	70.2	68	20	66
EBRT alone	81	78	87	77
^{125}I BT alone	145	71	43	71
^{103}Pd BT alone	124	74	69	77
EBRT + ^{125}I	45 (EBRT) + 108 (BT)	94	99	96
EBRT + ^{103}Pd	45 (EBRT) + 100 (BT)	103	100	104
EBRT + HDR	45 (EBRT) + 3 × 6 Gy (BT)	78	87	97

EBRT, external-beam radiation therapy; BT, brachytherapy; EUD, equivalent uniform dose; TCP, tumor control probability; LQ, linear-quadratic.

[a]For EBRT, 1.8-Gy fraction size assumed.

[b]LQ parameters:[256] $\alpha = 0.15\ Gy^{-1}$, $\alpha/\beta = 3.1$ Gy, $T_r = 16$ minutes, $T_d = 42$ days, $K = 1.1 \times 10^7$.

[c]LQ parameters:[300] $\alpha = 0.039\ Gy^{-1}$, $\alpha/\beta = 1.0$ Gy, $T_r = 1.9$ h and with repopulation effect ignored.

Cumulative EUD[a]	Permanent BT		HDR BT			
	I-125	Pd-103	2 Fractions	3 Fractions	4 Fractions	5 Fractions
68 Gy	50 Gy	34 Gy	5.8 Gy × 2	4.5 Gy × 3	3.8 Gy × 4	3.2 Gy × 5
72 Gy	57 Gy	40 Gy	6.7 Gy × 2	5.2 Gy × 3	4.3 Gy × 4	3.7 Gy × 5
80 Gy	72 Gy	53 Gy	8.4 Gy × 2	6.5 Gy × 3	5.4 Gy × 4	4.7 Gy × 5
90 Gy	92 Gy	70 Gy	10.2 Gy × 2	8.1 Gy × 3	6.8 Gy × 4	5.9 Gy × 5
100 Gy	112 Gy	87 Gy	12.2 Gy × 2	9.5 Gy × 3	8.0 Gy × 4	7.0 Gy × 5
110 Gy	133 Gy	106 Gy	13.8 Gy × 2	10.8 Gy × 3	9.2 Gy × 4	8.0 Gy × 5

EUD, equivalent uniform dose; EBRT, external-beam radiation therapy.

[a]LQ parameters[256]: $\alpha = 0.15\ Gy^{-1}$, $\alpha/\beta = 3.1$ Gy, $T_r = 16$ minutes, $T_d = 42$ days, $K = 1.1 \times 10^7$.

Figure 1-3. Examples of combining EBRT with HDR BT and Permanent BT

1.4 References

1. Khan FM. The physics of radiation therapy. 4th ed. Philadelphia: Lippincott Williams & Wilkins; 2010.

2. Tyldesley S, Boyd C, Schulze K, Walker H, Mackillop WJ. Estimating the need for radiotherapy for lung cancer: an evidence-based, epidemiologic approach. International journal of radiation oncology, biology, physics 2001;49:973-85.

3. Jones B, Bleasdale CM. Effect of overall time when radiotherapy includes teletherapy and brachytherapy: a mathematical model. Br J Radiol 1994;67;63-70

4. Dale RG, Jones B. The effect of tumor shrinkage on biologically effective dose, and the possible implications for the fractionated high dose brachytherapy. Radiother Oncol 1994;33;125-32.

5. Dale RG. The application of the linear-quadratic dose-effect equation to fractionated and protracted radiotherapy. Br J Radiol 1985;58:515–528.

6. Brenner DJ, Hall EJ. Fractionated high dose-rate versus low dose-rate brachytherapy of the cervix. I. General considerations based on radiobiology. Br J Radiol 1991;64:133.

7. Dale RG, Jones B. The clinical radiobiology of brachytherapy. Br J Radiol 1998;71(845):465–483.

8. Mohan, R., G. S. Mageras, B. Baldwin, L. J. Brewster, G. J. Kutcher, S. Leibel, C. M. Burman, C. C. Ling, and Z. Fuks. "Clinically relevant optimization of 3-D conformal treatments." *Medical physics* 19, no. 4 (1992): 933-944.

9. Niemierko A. A generalized concept of equivalent uniform dose (EUD) (Abstract).*Med Phys* 1999;26:1100.

10. Dale RG. Radiobiological assessment of permanent implants using tumor repopulation factors in the linear-quadratic model. *Br J Radiol*1989;62(735):241–244.

11. Armpilia C, Dale RG, Coles IP, Jones B, Antipas V. The determination of radiobiologically optimized half-lives for radionuclides used in permanent brachytherapy implants. Int J Radiat Oncol Biol Phys 2003;55(2):378–85

12. Thames HD, Withers HR, Peters LJ, Fletcher, GH. Changes in early and late radiation responses with altered dose fractionation: implications for dose-survival relationships. *Int J Radiat Oncol Biol Phys*1982;8(2):219–226.

13. Orin, CG. Correspondence 1987, *The British Journal of Radiology, 60,* 300-302

14. Dale RG. The use of small fraction numbers in the high dose-rate gynecological afterloading: some radiobiological considerations. Br J Radiol 1990;63:290-4.

15. Jacobs H. Breast conserving therapy: experience with HDR afterloading iridium implants. Brachytherapy HDR and LDR. Leersum, The Netherlands: Nucletron BV, 1990:251-6.

16. Rivard, M. J., Davis, S. D., DeWerd, L. A., Rusch, T. W., & Axelrod, S. (2006). Calculated and measured brachytherapy dosimetry parameters in water for the Xoft Axxent X-Ray Source: An electronic brachytherapy sourcea). *Medical physics*, *33*(11), 4020-4032.

17. Wuu, C. S., P. Kliauga, M. Zaider, and H. I. Amols. "Microdosimetric evaluation of relative biological effectiveness for 103Pd, 125I, 241Am, and 192Ir brachytherapy sources." International journal of radiation oncology, biology, physics 36, no. 3 (1996): 689-697.

18. Dale RG, Jones B. The assessment of RBE effects using the concept of biologically effective dose. Int J Radiat Oncol Biol Phys 1999;43(3):639–645.

19. Rajon, D., Bolch, W. E., & Howell, R. W. (2012). Survival of tumor and normal cells upon targeting with electron - emitting radionuclides. Medical physics, 40(1), 014101.

Chapter 2 Dynamic Modulated Brachytherapy (DMBT) for Rectal Cancer

2.1 Introduction

The idea of intensity-modulated brachytherapy (IMBT) using collimated brachytherapy source was first proposed by Ebert et al.[1] in 2002. That work investigated the advantages of having a radially asymmetric radiation point-source that was free to rotate about its axis for treatment of idealized targets. The idea takes advantage of the fact that an indexed rotation of the source about its axis would provide radial intensity modulation, which could compensate for variations in the spatial relationship between the source position and location of the target edge. The paper concludes that a collimation angle (resolution) of 22.5-45° and shielded-side transmission of <10% (leakage) are needed to see a worthwhile benefit of IMBT over conventional, non-shielded, brachytherapy implants. Since then, a number of different investigations into the potential implementation of anisotropic brachytherapy techniques have been conducted.[2-5] Ebert[2] and Shi et al.[3] looked at the benefits of a 3D anisotropic source for treatment of prostate and breast cancer, respectively, and found very positive results. However, they created their radiation profiles using computer simulations and did not outline how to create these distributions in practice. A similar idea was also investigated by Kim et al.[4] in 2003 and Shi et al.[5] in 2012 using MC simulations. However, the 2003 study laid out theoretical specifications as to how to achieve collimation using steel and/or tungsten alloy as the housing for a beta-producing $^{90}Sr/^{90}Y$ radioactive source, for intravascular brachytherapy.

The beta-producing source was chosen as a candidate since an unrealistic amount of shielding would be necessary to collimate a high-energy gamma-producing source such as that used in high dose rate (HDR) ^{192}Ir brachytherapy. Unfortunately, although these ground breaking works theoretically showed that significant improvements could be achieved with a collimated radiation profile; no further development ensued to implement them clinically.

This work builds upon the idea of IMBT for the treatment of rectal cancer. The management of rectal cancer has progressed significantly over the last few decades. The primary treatment modality is surgery, while preoperative chemo-and-radiation-therapy (CRT) has proven to be quite beneficial in long-term survival.[6-9] Therefore, the current standard for treating rectal cancer patients is preoperative chemotherapy and external-beam radiotherapy to the pelvis, followed by reduced field boost, and surgery 6-8 weeks later. This schedule improves local control and is more tolerable than postoperative CRT; however, toxicities are still quite significant with 27% acute and 14% late grade 3-4 GI toxicity.[6-12] These high toxicities are because the radiation needs to traverse a large volume of healthy tissues in the pelvis and chemotherapy sensitizes pelvic organs such as small bowel and rectum.[13,14] Damage from radiation to these and other surrounding organs can lead to problems or delays in post-surgical healing (e.g., anastomotic leak or perineal wound infection).[13] In addition, for non-surgical candidates, due to health or other contraindications, the problem is exacerbated since, in this situation, CRT is the only alternative modality and must be given in a more intense, definitive setting.

To reduce these toxicities while maintaining equivalent/better treatment outcome, investigators in Canada[10,15-17] conducted an exploratory clinical trial to study the potential role of HDR endocavitary brachytherapy. As an alternative to the preoperative CRT portion of the standard of care, an 8-channel applicator known as an Intracavitary Mold Applicator (ICMA, Nucletron, Netherlands).[18-21] was used. The occurrence of grade ≥3 acute proctitis went down to 1% vs. 27%, and pathologic complete response rate rose to 29% compared with 8-12% using CRT. In addition, the shorter treatment duration (1 week vs. 5 weeks), no need for chemotherapy, and less surgical complications were significant advantages. However, due to the near-isotropic nature of the HDR ^{192}Ir source, and limited use of shielding in the ICMA, there still is an appreciable amount of radiation delivered to surrounding tissues. As shown in this work, this is especially true for the tissues above and below the tumor, including the sphincter.

Building upon the foundations of early collimated IMBT work,[1-5] we have designed and carried out a study evaluating the use of a collimated ^{192}Ir source radiation profile for treating rectal cancer. The basic idea is to collimate the radiation beam using a cylindrical tungsten alloy shield, then dynamically rotate and translate this shield during treatment using robotic hardware to achieve intensity modulation. The idea is similar to the delivery of volumetric modulate arc therapy but from inside the rectal cavity. The moniker *Dynamic Modulated Brachytherapy* (DMBT) is chosen to distinguish it from the current IMBT-HDR brachytherapy techniques, such as ICMA, and two different segmented shielded applicators (Nucletron, Netherlands and Varian Medical Systems, Palo Alto, CA)[22,23] which are static after placement, in that the proposed applicator,

robotic in nature, is in full motion, with two degrees of freedom. This paper will discuss the concept, design, and performance analysis with 36 treatment plans clinically treated with the ICMA using Monte Carlo (MC) simulations of the shielded applicator using N-Particle Monte Carlo (MCNP5). This study aims to demonstrate that DMBT utilization of a dynamic shield during treatment can improve treatment plan evaluation metrics in comparison to the ICMA. While this investigation is limited to rectal cancer, the basic DMBT concept can be extended to other disease sites treated with HDR brachytherapy such as gynecological and breast.

2.2 Materials and Methods

A. System overview

The DMBT system proposed in this work uses a high-density tungsten-alloy shield, cylindrical in shape, with a small window on one side to encapsulate an HDR ^{192}Ir source, to create collimation that results in a highly directional radiation beam. Figure 2-1a-c illustrates our first shield design. The shield is cylindrical to allow smooth translation up and down the rectal cavity, guided by a rigid cylindrical bio-safe polycarbonate sheath that fits tightly around the shield. Figure 2-1d shows the design of our robotic applicator that will be used to step the shield precisely into a planned dwell positions. It consists of two precision EvoDrive ST-17 stepper motors with 1/500 degree accuracy.[24] The current gearing in the system allows for a translational and rotational stepping precision of 0.0125 mm and 0.012°, respectively.

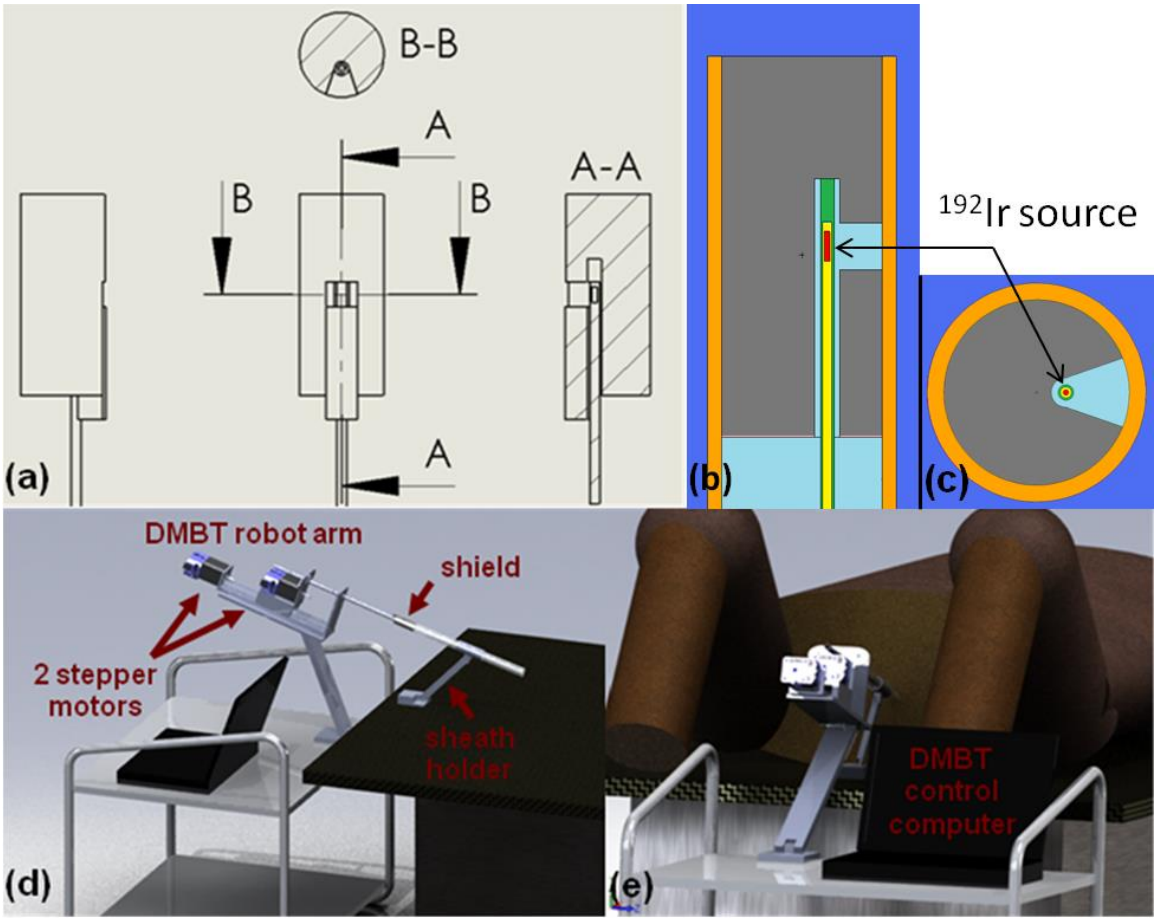

Figure 2-1. DMBT schematic overview. (a) A CAD drawing of our first tungsten alloy shield design. The shield is 19 mm in diameter and 45 mm in length, and has a moveable window that slides in and out to variable distances to create continuous window opening size. (b) A sagittal cross section of the shield. (c) In-plane cross section of the shield. Cartoon depictions of the (d) DMBT system overall setup and (e) the DMBT system in an envisioned treatment, with a patient on the table.

The treatment planning and delivery processes will be similar to that of current image-guided HDR ^{192}Ir brachytherapy procedures. Starting in the imaging room, the patient will be placed on a stabilization board in the supine position. An indexed cylindrical polycarbonate sheath, which is encapsulated by a unidirectional endocavitary balloon (e.g. Civco Medical Solutions, Kalona, IA) will be placed into the rectal cavity. The balloon is then inflated to move the healthy tissue away from the applicator site and

help stabilize the sheath within the cavity. Next, the sheath will be affixed to a mechanical arm which itself is attached to the stabilization board the patient is on. The CT and/or MRI imaging will commence, and after imaging is completed, the patient will be transported into the HDR room. Once the patient is in the room, the DMBT applicator will be locked into position inside the polycarbonate sheath. Figure 2-1e illustrates a cartoon depiction of the treatment setup. Once plan optimization had been completed, the treatment will commence with the approved plan. Figure 2 shows a simulated delivery of an envisioned treatment. At a given indexed translational position, the DMBT system carries out the treatment in a dynamic arc fashion, pre-programmed with angular dwell times and positions.

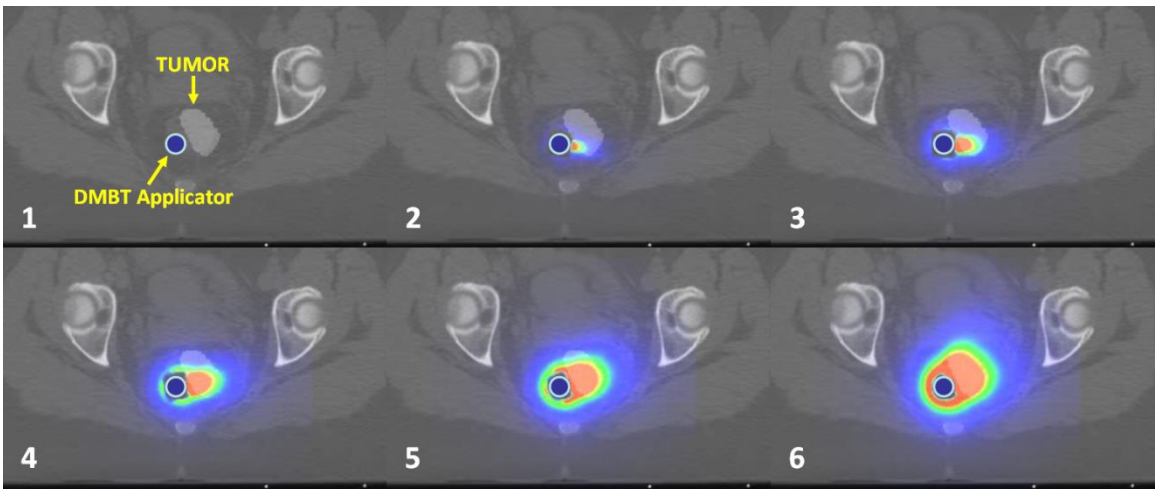

Figure 2-2. An example patient plan with snapshots of cumulative radiation dose distribution as the DMBT robotic applicator rotates counterclockwise to carry out the treatment delivery.

B. Intracavitary mold applicator (ICMA)

The ICMA applicator, which was used in the McGill University trial,[17,19-21] is the most widely used rectal applicator with the most promising dosimetric results.[10-12,15-17,25-27] This is the applicator that the DMBT system will be compared to in this work. The

custom designed 8-channel flexible applicator is 280 mm in length and 20 mm in diameter. It also comes with an optional 8 mm diameter tungsten alloy rod which can be inserted in the central cavity to create a modest directional radiation profile. An inflatable 30 ml endocavitary balloon (CIVCO Inc, Kalona, Iowa) can be wrapped tightly around the applicator to push the contralateral rectum away.

C. Patient dataset

Patient data was acquired from The McGill University, Canada.[17] The data set used was comprised of 36 treatment fractions (fx) of 13 patients each treated using the ICMA applicator. The patients were not surgical candidates due to health or other contraindications, and thus required radiotherapy in a definitive setting. For the purpose of this study, this patient group was chosen over more conventional surgical patients. Therefore, this cohort represented the most extreme cases that can be treated with HDR ^{192}Ir brachytherapy, and thus was a suitable group to evaluate the performance of the DMBT system. Due to the absence of surgery, a higher HDR ^{192}Ir prescription dose of 10 Gy/fx × 3 fxs was delivered, as opposed to 6.5 Gy/fx × 4 fxs. Most patients were first treated with the external-beam radiotherapy prescription dose of 2.5 Gy/fx × 16 fxs while some received 1.8 Gy/fx × 25 fxs prior to the HDR ^{192}Ir treatment. All cases evaluated were non-circumferential tumors for which no more than 3 channels were utilized in the applicator, The size of the clinical target volume (CTV) was 9.0 ± 3.5 cm^3. The inflatable balloon, mentioned in Section 2.2 A. and the tungsten alloy rod were used. Due to the limitations of the treatment planning software, the plans did not account for the tungsten alloy rod during dose calculations. Therefore, MCNP Monte Carlo (MC) simulations

were used to reconstruct the doses delivered to the identified critical structures. However, presence of the rod does not obstruct the CTV dose coverage if 3 or fewer channels are used, however.[20,21]

Figure 2-3 shows typical structures contoured for planning. The main critical structures are the contralateral rectum, superior spill, and inferior spill. The superior and inferior spills are cylindrical structures located above the distal and below the proximal edges of the CTV, respectively. Typically they were 10 mm in length and 40 mm in diameter. These structures are used to describe the extent of the radiation as seen in the coronal or sagittal view and become especially important if the CTV location is close to the sphincter (< 50 mm), in which case, an extra effort was made to spare this organ.

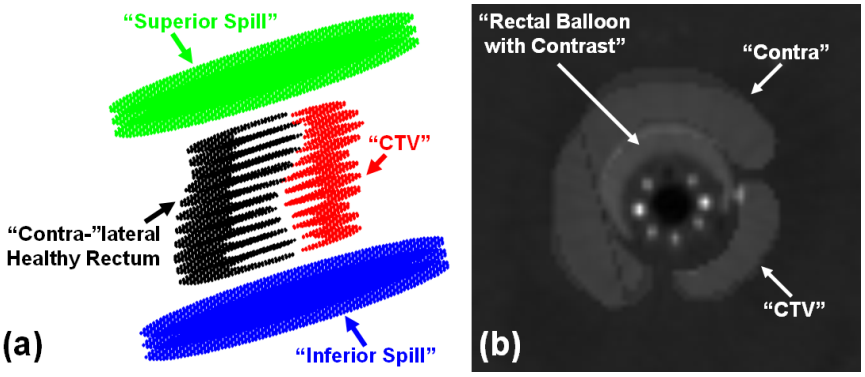

Figure 2-3. Typical structures contoured for treatment planning with the ICMA applicator. (a) 3D plot of the contours. (b) An axial CT slice with structures shown. Also seen is the endocavitary balloon filled with contrast.

D. Monte Carlo simulations

D.1 ^{192}Ir source

The ICMA applicator was used with the Nucletron afterloader. However, for completeness, both Nucletron and Varian sources were simulated with MCNP for comparison. Energy levels were specified according to the National Nuclear Data Center.[28] Patients were treated with the Nucletron mHDR-v2 source.[29] This design consists of an iridium core, which is 0.65 mm in diameter and 3.6 mm in length, and is surrounded by a steel capsule 5.0 mm in length and varying diameter from 0.9-1.10 mm. For the VariSource iX HDR source,[30] there are two identical adjoining cores 0.34-mm in diameter and 2.5 mm in length each, and are encapsulated by a 0.59 mm nitinol wire of density 6.45 g/cm^3.[31] In all simulations, unless explicitly stated, the Nucletron source was used.

D.2 ICMA applicator

The ICMA applicator is composed of flexible silicone rubber (density=1.14 g/cm^3), and is 280 mm in length and 20 mm in diameter.[20,21] The applicator contains 8 straight channels distributed every 45° and 3.5 mm inside from the edge and can be seen in Figure 2-3b. The central cavity is occupied by an 8 mm diameter and 254-mm long tungsten alloy rod (density=18.0 g/cm^3).

D.3 DMBT applicator

The tungsten alloy shield design presented here is cylindrical in shape to allow smooth translational motion along the polycarbonate sheath, as illustrated in Figure 2-1d. The shield has a density of 18.0 g/cm^3, the same as the ICMA applicator shield, and a

length of 45 mm. In order to load the ^{192}Ir source a 3 mm diameter hole was placed parallel to the axis of rotation extending 30 mm into the shield. As discussed in Section 2.2 G.1 , this hole is strategically located 3 mm radially away from the center of the shield (Figure 2-1c). The window opening is wedge-shaped in-plane and is 45° with respect to the radial center of the shield and tapered to match the edge of the central cavity. The window opening parallel to the axis of rotation is 5.5 mm. This length was chosen to allow up to ±1 mm in positioning uncertainty of the (active part of the) source and still have a relatively unobstructed fluence exiting the window. An indexed polycarbonate sheath (density=1.2 g/cm^3) was placed tightly around the shield as a barrier to protect the patient from the device and vice versa.

The shield and the iridium source were modeled as combinations of cylinders and other macro-bodies. All elements of the shield and the source were modeled according to their molecular composition and density.[32] By atomic fraction, the tungsten alloy used was 95% tungsten, 3.5% nickel, and 1.5% copper. In addition, the polycarbonate sheath was modeled with 75.6% carbon, 18.9% oxygen, and 5.5% hydrogen.

D.4 MCNP dose calculations

MC simulations were run with the MCNP code, version 2.6.0.[33] Cubical voxels with size of edge length 2.5 mm were used within a cubed region of length 50 mm and 5 mm cubed voxels were used beyond that. In addition, 0.833 mm voxels were used to fill in gaps directly next to the shield. The dose was measured in mean energy deposited over each cell (measured with the F6 tally in MCNP5). For each decay event of ^{192}Ir, 2.363 gamma emissions were generated.[34] Bremsstrahlung X-rays, electron-induced X-rays,

knock-on electrons and secondary electrons were used for photon interactions. Other interactions used were incoherent scattering, coherent scattering (Rayleigh scattering), fluorescence emission, Compton scattering, capture, and pair production. In order to achieve better simulation efficiency, a lower energy cutoff of 10 keV for electron transport simulations was enforced. All space outside of the applicator was treated as water.

E. Uncertainty analysis

There are a number of potential uncertainties in the delivery of DMBT treatment, including 1) uncertainty in the initial positioning of the applicator after movement from the CT room to the treatment room, 2) patient motion relative to the applicator, and 3) uncertainty in the ^{192}Ir source positioning with a commercial afterloader. These were evaluated with 1) systematic translational shield misplacement of 1-5 mm, 2) systematic rotational misplacement of 1-20°, and 3) source positioning uncertainty of ±1 and ±2 mm inside the shield. Each scenario was examined on all 36 plans. For the shield misplacement simulations, the shield and the source were offset together with respect to the patient anatomy, whereas for the source positioning uncertainty analysis, the MCNP dose calculation was performed for each source positional offset within the shield, and that resulting dose distribution was used for plan evaluation.

F. DMBT plan optimization

F.1 The optimization model

For the DMBT plan optimization algorithm, for almost all cases the resolution of dwell positions was set to 5 mm and 1° steps in the translational and angular directions,

respectively. In one case, the translational step size was set at 2 mm in order to compare to the 5 mm step size and validate that choice. The complete set of all dwell positions is denoted by T. Dwell times, which are the decision variables to be optimized, are given for each dwell position, $j \in T$, as x_j. The set of voxels inside each contoured structure (Figure 3) is given by V. From here, we denote z_i as the dose to voxel $i \in V$, and the prescribed dose to that same voxel as p_i. In addition, each voxel $i \in V$ is assigned a user defined importance weight, w_i. This weight is set heuristically to achieve the best results for each plan. The voxel dose is calculated as $z_i = \sum_{j \in T} D_{ij} x_j$ where D is the dose deposition coefficient matrix where D_{ij} represents the dose to voxel $i \in V$ by dwell position $j \in T$ per unit time. The dose deposition vector $\boldsymbol{d_i}$ is the set of doses received by voxel $i \in V$ by each dwell position $j \in T$ such that $\boldsymbol{d_i}(j)=D_{ij}$. It is related to the voxel dose, z_i, by $z_i = d_i^T x$. We construct our objective function, $F(x)$, in a quadratic form to ensure convexity as:

$$\min_x F(x) = \frac{1}{2} \sum_{i \in V} w_i (d_i^T x - p_i)^2 \qquad \text{subject to } x_i \geq 0, \forall\ i \in V \tag{2.1}$$

The above equation can be rewritten in the form:

$$\min_x F(x) = \frac{1}{2} x^T H x + f^T x \qquad \text{subject to } x_i \geq 0, \forall\ i \in V \tag{2.2}$$

where

$$H \equiv \sum_{i \in V} w_i d_i (d_i)^T \tag{2.3}$$

and

$$f \equiv -\sum_{i \in V} w_i p_i (d_i)^T \ . \tag{2.4}$$

Notice the linear term, $\frac{1}{2}p_i^2$, has been dropped for convenience, since it is just a constant offset.

F.2 The optimization algorithm

As mentioned, the objective function is convex quadratic. Therefore, the direction of the steepest decent is that of the negative gradient. However, our decision variables, which are the dwell times, $\boldsymbol{x}$, must be non-negative (i.e., cannot have a dwell time < 0 seconds). Thus, optimizing along the path of the steepest decent may lead to unacceptable solutions so a gradient projection method was used to limit our dwell times to be ≥ 0. This method is iterative and begins by forcing the gradient to be partially along the boundary of the feasible space, and subsequently project the unconstrained solution from that step into the feasible space.[3540,36] To do this, first, it is necessary to define the initial condition $\boldsymbol{x^0}$. The initial condition must lie within the constrained space, so that all elements are non-negative. Although any initial guess leads to an optimized solution eventually, an educated initial guess can reduce the number of iterations necessary for convergence. To do this, we set $\boldsymbol{x^0}(i) = c$ (constant) if that dwell position points toward the target volume and zero otherwise. The constant, c, was selected such that the initial mean dose to the target volume equals the prescription dose. The projected gradient direction is given by:

$$g_j^k = \begin{cases} \nabla_j F\left(x^k\right) & \text{if } x_i^k > 0 \\ \min\left\{0, \nabla_j F\left(x^k\right)\right\} & \text{if } x_i^k = 0 \end{cases} \qquad (2.5)$$

Here, k denotes the iteration number and $\boldsymbol{\nabla F(x^k)}$ is the gradient of $F(\boldsymbol{x})$ at $\boldsymbol{x^k}$. This gradient direction is used to find the next step:

$$x^{k+1} = \left(x^k - \alpha^k g^k\right)_+ \tag{2.6}$$

where $(*)_+ = \max\{0,*\}$.

The optimal step size, denoted by α^k, is given by:[37]

$$\alpha^k = \frac{(g^T)^k \nabla F^k(x)}{(g^T)^k H g^k} \tag{2.7}$$

In summary, the pseudo code for our algorithm can be summarized as:

Initialization

(1) Let $k = 0$
(2) Select an initial solution $\boldsymbol{x^0}$ such that $\boldsymbol{x^0} \geq 0$.

Main iterative loop

(3) Calculate g^k
(4) Calculate α^k
(5) Calculate $x^{k+1} = \left(x^k - \alpha^k g^k\right)_+$
(6) If $\left|F\left(x^{k+1}\right) - F\left(x^k\right)\right| / F\left(x^{k+1}\right) < \delta$, then stop; else $k = k + 1$, and go back to step (3). In this work the stopping criterion was set at $\delta = 10^{-5}$.

We implemented this algorithm on an Intel Core i7 CPU. Due to the high degree of vector algebra in the optimization process, MATLAB (MathWorks Inc, Natick, MA) was a suitable choice for coding.

Our algorithm does not put any constraints on the solution other than requiring non-negativity. However, after each completed optimization, we enforced a criterion that the 98% of the CTV receives the prescription dose. This constraint was easily enforced by scaling the final dose distribution, without altering the final solution. This is possible because it is mathematically equivalent to increasing the target prescription dose, which

only acts to scale the function $F(x)$, and does not change its shape and, therefore, the solution is unchanged.

F.3 Plan comparison indices

The mean dose, the maximum dose delivered to 98% of the volume (D_{98}), and the maximum dose delivered to 5% of the volume (D_5) were calculated for all structures. The dose heterogeneity index (DHI),[41] defined as $(D_{max}-D_{min})/D_{mean}$, was calculated as well, where D_{max}, D_{min}, and D_{mean} represent the maximum, minimum, and mean dose received by the CTV, respectively. Lastly, the total cumulative dwell time (i.e., treatment time) was calculated assuming an air-kerma strength of 40.25 kU (i.e., 10 Ci).

G. DMBT shield design

G.1 Radial source position

The radial location of the ^{192}Ir source within the shield affects both the radiation anisotropy and the overall treatment time. As the location moves radially towards the surface, the contralateral side of the shield opening allows greater attenuation, and hence less leakage, while the collimated beam becomes wider and decreases in directionality. At the extreme when the source is at the surface, it becomes like the ICMA design. These effects were analyzed by simulating and optimizing with the source in the center, radially offset by 3 mm, and 6 mm. Unless otherwise specified, the results are based on the 3 mm radial offset design as shown in Figure 1c.

H. Diameter of the shield

Diameters of 10, 15, 19, 25, and 30 mm were simulated. The diameter of 19 mm was chosen instead of 20 mm so that, with the addition of the polycarbonate sheath (1

mm thick), the total diameter would closely match that of the ICMA applicator (i.e., 20 mm). The length of the shield and window opening were kept the same while the diameter was scaled.

The patient plans, described in Section 3.2 E. , could not be used to compare different shield diameters because they were planned with the ICMA applicator, which is 20 mm in diameter. Instead, scalable phantom geometries were used. They were cylindrical in shape, and the CTV was comprised of a 90° wedge cylindrical shell and 40 mm in length, and the diameter of the cylinder was adjusted to fit tightly around the DMBT shield size being evaluated. The size of the CTV was adjusted radially to fix the volume at 10 cm^3. All plans were generated using the same conditions set forth in the optimization code described in Section 3.2 H.

2.3 Results

A. MCNP dose calculations

In all simulations, a sufficient number of decay events were simulated to keep the variance to all voxels under 5%. In most regions of interest, the variance was kept under 1%. For example, 10 mm from the shield opening for the 19 mm diameter shield the variance was about 0.1%, while 10 mm from the shield on the back side the variance was 0.5%. The high variance regions occurred in the areas with the highest degree of shielding and therefore would not be directed towards the tumor volume. The end results for open source simulations were compared and normalized to the TG-43[39,40] standard. We found the radial dose function to be in agreement with TG-43 within 2%.

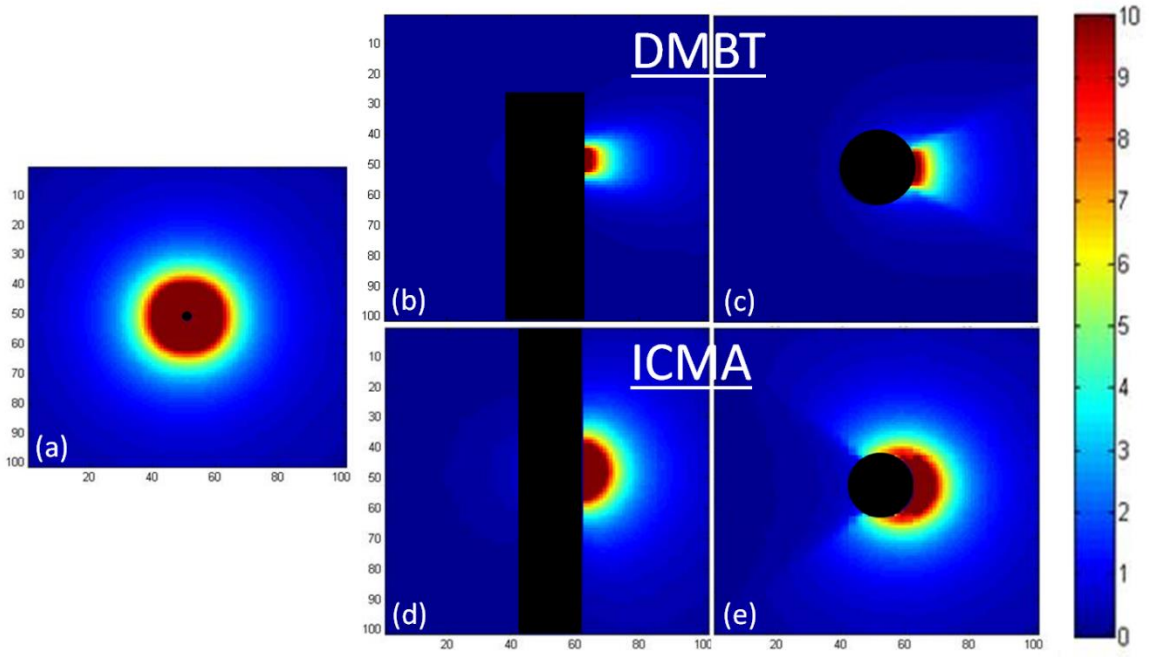

Figure 2-4. MCNP simulation results in [cGy/s]. (a) ^{192}Ir open source in water, (b) sagittal cross section of and (c) axial cross section of the collimated beam profile of a DMBT shield design in Figure 2-1 (19 mm diameter), and (d) sagittal cross section of and (e) axial cross section of the ^{192}Ir source in one of the channels in the ICMA applicator, with the tungsten alloy rod inserted.

B. ICMA vs. DMBT plan quality

Figure 2-4 shows the resulting dose distributions for an open source, DMBT and ICMA applicators in a homogenous water phantom. The DMBT shield design gives a more collimated radiation profile with reduced dose spills in all directions around the ^{192}Ir source, except for radiation from the source directed towards the solid angle covering the window opening. The rotational and translational flexibility of the device adds more degrees of freedom than the multichannel ICMA applicator, leading to superior overall dose conformality, especially for irregular tumor shapes. Figure 2-5 illustrates a typical plan obtained with the ICMA and DMBT applicators, as well as the differential dose. As the arrows indicate, the DMBT plan produces a more conformal

plan with minimal spill to the contralateral healthy rectum. This trend was consistent for all plans and is demonstrated in Figure 2-6 and Table 2-1. As the figure and the table show, per equal CTV coverage (D_{98}), the DMBT plans provide >30% decrease in D_5 (high dose volume) resulting in a ~40% decrease in DHI. In addition, mean dose, D_{98}, and D_5 showed a marked reduction (typically 40-60%) on all critical structures evaluated. However, there was an increase in total treatment time from 7.62 to 20.78 minutes.

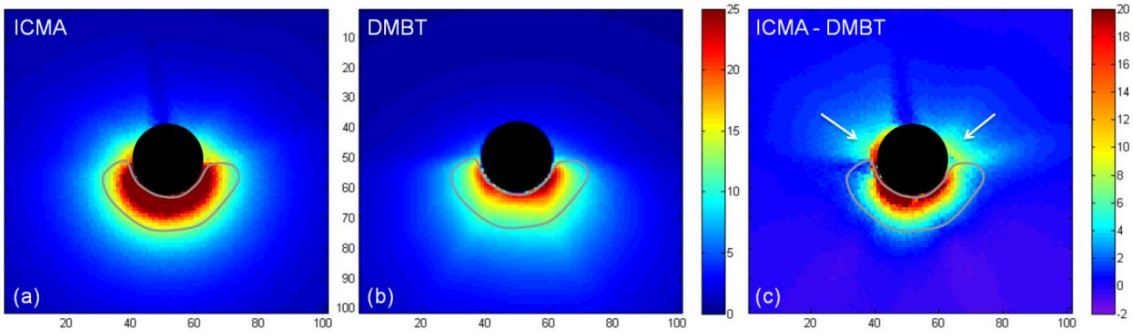

Figure 2-5. A typical dose distribution for a plan generated by (a) ICMA, (b) DMBT, and (c) the relative difference between the two in Gray [Gy] for a 10 Gy prescription dose.

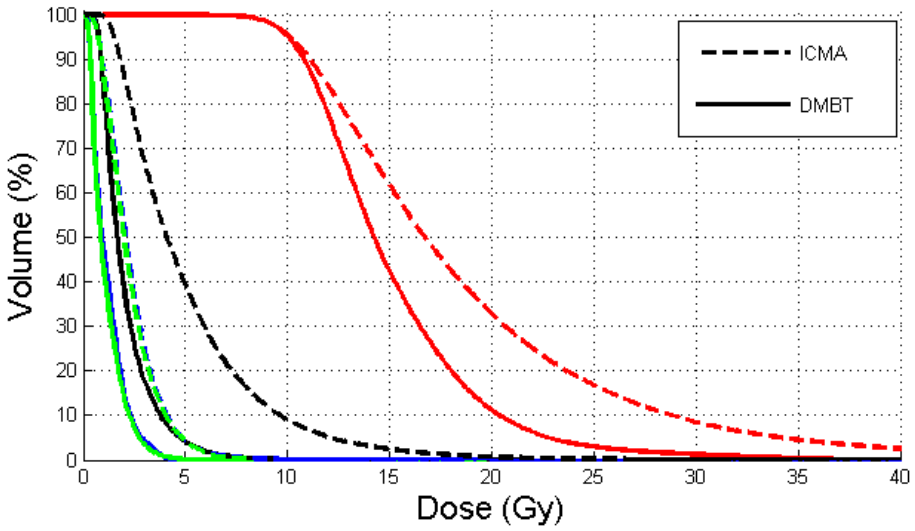

Figure 2-6. Average DVH comparing the ICMA (dashed) and DMBT (solid) plans, which were averaged over all 36 patient cases Shown are the for CTV(red), contralateral rectum (black), inferior spill (green), and superior spill (blue). Prescription dose was 10 Gy.

Table 2-1. Comparison between the ICMA and DMBT plans. % Diff is defined as = 100% × (ICMA-DMBT)/ICMA.

Structure	Index	ICMA	DMBT	Mean %Diff	STDEV
CTV [Gy]	Mean Dose	19.89	16.39	-17.02	9.41
	D_{98}	10.00	10.00	NA	NA
	D_5	32.40	21.97	-31.23	9.17
Contralateral Rectum [Gy]	Mean Dose	6.19	2.29	-60.01	9.92
	D_{98}	2.49	0.97	-51.61	20.78
	D_5	12.78	4.92	-59.38	8.44
Inferior Spill [Gy]	Mean Dose	2.57	1.32	-47.46	9.95
	D_{98}	0.99	0.40	-56.33	13.71
	D_5	4.81	2.84	-39.43	11.09
Superior Spill [Gy]	Mean Dose	3.00	1.31	-54.93	10.08
	D_{98}	1.05	0.34	-64.15	12.53
	D_5	6.02	3.02	-48.42	11.91
	Time [min]	7.62	20.78	179.03	41.64
	DHI	1.95	1.17	-38.35	11.22

C. DMBT shield design

C.1 ^{192}Ir source type

The Nucletron and Varian ^{192}Ir sources yielded similar results. The Nucletron source had a slightly higher DHI and reduced D_5 to the spills by ~3% while increasing D_{95} about the same amount due to the shorter length of the "active" source, which produces a more directional beam per given window opening. However, due to this more

collimated beam, the treatment time increased by ~4.5%, compared to the Varian source. Otherwise, the difference between the two source types was statistically insignificant.

Table 2-2. Dependence of the plan quality indices on the radial position of the 192Ir source inside the DMBT shield. The parenthetical value, % Opt., is the percentage of fractions in which that design gave the best value among the three options.

Structure	Radial Position [mm]	0 (% Best)	3 (% Best)	6 (% Best)
CTV [Gy]	Mean Dose	16.47 (52.8)	16.39 (30.6)	16.84 (16.7)
	D_{98}	10.00	10.00	10.00
	D_5	21.95 (55.6)	21.97 (33.3)	23.78 (11.1)
Contralateral Rectum [Gy]	Mean Dose	4.32 (0.0)	2.29 (0.0)	1.68 (100.0)
	D_{98}	2.35 (0.0)	0.97 (0.0)	0.44 (100)
	D_5	6.84 (0.0)	4.92 (52.8)	5.12 (47.2)
Inferior Spill [Gy]	Mean Dose	1.54 (2.8)	1.32 (86.1)	1.49 (11.1)
	D_{98}	0.79 (0.0)	0.40 (0.0)	0.22 (100.0)
	D_5	2.71 (75.0)	2.84 (19.4)	3.67 (5.6)
Superior Spill [Gy]	Mean Dose	1.48 (5.6)	1.31 (83.3)	1.49 (11.1)
	D_{98}	0.67 (0.0)	0.34 (0.0)	0.20 (100.0)
	D_5	2.80 (86.1)	3.02 (5.6)	3.80 (8.3)
	Time [min]	32.72 (0.0)	20.78 (0.0)	12.03 (0.0)
	DHI	1.19 (41.7)	1.17 (41.7)	1.26 (16.7)

C.2 Radial source position in the shield

Among the various positions of the ^{192}Ir source within the shield, for the average patient, the 3-mm offset design produced the best overall results. As shown in Table 2-2,

on average, the design with the source located in the center reduced the D_5 values by less 8% compared to the 3-mm offset for all the critical structures while performing the worst in many other indices, including D_5 for the contralateral rectum. The 3-mm offset design was a good balance in many areas as well as outperforming either other design in the mean dose to all structures except the contralateral rectum where it had the best D_5 result. Finally, the 6-mm offset design produced a mixed result giving the best sparing in low doses to the contralateral rectum as well as D_{95} to the spill and had the lowest delivery time, but the worst results for many of the remaining parameters.

It is important to note that although these are the average results, they cannot be generalized to every patient case. While D_{95} to all structures, D_{mean}, and time were all consistent across all fractions, there were some variations in all other comparisons. The biggest variation was to the CTV with no design being optimal for more than 56% of the fractions. The parenthetical values in Table 2-2 give the percent of fractions in which the given design was the best of the three designs for that value.

C.3 Diameter of the shield

As expected, the thicker shields produced less back-side leakage. There is a near exponential decrease in the leakage as a function of the shield diameter. For shield diameters of 10, 15, 20, 25, and 30 mm, the transmission coefficients were 9.7, 4.4, 2.3, 1.2, and 0.7%, respectively.

Table 2-3 shows the impact of the shield size on plan quality. In all indices, except the treatment time, there is an improvement as the shield size is increased. The

treatment time scales linearly with the shield diameter, due to the fact that the source is geometrically further away from the CTV as the shield size is increased.

Table 2-3. Dependence of the plan quality indices on the DMBT shield size.

Structure	Diameter [mm]:	10	15	19	25	30	ICMA (20)
CTV [Gy]	Mean Dose	22.52	21.37	18.84	16.59	15.64	20.75
	D_{98}	10.00	10.00	10.00	10.00	10.00	10.00
	D_5	44.18	38.39	30.41	24.11	21.80	40.31
Contralateral Rectum [Gy]	Mean Dose	7.34	4.48	3.31	2.34	1.95	7.24
	D_{98}	2.80	1.55	0.99	0.60	0.39	1.10
	D_5	15.99	10.49	9.47	7.86	7.85	17.36
Inferior Spill [Gy]	Mean Dose	2.87	1.99	1.55	1.16	1.00	3.64
	D_{98}	0.90	0.53	0.40	0.26	0.20	0.61
	D_5	6.99	5.49	4.40	3.48	3.05	7.05
Superior Spill [Gy]	Mean Dose	2.76	1.90	1.41	1.02	0.90	3.85
	D_{98}	0.86	0.51	0.38	0.24	0.19	0.61
	D_5	6.62	5.16	3.81	2.84	2.56	7.79
	Time [min]	12.02	16.45	21.68	28.76	38.85	7.18
	DHI	2.68	2.24	1.73	1.39	1.38	2.63

D. Uncertainty analyses

D.1 Translational shield misplacement

The greatest impact of translational shield misplacements on plan quality to the CTV was on the D_{98} (low dose). At 5 mm shift, the CTV D_{98} dropped by 24%. The D_5 (high dose volume) increased by 6% and 19% for the 3 mm and 5 mm offset, respectively, as shown in Table 2-4. Changes of up to 2 mm led to up to 3% changes in dose while dose to the contralateral rectum increased by 5-10%. The biggest change was to the spill structure in the direction of the shift, where dose was increased by 10-15%.

Table 2-4. Impact of the systematic translational shield misplacement on the plan quality indices.

Structure	Shift [mm]:	0	1	2	3	5
CTV [Gy]	Mean Dose	16.39	16.82	16.78	16.78	17.89
	D_{98}	10.00	9.84	9.48	8.80	7.66
	D_5	21.97	22.69	22.94	23.37	26.12
Contralateral Rectum [Gy]	Mean Dose	2.29	2.44	2.43	2.43	2.58
	D_{98}	0.97	1.07	1.05	1.02	1.04
	D_5	4.92	5.13	5.12	5.13	5.54
Inferior Spill [Gy]	Mean Dose	1.32	1.50	1.58	1.66	1.91
	D_{98}	0.40	0.45	0.46	0.47	0.52
	D_5	2.84	3.24	3.46	3.67	4.30
Superior Spill [Gy]	Mean Dose	1.31	1.30	1.21	1.13	1.07
	D_{98}	0.34	0.37	0.36	0.35	0.35
	D_5	3.02	2.88	2.64	2.43	2.25

D.2 Rotational shield misplacement

Systematic rotational shield misplacements cause the entire dose distribution to rotate away from the CTV towards the contralateral healthy rectum, thus compromising target coverage and normal tissue sparing. However due to the cylindrical nature of the rectal cavity, the spills structures did not see any change. These effects are reflected in Table 2-5. Rotations of 5 degrees changed the mean dose to the CTV by 8% while D_5 and D_{98} increased by <3%. At larger rotational shifts, however, the dosimetric indices begin to change by larger amounts, with the mean dose dropping an additional 10-15% per 5 degrees of rotation. In all cases, the mean dose to the CTV was increased by around 10% and the D_5 increased approximately proportionally with the rotation with a 22% increase for a 20 degree rotation.

Table 2-5. Impact of the systematic rotational shield misplacement on the plan quality indices.

Structure	Shift [Degree]:	0	1	5	10	15	20
CTV [Gy]	Mean Dose	16.39	16.81	16.58	16.62	15.98	15.86
	D_{98}	10.00	10.00	9.24	7.88	6.29	5.38
	D_5	21.97	22.57	22.48	22.84	22.47	22.86
Contralateral Rectum [Gy]	Mean Dose	2.29	2.45	2.44	2.54	2.60	2.80
	D_{98}	0.97	1.08	1.07	1.08	1.06	1.08
	D_5	4.92	5.16	5.17	5.68	6.36	7.61

Table 2-6. Impact of the ^{192}Ir source positioning uncertainty, inside the shield, on the plan quality indices.

Structure	Source Pos.:	Inf 2-mm	Inf 1-mm	0-mm	Sup 1-mm	Sup 2-mm
CTV [Gy]	Mean Dose	17.79	16.49	16.39	16.55	18.09
	D_{98}	10.10	9.64	10.00	9.75	10.43
	D_5	24.25	22.27	21.97	22.33	24.62
Contralateral Rectum [Gy]	Mean Dose	2.57	2.41	2.29	2.44	2.67
	D_{98}	1.12	1.05	0.97	1.07	1.17
	D_5	5.42	5.07	4.92	5.14	5.61
Inferior Spill [Gy]	Mean Dose	1.63	1.45	1.32	1.33	1.38
	D_{98}	0.47	0.43	0.40	0.42	0.45
	D_5	3.55	3.13	2.84	2.80	2.87
Superior Spill [Gy]	Mean Dose	1.14	1.31	1.31	1.43	1.66
	D_{98}	0.36	0.37	0.34	0.39	0.43
	D_5	2.76	2.91	3.02	3.25	3.84
	DHI	23.75	22.10	20.78	22.15	24.24

D.3 Source positioning uncertainty

The effect of a translational source positioning offset is to tilt the dose distributions in the craniocaudal direction, resulting in the dose to the spills structures to increase in the opposite direction of the source shifts and vice versa. Table 2-6 lists the dosimetric changes. For the target coverage, the changes are less than 4% within ±1 mm shifts and with ±2 mm shifts there is an increase of around 10% for D_5 and D_{98}. The dose

changes to the spills were greater with D_5 changing by as much 10% and 30% for the 1 mm and 2 mm offsets, respectively. Even if dose escalation is used to match the prescription dose, shifts of 1 mm still outperform ICMA from a dosimetric standpoint. This shift is within the positioning accuracy for the considered current commercial afterloaders.[42,43]

D.4 Translational Step Size

The dwell position step resolution of 5mm was chosen to reflect the size of the iridium seed. A step size of 2 mm was also simulated and it was found that this higher resolution had less than 1% improvement to all indices, while greatly increasing the optimization time.

2.4 Discussion

A. Overall system design

The concept of a dynamic applicator proposed here is novel and represents a significant step forward in HDR ^{192}Ir brachytherapy technology. Dynamic motion of the applicator in combination with collimation of the radiation beam is the key innovation. We have compared and analyzed 36 clinical ICMA-based plans, and have shown that the DMBT dosimetric results are superior.

B. ICMA vs. DMBT plan quality

The DMBT plans showed significant improvements over the 36 ICMA plans. The CTV DVH in Figure 6 showed a steeper dose drop-off beyond the prescription point. This means that the severity of high dose volumes in the CTV will be less and perhaps with that an opportunity exists to escalate the dose, since dose to rectal mucosa typically

limits the prescription. Simultaneously, all critical structures were spared with a dose reduction of 40-60% which should lead to decreases in clinical complications.[17,19-21]

The DMBT design increases the treatment time (i.e., total dwell times) from on average 7.62 to 20.78 minutes. However, such an increase should still be within clinically acceptable range since the overall treatment takes about 1 hour from setup, imaging, planning, to delivery, and all this with patient in the lithotomy treatment position. In addition, our comparison was presented for a 10 Gy/fx prescription, employed for the relatively rare inoperable patients. For a more common HDR ^{192}Ir treatment involving surgery (6-8 weeks later), the prescription is 6.5 Gy/fx. This translates into treatment times of approximately 13.5 minutes. Furthermore, by including an adjustable window size as part of our plan optimization, we can likely reduce the treatment times even further.

C. DMBT shield design

C.1 Diameter

As the shield diameter increased, there was a pattern of consistent decrease in dose to all critical structures, while keeping the prescription dose constant. However, the improvements begin to plateau as the size approached 30 mm diameter as a result of the CTV size chosen. Because most of the CTV volume was sufficiently close to the opening of the shield for this shield size, the dynamic aspect of the treatment was under-utilized and was limited to a few angular dwell positions, thus reducing the benefits of the dynamic motion.

Shield sizes, as small as 10 mm in diameter, performed better than the ICMA applicator. Recall that Ebert's 2002 study[1] (discussed in Introduction) concluded that, for an effective IMBT, a collimation angle of 22.5-45° and shielded-side transmission of <10% (leakage) are needed to see a worthwhile improvement. The 10 mm diameter shield satisfied these criteria. This gives DMBT a greater degree of freedom to treat a variety of patients. Not all patients are equally capable of tolerating devices as large as 20 mm in diameter, which means having the potential option of smaller shields is beneficial. In addition, some applicators such as the CAPRI™ system (Varian Medical Systems, Palo Alto, CA)[44] used in GYN and rectal sites, are as large as 30 mm in diameter. Therefore an equally large DMBT shield, which provides better plans than the 19 mm shield evaluated in this study, may be advantageous for some patients. Depending on the clinical need and the patient tolerance, an optimal shield size should be selected to maximize the therapeutic ratio.

C.2 Radial Source Position

As discussed in Section 3.3 C.1 , although on average having the source 3 mm offset within the shield is optimal, this result cannot be generalized to all patient fractions. Even within a single patient's set of fractions, the best choice may vary. However, the 3 mm offset design was the only one to consistently outperform ICMA for all fractions in all areas except delivery time. Therefore, it is the best option if it is only feasible to have a single choice, but if more options are available, it is advisable to decide the shield to be used in a case-by-case basis.

D. Uncertainty analysis

Commercial afterloaders have a maximum positioning uncertainty of ±1 mm.[41,42] In addition, from experience with image guided brachytherapy treatments, including accelerated partial breast irradiation applicators, the anticipated positioning uncertainty of the applicator with respect to the tumor volume should be around 1° and 2 mm in angular and translational positions, respectively. In this range of uncertainties, the plan quality indices did not vary by more than 5%. Various combinations of uncertainties were not simulated thoroughly, as the intent of this paper was to present the concept and design of the DMBT system. In addition, since the DMBT plans are much more conformal, there is room to add some small margins to incorporate the uncertainties as well. This and other issues related to the design will be examined in a more thorough follow up study.

E. Future work

The optimization algorithm can be accelerated with GPU coding.[45] The goal is that plans can be optimized near real-time. In addition, the algorithm will be updated to allow for more DVH constraints, which may require the use of hybrid-stochastic methods.[46]

Additionally, work will be conducted on the hardware aspects of DMBT. The results presented herein are exclusively obtained through simulations. Therefore, it is a necessary next step to build a working prototype of the device which can be experimentally validated. From there, guidelines for quality assurance can be created.

2.5 Conclusion

Dosimetric properties of a novel DMBT system have been described and evaluated. Comparison with the ICMA commercial applicator has shown its potential as a clear step forward in high-dose-rate ^{192}Ir brachytherapy technology. Dynamic motion of an applicator during treatment, to any site in general, can provide additional degrees of freedom that, if properly considered, can potentially increase the plan quality significantly. The design presented in this paper is by no means complete. There are many aspects of the system that can be improved, such as the use of a variable window opening as an added degree of freedom to further fine-tune the dose distribution, development of DVH constrained, uncertainty-robust, and faster optimization algorithms, a smaller applicator design, and more systematic uncertainty analysis.

2.6 Acknowledgements

The text of Chapter 2, in part or in full, is a reprint of the material as it appears in the following publication: Webster M.J., Devic S, Vuong T, Han D, Park JC, Scanderbeg D, Lawson J, Song B, Watkins WT, Pawlicki T, Song WY. Dynamic modulated brachytherapy (DMBT) for rectal cancer. Med Phys 2013;40(1):011718-1-011718-12. The dissertation author was the primary researcher and author, and the co-authors listed in this publication directed and supervised the research which forms the basis for this chapter.

2.7 References

1. M. A. Ebert, “Possibilities for intensity-modulated brachytherapy: Technical limitations on the use of non-isotropic sources,” Phys. Med. Biol. 47, 2495-2509 (2002).

2. M. A. Ebert, “Potential dose-conformity advantages with multi-source intensity-modulated brachytherapy (IMBT),” Australas Phys Eng Sci Med. 29(2), 165-71 (2006);

3. C. Shi, B. Guo, C. Y. Cheng, C. Esquivel, T. Eng, and N. Papanikolaou. “Three dimensional intensity modulated brachytherapy (IMBT): dosimetry algorithm and inverse treatment planning,” Med. Phys. 37(7) 3725-3737 (2010).

4. S. Kim, E. Han, J. R. Palta, and S. W. Ha, “Conceptual source design and dosimetric feasibility study for intravascular treatment: A proposal for intensity modulated brachytherapy,” J. Kor. Soc. Ther. Radiol. Oncol. 36, 158-166 (2003).

5. V. Chaswal, B. R. Thomadsen, and D. L. Henderson, “Development of an adjoint sensitivity field-based treatment-planning technique for the use of newly designed directional LDR sources in brachytherapy,” Phys. Med. Biol. 57(4) 963-982. (2012).
6. R. Sauer, H. Becker, W. Hohenberger, C. Rödel, C. Wittekind, R. Fietkau, P. Martus, J. Tschmelitsch, E. Hager, C. F. Hess, J.H. Karstens, T. Liersch, H. Schmidberger, and R. Raab, “Preoperative versus postoperative chemoradiotherapy for rectal cancer,” N. Eng. J. Med. 351, 1731-1740 (2004).

7. V. Valentini, R. Beets-Tan, J. M. Borras, Z. Krivokapić, J. W. Leer, L. Påhlman, C. Rödel, H. J. Schmoll, N. Scott, C. Van de Velde, and C. Verfaillie, “Evidence and research in rectal cancer,” Radiother. Oncol. 87, 449-474 (2008).

8. J. Y. Wo, H. J. Mamon, D. P. Ryan, and T. S. Hong, “T3N0 Rectal cancer: Radiation for all?” Sem. Rad. Oncol. 36, 362-369 (2011).

9. J. H. W. de Wilt, M. Vermaas, F. Ferenschild, and C. Verhoef, “Management of locally advanced primary and recurrent rectal cancer,” Clin. Col. Rect. Surg. 20, 255-264 (2007).

10. T. Vuong, C. Richard, T. Niazi, S. Liberman, F. Letellier, N. Morin, K. Hu, D. Anderson, and S. Devic, “High dose rate endorectal brachytherapy for patients with curable rectal cancer,” Sem. Col. Rect. Surg. 21, 115-119 (2010).

11. A. Sun Myint, T. Mukhopadhyay, V. S. Ramani, K. Perkins, A. J. Snee, F. Jelley, H. Wong, and C. D. Lee, “Can increasing the dose of radiation by HDR brachytherapy

boost following pre operative chemoradiotherapy for advanced rectal cancer improve surgical outcomes?" Colorectal. Dis. 12, 30-36 (2010).

12. A. Sun Myint, C. D. Lee, A. J. Snee, K. Perkins, F. E. Jelley, and H. Wong, "High dose rate brachytherapy as a boost after preoperative chemoradiotherapy for more advanced rectal tumours – the Clatterbridge experience," Clin. Oncol. 19, 711-719 (2007).

13. B. D. Kavanagh , C. C. Pan, L. A. Dawson, S. K. Das, X. A. Li, R. K. Ten Haken, and M. Miften, "Radiation dose-volume effects in the stomach and small bowel," Int. J. Radiat. Oncol. Biol. Phys. 7, S101–S107 (2010).

14. I. Yau, T. Vuong, A. Garant, T. Ducruet, P. Doran, S. Faria, S. Liberman, C. Richard, F. Letellier, P. Charlebois, R. Loungnarath, B. Stein, and S. Devic, "Risk of hypogonadism from scatter radiation during pelvic radiation in male patients with rectal cancer," Int. J. Radiat. Oncol. Biol. Phys. 74, 1481-1486 (2009).

15. T. Vuong, S. Devic, and E. Podgorsak, "High dose rate endorectal brachytherapy as a neoadjuvant treatment for patients with resectable rectal cancer," Clin. Oncol. 19, 701-705 (2007).

16. T. Vuong, S. Devic, B. Moftah, M. Evans, and E. B. Podgorsak, "High-dose-rate endorectal brachytherapy in the treatment of locally advanced rectal carcinoma: technical aspects," Brachyther. 4, 230-235 (2005).

17. T. Vuong, S. Devic, and E. Podgorsak, "Chapter 17: High-dose-rate preoperative endorectal brachytherapy for patients with rectal cancer," Editors: B. G. Czito and C. G. Willett, Rectal Cancer: International Perspective on Multimodality Management (Current Clinical Oncology). Springer Science+Business Media, LLC (2010).

18. S. Devic, T. Vuong, B. Moftah, M. Evans, E. B. Podgorsak, E. Poon, and F. Verhaegen, "Image-guided high dose rate endorectal brachytherapy," Med. Phys. 34, 4451-4458, (2007).

19. S. Devic, T Vuong, and B. Moftah, "Advantages of inflatable multichannel endorectal applicator in the neo-adjuvant treatment of patients with locally advanced rectal cancer with HDR brachytherapy," J. Appl. Clin. Med. Phys. 6, 44-49 (2005).

20. E. Poon, B. Reniers, S. Devic, T. Vuong, and F. Verhaegen, "Dosimetric characterization of a novel intracavitary mold applicator for 192Ir high dose rate endorectal brachytherapy treatment," Med. Phys. 33, 4515-4526 (2006).

21. E. Poon, J. F. Williamson, T. Vuong, and F. Verhaegen, "Patient-specific Monte Carlo dose calculations for high-dose rate endorectal brachytherapy with shielded intracavitary applicator," Int. J Radiat. Oncol. Biol. Phys. 74, 1259-1266 (2008).
22. Applicator Guide 2008: Applicators and accessories for HDR and PDR brachytherapy, Nucletron, (2008).

23. Varian Brachytherapy: Applicators and Accessories, Varian Medical Systems, (2011).

24. "Evo Drive Stepper Motor Controllers," Eva Robotics (2011)

25. L. Petrokikkinos, K. Zourari, E. Pantelis, A. Moutsatsos, P. Karaiskos, L. Sakeelliou, I. Seimenis, E. Georgiou, and P. Papagiannis, "Dosimetric accuracy of a deterministic radiation transport based 192Ir brachytherapy treatment planning system. Part II: Monte Carlo and experimental verification of a multiple source dwell position plan employing a shielded applicator," Med. Phys. 38, 1981-1992 (2011).

26. I. K. K. Kolkman-Deurloo, J. J. Nuyttens, P. E. J. Hanssens, and P. C. Levendag, "Intraoperative HDR brachytherapy for rectal cancer using a flexible intraoperative template: standard plans versus individual planning," Radiother. Oncol. 70, 75-79 (2004).

27. P. J. Hoskin, S. M. de Canha, P. Bownes, L. Bryant, and R. G. Jones, "High dose rate afterloading intraluminal brachytherapy for advanced inoperable rectal carcinoma," Radiother. Oncol. 73, 195-198 (2004).

28. H. Yanagi, M. Kusunoki, and T. Yamamura, "The effectiveness of preoperative intraluminal brachytherapy in preventing wall penetration and nodal involvement of rectal carcinomas," Surg. Today. 30, 410-415 (2000).

29. National Nuclear Data Center: http://www.nndc.bnl.gov/

30. G. M. Daskalov, E. Löffler, and J. F. Williamson, "Monte Carlo-aided dosimetry of a new high dose-rate brachytherapy source," Med. Phys. 25, 2200-2208 (1998).

31. VariSource iX, iX(t) HDR Afterloader: http://www.varian.com/brachytherapy

32. S. Civjan, E. F. Huget, and L. B. DeSimon, "Potential applications of certain nickel-titanium (nitinol) alloys," J. Dent. Res. 54, 89-96 (1977).

33. Compositions of Materials Used in STAR Databases: http://physics.nist.gov/cgi-bin/Star/compos.pl

34. MCNP – A General Monte Carlo N-Particle Transport Code, Version 5: http://mcnp-green.lanl.gov/pdf_files/MCNP5_manual_VOL_I.pdf

35. J. Borg and D. W. O. Rogers, "Monte Carlo Calculations of Photon Spectra in Air from 192Ir Sources," NRC Report PIRS-629r: http://www.irs.inms.nrc.ca/inms/irs/papers/PIRS629r/ pirs629r.html (1998).

36. P. H. Calamai and J. J. Moré, "Projected gradient methods for linearly constrained problems," Math. Program. 39, 93-116 (1987).

37. M. S. Bazaraa, H. D. Sherali, and C. M. Shetty, "Nonlinear Programming: Theory and Algorithms, 2nd ed.," Hoboken, NJ: Wiley (1993).

38. J. Nocedal and S. J. Wright, "Numerical Optimization. Springer Series in Optimizations Research," New York: Springer-Verlag (1999).

39. R. Nath, L. L. Anderson, G. Luxton, K. A. Weaver, J. F. Williamson, and A. S. Meigooni, "Dosimetry of interstitial brachytherapy sources: Recommendations of the AAPM Radiation Therapy Committee Task Group No. 43," Med. Phys. 22, 209-234 (1995).

40. M. J. Rivard, B. M. Coursey, L. A. DeWard, W. F. Hanson, M. S. Huq, G. S. Ibbott, M. G. Mitch, R. Nath, and J. F. Williamson, "Update of AAPM task group No. 43 report. A revised AAPM protocol for brachytherapy dose calculations," Med. Phys. 31, 633-674 (2004).

41. V. Coen, E. Lartigau, C. Haie-MEder, P. Lambin, H. Marsiglia, E. Briot, and A. Gerbaulet, "The heterogeneity index (HI) : a new parameter to evaluate tumor local control and late morbidity in interstitial brachytherapy," Rad. Oncol. 39, 9-9 (1) (1996).

42. G. Kertzscher, C. E. Andersen, F. A. Siebert, and S. K. Nielsen, "Identifying afterloading PDR and HDR brachytherapy errors using real-time fiber-coupled AL2O3 dosimetry and a novel statistical error decision criterion," Radiother. Oncol. 100, 456-462 (2011).

43. B. Plamer, N. Davis, and L. DeWerd, "Kinematics of Varian Varisource high dose rate afterloading system when subjected to obstruction," University of Wisconsin Medical Radiation Research Center Report.

44. CAPRI™ Applicator: http://varian.mediaroom.com/index.php?s=43&item=850

45. C. Men, H. E. Romeijn, X. Jia, and S. B. Jiang, "Ultrafast treatment plan optimization for volumetric modulated arc therapy (VMAT)," Med. Phys. 37, 5787-5791 (2010).

46. S. Webb, “Optimization of conformal radiotherapy dose distributions by simulated annealing,” Phys. Med. Biol. 34, 1349-1370 (1989).

Chapter 3 HDR Brachytherapy of Rectal Cancer Using a Novel Grooved-Shielding Applicator Design

3.1 Introduction

Improvements in imaging technologies have made tumor localization increasingly accurate.[1,2] While external-beam radiotherapy (EBRT) has been able to capitalize on these advancements with non-uniform beam intensities, brachytherapy has not kept up in delivering dose distributions that are congruent to the tumor volume. Even so, brachytherapy offers significant advantages in treatment of certain sites, including rectal, when compared to EBRT. A major reason for this is that EBRT delivers an appreciable dose to all the tissue the beam traverses while targeting the tumor volume; this problem is exacerbated because chemotherapy sensitizes pelvic organs such as the small bowel and rectum.[3,4] Damage from radiation to these and other surrounding organs can lead to problems or delays in post-surgical healing (e.g., anastomotic leak or perineal wound infection).[3] The situation is even worse for non-surgical candidates, due to health or other contraindications, since in those cases the only alternative treatment modality is chemo-and-radiation-therapy (CRT) in a more intense, definitive setting. Therefore, it is highly desirable to have a brachytherapy applicator that could surpass the tumor conformality of EBRT, thus avoiding dosing much of the healthy pelvic organs. This can be achieved through judiciously designed intensity modulated brachytherapy (IMBT) applicators.

Various studies have shown that preoperative high-dose rate (HDR) brachytherapy, instead of the typical preoperative CRT, has proven to be quite beneficial

in recurrence rates and long-term survival.[5-7] The most exciting improvements have come from use of the intracavitary mold applicator (ICMA) (Nucletron, Netherlands)[8-11], which is an 8-channel cylindrical applicator. When using this applicator, the occurrence of grade ≥3 acute proctitis went down to 1% vs. 27%, and pathologic complete response rate rose to 29% compared with 8-12% using CRT. In addition, the shorter treatment duration (1 week vs. 5 weeks), no need for chemotherapy, and less surgical complications were significant advantages. One reason for large benefits seen from this applicator is the optional shielding, which is in the form of an 8-mm diameter tungsten rod, which can be used for treatment of non-circumferential tumors.[10]

While the tungsten allows for some dose anisotropy, the geometry of the design places the ^{192}Ir seed 2.5-mm away from the shield surface, resulting in a 285° spread of completely unshielded cross-sectional dose,[6] thus limiting how conformal the delivered radiation profile can be. Therefore, while outcomes with the ICMA have been very encouraging, there still exists a large potential for improvement in dose congruence. Our previous design of an applicator we called Dynamic Modulated Brachytherapy (DMBT)[12] has shown that by insetting the ^{192}Ir seed into an intelligently designed shield itself, extreme improvements in dose conformality and sparing of the healthy tissues can be achieved. The reason for the DMBT's extreme improvements in results is that it takes shielding to its logical extreme, creating a highly collimated dose profile which then could be modulated by rotating and translating the entire system to direct the dose exactly as desired for optimal dose distributions. While this design gave extraordinary results, it

had some drawbacks including increased treatment time and complexity of setup and delivery.

With these issues in mind, a new IMBT applicator has been designed to strike a balance between the ICMA and DMBT. This novel applicator retains the stationary multi-channel design of ICMA, but insets the channels into grooves within a larger shield, borrowing from the ideas of DMBT. This way, a much greater amount of shielding is introduced, allowing for more directional dose profiles. A 2002 study by Ebert found that for an effective IMBT, a collimation angle of 22.5-45° and shielded-side transmission of <10% (leakage) are needed to see a worthwhile improvement.[13] While ICMA produces 5% leakage, the collimation angle of 285° is well above the values suggested by Ebert. There are also a couple of available shielded applicator sets (Nucletron, Netherlands and Varian Medical Systems, Palo Alto, CA)[14,15] which have collimation angles of 90 or 180°, but these is still well short of the recommended value. These applicators are also single channeled, thus greatly reducing the available degree of dose modulations. While the grooved design put forth here would lack the extremely high conformality of the DMBT, it would be able to achieve these criteria recommended by Ebert and represents a major improvement in the potential of treatment using immobile applicators for IMBT. This current investigation examines the dosimetric benefits of such a design. Multiple variations of this applicator are simulated and compared to both the ICMA and DMBT. The new applicators should not only increase the possibility of conforming to the target volume, but also sparing of relevant sensitive structures without increasing complexity of setup and treatment (e.g., no moving parts during treatment).

3.2 Methods and Materials

A. System overview

The tungsten-alloy shields simulated in this study were all 16-mm in diameter, with equally spaced grooves running longitudinally along the entire edge of the shield. The alloy used in this work was comprised of 95% tungsten, 3.5% nickel, and 1.5% copper; this is the highest density tungsten alloy available which is completely non-magnetic, thus making it MR-compatible. Each shield design was simulated at a length of 60-mm, with every groove, 1.2-mm in width running the entire length of the shield. The source was located inside a catheter, which was 1.2-mm in diameter, matching the channel size, at the base of the groove, putting the source center 0.6-mm from the deepest point in the groove. The applicator was then encapsulated in a 2-mm thick indexed silicon sheath, giving the entire system a total diameter of 20-mm.

The treatment planning process would follow the same procedure as other existing image-guided HDR ^{192}Ir brachytherapy devices. While in the imaging room, the patient will be placed on a stabilization board in the supine position. The silicon sheath, which would be encapsulated in a unidirectional endocavitary balloon (e.g. CIVCO Medical Solutions, Kalona, IA), would then be inserted into the rectal cavity. In order to assure dwell position accuracy, the sheath will be affixed to the stabilization board. This would not only keep it from moving laterally, but would also allow for rotational fixation. Furthermore, in order to avoid geometrical discrepancies that may arise from inserting the shield, it may be necessary to have a dummy shield, which is transparent to CT in place while imaging. In addition, this would allow for the placement of a dummy source

for easy catheter identification. The balloon would then be inflated in order to displace the healthy tissues away from the applicator and stabilize the sheath within the cavity. Imaging will then be done and the patient will be transported to the HDR room. Once there, the tungsten shield will be placed within the sheath and locked into place. Once this has been completed, an optimized treatment plan will be delivered.

B. Modeling of the ^{192}Ir HDR source

The ^{192}Ir source used in our clinic is the VariSource iX HDR source.[16] The source is comprised of two identical adjoining cores, each 0.34-mm in diameter and 2.5-mm in length, which are encapsulated together by a 0.59-mm diameter nitinol wire of density 6.45 g/cm^3.[17] The energy levels used were in accordance with the National Nuclear Data Center.[18]

C. Shield design variations

A systematic approach was used to identify the optimal design(s) for a grooved channel system. Three different groove depths and five channel counts were used to make fifteen simple designs and then one complex design with two usable dwell positions per channel were used for a total of sixteen different variations simulated and optimized for this work. In the different variations, there were a total of 8, 10, 12, 14, or 16 equally spaced longitudinal grooves. The range of channels was chosen to reflect the fact that more channels means a greater degree of freedom for optimization, but it does so at the cost of reduced shielding. That is, more dwell positions mean a less anisotropic dose distribution for each dwell position. A lower limit of 8 channels was chosen to allow sufficient overlap of doses delivered by adjacent dwell positions and therefore severe

hotspots would not become an issue. Conversely, a maximum of 16 channels was chosen simply because it would be impractical to attempt any more than that on a shield with a 16-mm diameter.

For each groove count, three designs were considered, each with the groove at a different depth. Similar to the tradeoff of adding more channels, making each groove deeper has advantages and disadvantages. Specifically, a deeper channel means that the dose distribution becomes more directional, but then there is a greater degree of transmission to the contralateral side of the shield. Also, a deeper set source would require more total time to deliver the same dose as a source near the shield's surface. To analyze these issues, designs with the source centered at 1, 2, and 3-mm from the surface of the tungsten were looked at. This was done for each number of channels, making 15 total designs of this nature, the schematics for which can be seen in Figure 3-1. For convenience, the format ***a.b*** will be used to refer to specific designs, where ***a*** and ***b*** represent the number of channels and the depth of the source, in millimeters, for that particular design, respectively.

In addition to these, one more unique design was considered, in which two channels were constructed per groove. See Figure 3-1 ("Dual Depth" design on bottom left). Using a design with 10 channels, each groove contained two catheter channels, creating a total 20-channel system. The depths were chosen to be 1 and 2.5-mm because it was concluded that, given the tradeoffs previously mentioned, these two would generate the best results. Only the 10-channel system was considered because the VariSource iX HDR afterloader has a maximum of 20 allowable channels.[19] Therefore,

while similar designs with more channels may produce better results, they would be impractical to implement with the currently available clinical tools.

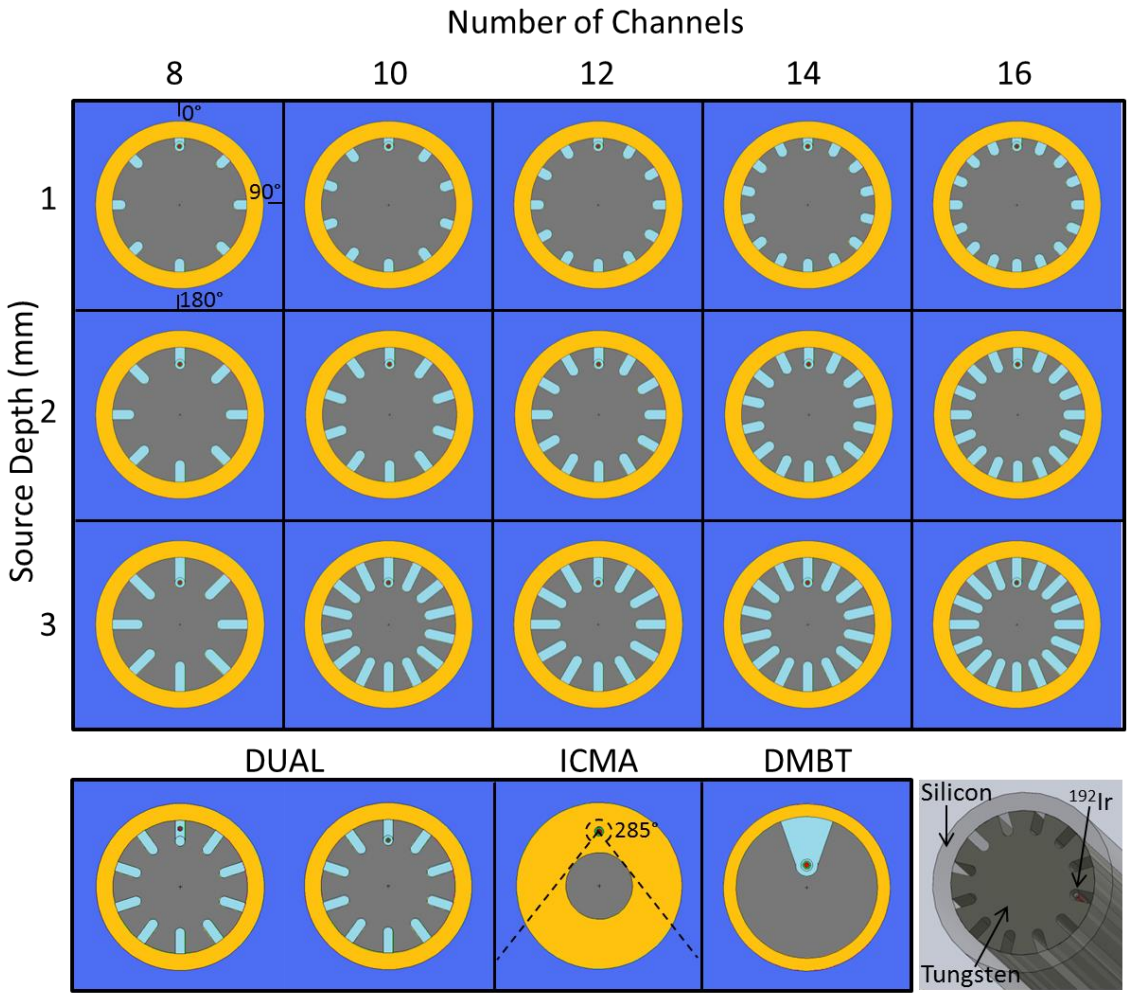

Figure 3-1. A transverse cross section of the design schematics for all applicators. Shown are the 15 grooved designs with a single dwell position depth, the 10-channel design with two dwell position depths, ICMA, and DMBT. Finally the bottom right image shows a 3D CAD rendering of the 12-channel applicator with the source located 2-mm deep from the edge of the tungsten, for example.

D. Reference applicators (ICMA and DMBT)

To assess the quality of the shield designs in comparison to currently available commercial IMBT applicators, they were evaluated against the ICMA. The ICMA was chosen as a baseline point of comparison because it is a widely used rectal applicator and has the most promising dosimetric results.[5-11] The ICMA system is comprised of a flexible silicon applicator, 280-mm in length and 20-mm in diameter. See Figure 3-1 ("ICMA"). For non-circumferential target volumes, for which no more than 3 consecutive channels of the applicator are used, sparing can be improved by inserting an 8-mm diameter tungsten rod into the center of the applicator. In addition, an inflatable 30 ml endocavitary balloon (CIVCO Inc, Kalona, Iowa) may be used to distance the healthy tissues from the applicator.

All the designs listed were also compared against the DMBT applicator.[12] By using a shield with single small opening to create a very narrow dose profile and then rotating and translating the shield itself with specialized robotics it is possible to create a very conformal dose distribution, far better than ICMA. Therefore, this applicator was also considered, as a gold standard of comparison for our applicators. See Figure 3-1 for design ("DMBT"). While, several design options for DMBT were outlined previously,[12] for this work, the design used was a 45-mm long, 19-mm diameter, tungsten cylinder with the source located 3-mm from the radial center of the shield at the vertex of a 45° wedge-shaped opening that was 5.5-mm long. For this applicator, a 1-mm thick polycarbonate sheath was placed around the outside of the shield.

E. Patient dataset

To quantify the quality of the applicators, patient geometries were used from planning datasets acquired from McGill University, Canada.[20] From this dataset, 36 clinical treatment plans from 13 patients previously treated with ICMA were used. Due to health or other contraindications, these patients were not candidates for surgery and required higher, more definitive prescription of 10 Gy × 3 fractions, as opposed to 6.5 Gy × 4 fractions. In addition, these patients presented with non-circumferential tumors, making the geometries ideal for treatment with applicators with higher dose conformality capabilities. In fact, the CTV for each fraction was suitably shaped such that no more than 3 channels were used with the ICMA, thus allowing for the use of the tungsten rod for shielding during treatments. The average volume of the CTV was 9.0 ± 3.5 cm^3. Finally, in all cases, the inflatable balloon mentioned previously was utilized. The organs at risk (OAR) which were used in treatment planning were the contralateral rectum, defined as the healthy rectum with the same inferior and superior edges as the CTV, and the inferior and superior spills. The inferior and superior spills were cylindrical structures, typically 10-mm in length and 40-mm in diameter located approximately 10-mm from the inferior or superior edge of the CTV, respectively. These structures did not represent any physical structures, but were used to limit and assess the extent of radiation being delivered above or below the applicator. See Figure 3-2. The inferior spill is especially important in limiting the dose to the sphincter, since sphincter preservation is a high priority in these treatments.

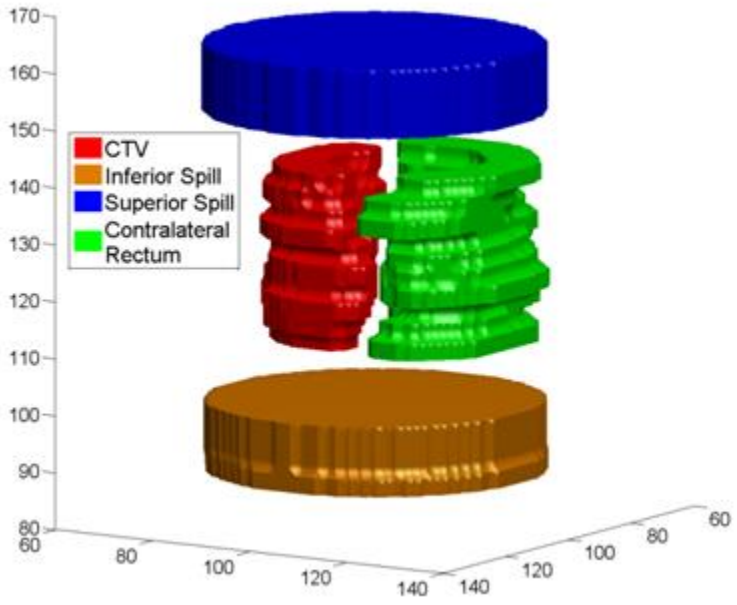

Figure 3-2. Sample patient geometry with all of the relevant structures. Distances are in-mm.

F. MCNP5 dose calculations

Every applicator mentioned thus far was simulated using an MCNP Monte Carlo code, version 2.6.0,[21] including the tungsten shields in ICMA, grooved-applicators proposed here, and DMBT. All components of the devices which would be present during treatment were created using the set of built-in macro-bodies. For each simulation, the specifics of the dose calculations and voxel geometry are the same as from the previous DMBT work.[12] For each decay event simulated, on average 2.363 gamma emissions were generated.[22] Bremsstrahlung X-rays, electron-induced X-rays, knock-on electrons and secondary electrons were used for photon interactions. Other interactions used were incoherent scattering, coherent scattering (Rayleigh scattering), fluorescence emission, Compton scattering, capture, and pair production. In order to achieve better simulation efficiency, a lower energy cutoff of 10 keV for electron transport simulations

was enforced. All space outside of the applicator was treated as water. All simulations were run through the San Diego Supercomputer Center, using 512 CPU cores, each simulating 100,000 particles. Due to the rotational symmetry of the applicators, it was only necessary to simulate one dwell position for each design.

G. Plan Comparison Indices

To assess the plan qualities of each design, the mean dose, D98, and D5 were calculated for all critical structures, where D98 and D5 represent the maximum dose which is delivered to 98% and 5% of the structure volume, respectively. In addition, the dose heterogeneity index (DHI)[23] was calculated, which is given by $(D_{max}-D_{min})/D_{mean}$, where D_{max}, D_{min}, and D_{mean} represent the maximum, minimum, and mean dose received by the CTV, respectively. Finally, total dwell times were calculated assuming source strength of 40.25 kU (10 Ci). To ensure a fair comparison, all plans for both ICMA and the grooved applicators, were normalized such that 95% of the CTV volume received at least 95% of the 10Gy prescription dose.

H. Dose optimization

All plans calculated were done so using an in-house coded gradient projection convex optimization algorithm. A quadratic objective function was used to minimize the dose to the OARs while keeping the CTV dose as uniform as possible. Except for a non-negativity condition on the dwell times, no dose constraints were implemented. A rigorous explanation of the optimization process used is presented in the DMBT work.[12] For all applicators, including the DMBT and ICMA, a lateral dwell position resolution of

5-mm was used. For all the multi-channel applicators, every available channel was optimized on, while 360 rotational steps were considered for the DMBT.

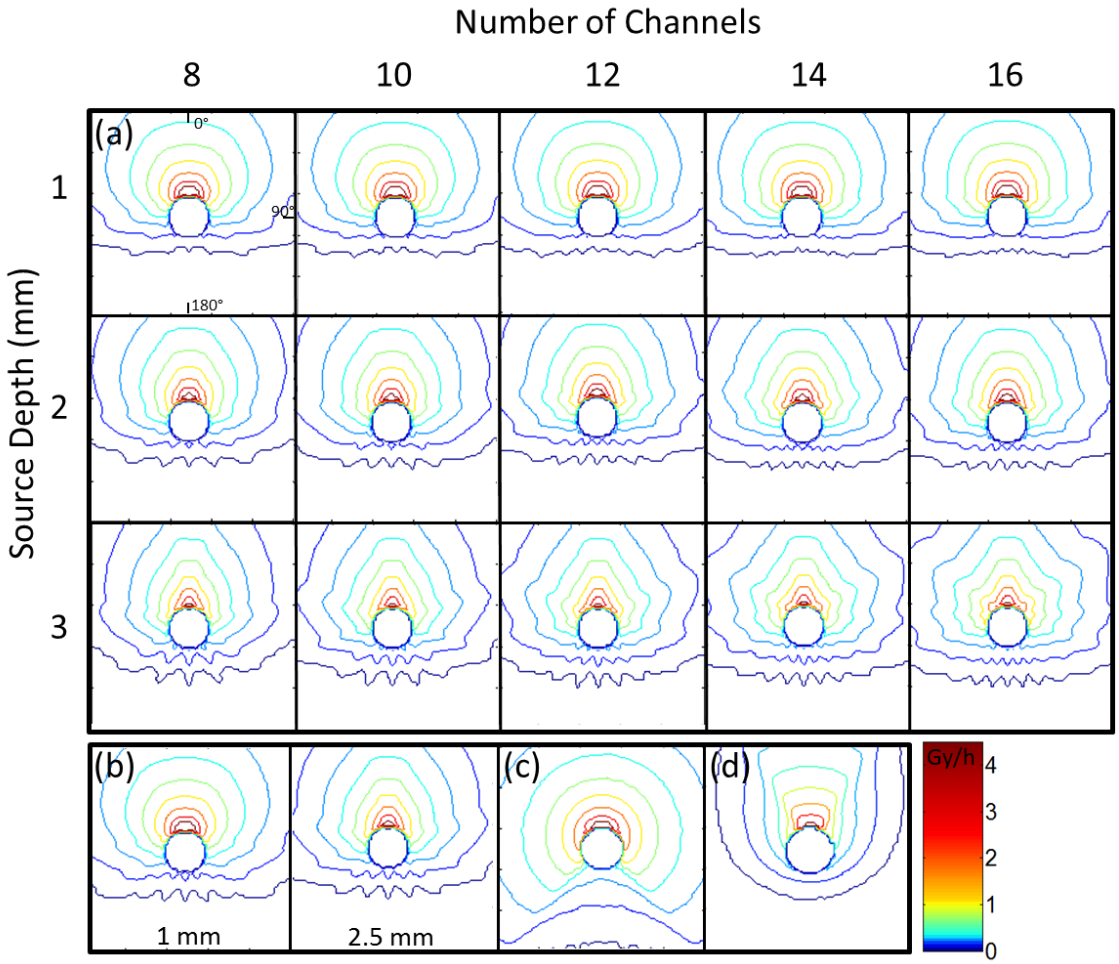

Figure 3-3. Transverse cross sections of the isodose plots for the applicator designs. Included are the 15 grooved designs with a single dwell position depth (a), the 10-channel design with two dwell position depths (b), ICMA (c), and DMBT (d). Each isodose line is a factor of two different from the adjacent lines.

3.3 Results

A. MCNP dose calculations

Each simulation required approximately 1.5 hours to complete on the super computer cluster. The characteristic isodoses for each applicator are shown in Figure 3-3. The isodose lines are given in Gy/h, with each line representing a factor of two difference from the adjacent lines. In all simulations, a sufficient number of decay events were simulated to keep the variance to all voxels under 5%. In most of the regions of interest, the variance was kept under 1%. Typically, the variance 10-mm from the shield surface was 0.1% at the point nearest the source and around 0.5% for the point 10-mm from the shield surface and directly behind the source. The regions of high variance occurred where a large amount of shielding was present and therefore would not be directed towards the tumor volume. The end results for open source simulations were compared and normalized to the TG-43 standard.[24,25] We found the radial dose function to be in agreement with TG-43 within 2%, as shown in Figure 3-4. In addition, the simulated Air Kerma strength was found to be in high agreement (<1%) with reported values. Within 5-cm of the source, the anisotropy function was within 1.5% for $\theta = 0°$ with up to 5% error for up to $\theta = 80°$. Beyond this, the accuracy diminished, but this was not view as a being detrimental to the to the results since in the design simulations most of this region was either contained within the applicator was sufficiently far away from the source to cause any appreciable change in the results.

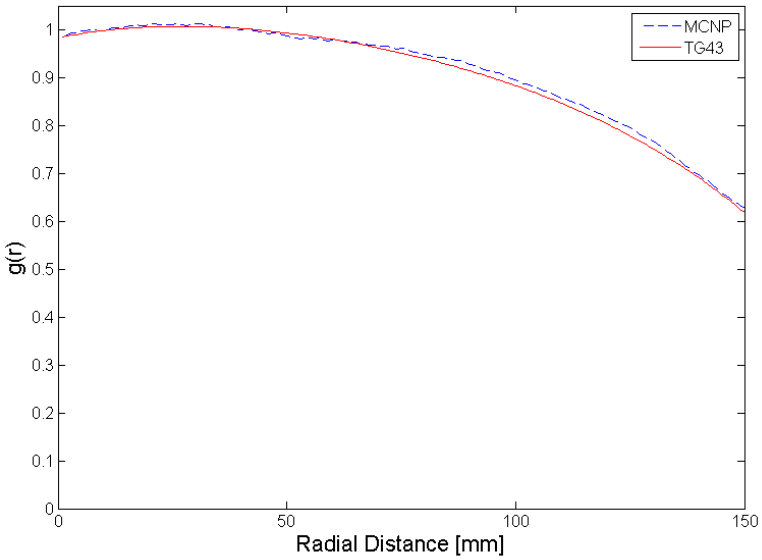

Figure 3-4. MCNPX (dashed blue) and TG-43 (solid red) calculations of the radial dose function of the VariSource iX HDR source.

Table 3-1. The simulated dosimetric data for all applicators. For each applicator, the given values are the average for that design over all 36 plans optimized and simulated. All doses are in Gy. Dwell times are in minutes. Dose was normalized such that 95% of the CTV volume received at least 95% of the 10 Gy prescription dose.

		CTV		Spill			Contra			Dwell	
Depth	Channels	Mean	D5	Mean	D98	D5	Mean	D98	D5	Times	DHI
	8	15.35	22.78	1.84	0.21	4.71	1.84	0.44	5.37	8.33	1.42
	10	15.26	22.49	1.83	0.22	4.64	1.97	0.46	5.53	7.96	1.41
1	12	15.13	22.17	1.79	0.21	4.58	1.83	0.43	5.26	8.04	1.4
	14	15.11	22.12	1.79	0.21	4.59	1.88	0.44	5.33	7.95	1.38
	16	15.08	22.06	1.81	0.21	4.56	1.92	0.44	5.39	7.85	1.38
	8	15.41	22.78	1.87	0.26	4.63	2.13	0.63	5.52	11.24	1.47
	10	15.15	22.01	1.83	0.26	4.55	2.14	0.63	5.45	10.85	1.4
2	12	15.1	21.86	1.85	0.27	4.56	2.21	0.63	5.53	10.33	1.38
	14	14.92	21.5	1.83	0.27	4.47	2.25	0.65	5.62	10.24	1.34
	16	14.99	21.71	1.89	0.28	4.5	2.39	0.67	5.93	9.72	1.32
	8	15.97	24.27	2	0.35	4.8	2.66	0.94	6.08	15.05	1.6
	10	15.61	23.4	2.09	0.38	4.7	3.04	0.99	6.96	12.62	1.52
3	12	15.24	22.09	1.96	0.35	4.57	2.73	0.93	6.2	13.44	1.37
	14	15	21.64	1.96	0.36	4.49	2.81	0.94	6.38	12.69	1.34
	16	15.09	21.91	2.02	0.36	4.53	2.91	0.95	6.67	12.16	1.32
	Dual 10	15.35	22.78	1.84	0.21	4.71	1.84	0.44	5.37	8.33	1.42
	ICMA	15.66	23.99	2.09	0.55	4.34	3.84	1.25	8.31	5.51	1.50
	DMBT	13.80	18.54	1.10	0.29	2.54	1.92	0.82	4.11	17.57	1.18

B. Plan quality comparison

The results presented hereafter represent the average outcomes. For each applicator, the given values are the average for that design over all 36 plans optimized and simulated. The dosimetric data is given in Table 1. Figure 3-5 shows the average of all designs divided by the corresponding ICMA value with the standard deviation for the DHI, contralateral D5, spill D5, and total dwell time. The raw data was sorted based on several criteria, such as CTV volume or depth, but no correlation was seen in how these affected the preference of one shield design over another. While some of the standard deviations were somewhat large, it is immediately clear that, while the grooved designs failed to match DMBT in many areas, they were still consistently better than the ICMA. Also, although there is a fair amount of variation in the data comparing the grooved-designs to each other, there are some clear trends in the data that are discussed in the following sections.

A typical patient plan is shown for ICMA, DMBT and the 12.1 applicator in Figure 3-6. The differences between the dose distributions delivered by the different applicators can be clearly seen in this figure. It is seen that the ICMA applicator has the least dose conformity, with the prescription isodose reaching well into the contralateral rectum. All grooved-designs exhibited a spill to this region as well, but in this case it was much smaller and often the prescription dose barely reached the contralateral rectum region, if at all. Finally, the DMBT design preformed the best, conforming nearly perfectly.

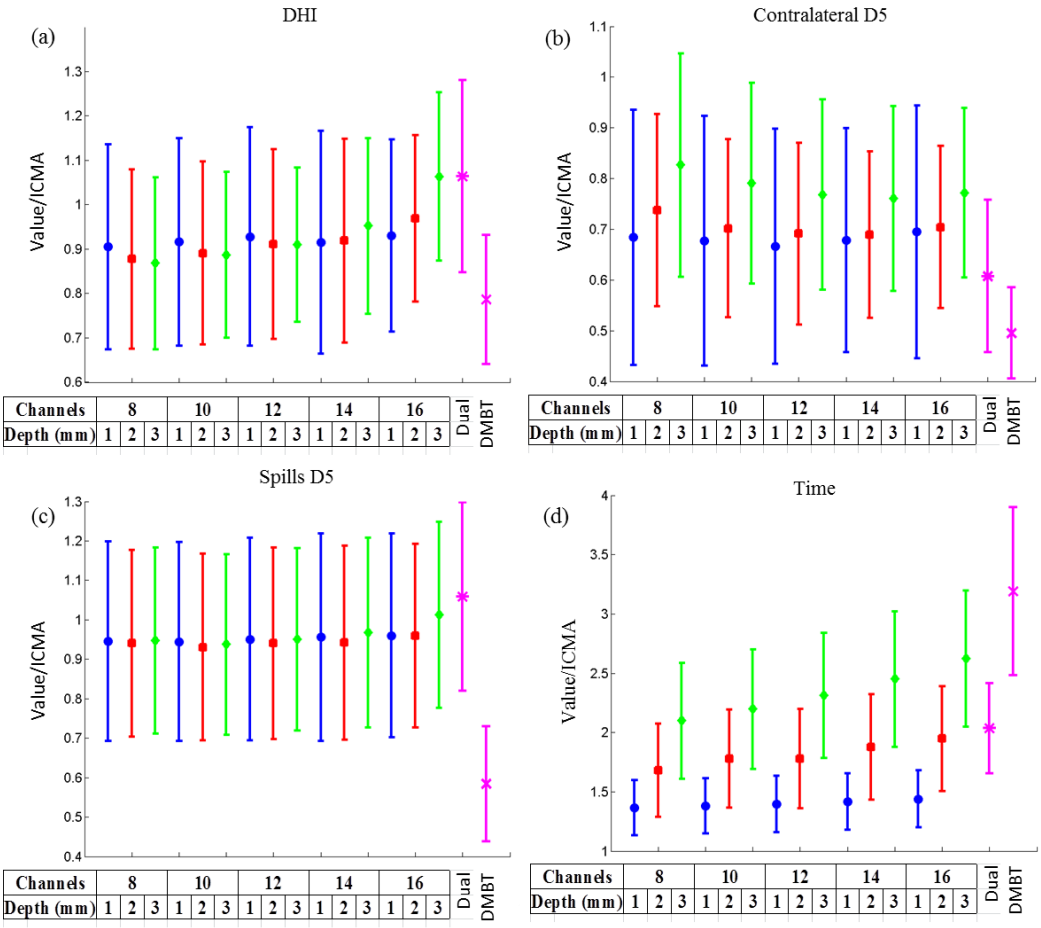

Figure 3-5. A comparison of the 15 single-depth grooved designs, 10 channel dual-depth grooved design, and DMBT. The comparison indices are (a) the DHI, (b) the contralateral D5, (c) the spills D5, and (d) total delivery time. Values were calculated as the mean of that applicator's value divided by ICMA.

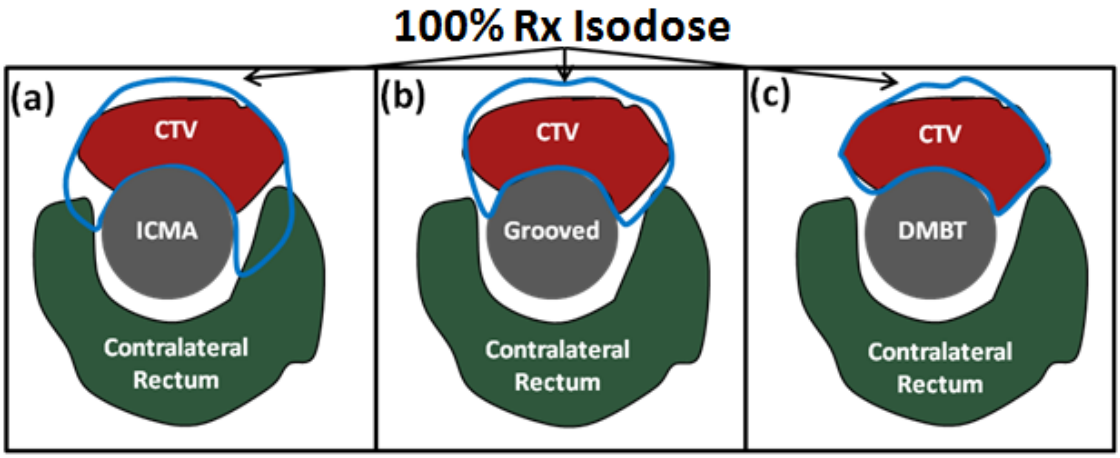

Figure 3-6. Typical dose distributions for (a) ICMA, (b) the grooved type applicator with 12-channel and 1-mm source depth, and (c) DMBT.

C. Standard designs

C.1 Source depth

The dose distributions from the different applicator designs can be seen in Figure 3-3. Optimized plans on the patient data showed almost all the new applicator designs outperforming that of the ICMA in every metric. This was especially apparent regarding the sparing of the healthy rectal tissues. While none of them managed to do as well as DMBT, a dose reduction of up to 50% compared to ICMA was seen. The dose to the spill regions was also reduced and the dose conformality to the CTV saw a benefit or no change with each of the grooved designs, with one exception. The exception was the 8.3 design. This shield gave a dose profile that was too directional, while lacking a sufficient number of channels, meaning that severe hot spots were induced in some areas, both in the tumor and healthy tissues to achieve the prescribed dose to the entire CTV. While this effect was less prevalent in the other designs with the source located at this depth, they

still yielded poorer results than the other options. For the same number of channels, with the exception of the DHI, the 2-mm depth designs, on average, did better than their 3-mm depth counterparts in every single metric measured.

For the remaining two depths considered, the shallowest 1-mm depth designs gave the best sparing to both the contralateral rectum and the spill regions, but failed to match the 2-mm depth designs in terms of CTV coverage. For any given number of channels, the maximum sparing to the contralateral rectum was achieved with the source placed at a depth of 1-mm. Depending on the number of channels, the difference in the mean dose to the contralateral rectum was increased 11-18% by increasing the depth of the grooves, with the greatest effect seen for the designs with more channels. Similarly, there was approximately a 30% increase in the D98 dose to the contra for the same shifts. In terms of CTV coverage, the shallowest channels preformed slightly worse, with the 2-mm depth performing the best. However, the changes in these values were typically under 3%. Furthermore, for each 1-mm increment in depth, an approximate increase of 20% in total dwell times was observed. With all elements considered, it appears that the 1-mm depth designs give the best overall performance.

C.2 Channels

The shields with 8 channels preformed noticeably worse than the rest of the grooved designs. For these designs, especially with the deeper depth channels, the optimizer struggled to deliver a conformal dose to the CTV, often at the cost of the contralateral rectum sparing. Up until 14 channels, adding more grooves improved the average CTV dose conformality, with the 16-channel system being a slight step down

from 14. With regards to contralateral rectum and spill region sparing, the best designs were those with 12 channels. Finally, the total dwell times decreased marginally with each additional pair of channels, with the difference between 8 and 16 channels being approximately 3 seconds per Gy delivered (e.g., a 10 Gy prescription had a 30-second difference).

When combining the effects of the different parameters, two of the applicators stood out as being superior to the rest. These were the 12.1 and 14.2 designs. These two designs were selected as the ones with the best sparing of the healthy tissues and best coverage of the CTV, respectively. The 12.1 design gave the best sparing of the healthy tissues in all categories except that of the D5 dose of the spills, for which the 14.2 design was optimal. The 14.2 design also gave the best average conformality to the CTV. The only dosimetric values that neither of these designs showed the best average results for, of the 15 designs, were the total dwell time and the DHI, which had the best results for the 16.1 and 16.3 designs, respectively.

D. Dual depth design

The final design considered, the dual depth 10-channel system yielded better results than any of the other 15 single depth designs. This setup gave both the best balance of CTV coverage and OAR sparing. The difference in the CTV dose conformality between this design and the 14.2 shield was minimal. It also yielded comparable results to the 12.1 design with regards to sparing, achieving slightly better, 2-5% sparing, in terms of D5 dosages. While failing to outright outperform every other design in every metric, this balance easily makes it better on the whole than any of the

single depth options simulated, despite not being able to have as many total grooves as the designs it was compared against. The DVH for this applicator, as well as ICMA, DMBT, and the two best results of the single channel design are shown in

Figure 3-7.

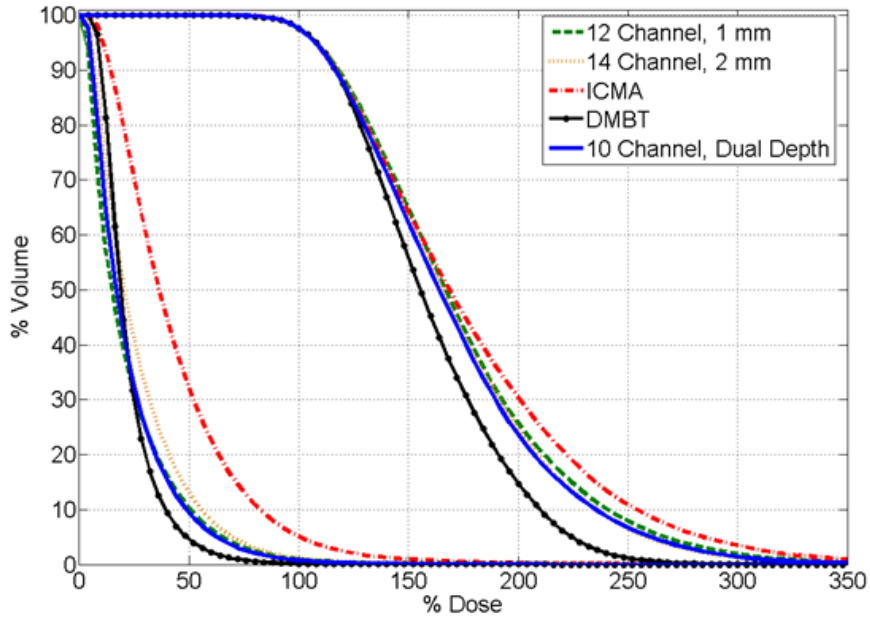

Figure 3-7. The mean DVHs for DMBT, ICMA, the dual depth 10-channel design, and the two best single depth designs, 12.1 and 14.2. For each applicator, the given values are the average for that design over all 36 plans optimized and simulated The two groups of DVHs shown are for the CTV (right) and Contralateral Rectum (left).

3.4 Discussion

It is clear from the simulations that a recessed groove-type applicator is capable of delivering a plan that is superior to the existing ICMA applicator. The increased degree of shielding makes it so that an applicator of this design is capable of reducing the radiation dose to healthy tissues while maintaining equivalent or better dose conformality to the CTV. This is a direct result of the increase in shielding given to the applicator and,

to a smaller extent, an increase in the number of channels. By recessing the source into the shield, as opposed to having it 2.5-mm from the shield surface, which is the case for ICMA, and doubling the shield size, the amount of dose exiting the applicator anywhere except directly out the front is greatly reduced. As previously mentioned, the dose collimation of ICMA is at 285° (see Figure 3-1 and Figure 3-3), while these new designs have collimation angles of 10-30°. A drawback of the additional shielding is that it requires more time to deliver the same amount of dose. The various designs showed an increase of 36-145% in comparison to ICMA. For a 40.25kU (10 Ci) source, the increased time, of up to 10 additional minutes should be acceptable. This is partly because the total treatment time is not limited to the delivery time. There is also setup, imaging, and dose planning to consider leading to a total treatment time around an hour, regardless of the applicator. However, for weaker sources the delivery time could as much as double the delivery times given in Table 3-1. This should still not create too much concern since, for the two recommended applicators, 12.1 and 14.2, this would only generate a total of 4.5 and 7 minutes of additional treatment, compared to ICMA, an acceptable tradeoff for the superior treatment plans.

Normalizing the dose to a point 10-mm from the shield edge, closest to the source, the degree of shielding can be directly compared between the ICMA and grooved applicators. The dose lateral to the shield is consistently around 25% that of the ICMA dose for all the applicators, while the dose on the contralateral side falls to around 20-35% of the ICMA, with the best results coming from the shallower grooves. The most extreme difference is in the area below the midpoint of the shield where the tungsten rod

of the ICMA applicator fails to block the dose. That is, between 90 and 142.5° from the source. The top left subfigure of Figure 3-3 shows the coordinate system used in this description. Furthermore, the 142.5° mark can be inferred by looking at the isodose lines shown in ICMA plot of Figure 3-3. In this region, the dose is at 5-15% of the ICMA, again with the shallower grooves yielding the best results. This makes it clear why the mean dose and D98 dose values drop so significantly when using the grooved type applicators.

While not as extreme, similar effects can be seen with regards to the spill regions superior and inferior to the CTV. While the D5 value was better for the grooved designs, the biggest difference came from the mean dose and D98. This is important because the inferior spill region often can correspond to the dose delivered to the sphincter and reducing the dose can help increase the chance of preserving it. In addition, previous studies have shown that higher treatment doses can improve outcomes. In one study, it was found that patients receiving greater than 93Gy biological effective dose had 5 year disease-free survival rate of 77%, compared to 50% for patients who received less than 93 Gy biological effective dose.[26] The use of the proposed groove-type applicators would make dose escalation like this more feasible and could even allow for even higher doses without increasing the risk of normal tissue complications.

Although some clear trends did emerge concerning the optimal number of channels and depth of the radioactive seed, it should be stressed that these were average results, with noticeable variations in the shield rankings for different patient geometries, especially regarding the ideal number of channels. This indicates that the tumor shape

and position may play a role in which applicator is ideal, and therefore it may be prudent to have multiple applicators available so that the best possible treatment can be delivered for each and every patient. With our design, this would be straightforward to implement in clinic. This is because the silicon sheath would be first inserted and fixed in place before imaging would be conducted. After which, any one of the applicators chosen could be inserted into the silicon sheath before the treatment commences.

These inter-patient variations may be diminished or even removed altogether if greater care was given to the initial setup, however. In the results presented, the applicators were setup so that the first channel of each one was consistently aligned with an arbitrarily selected 0° mark (i.e., the 12 o-clock position). It is perhaps the case that if more attention was given to the exact rotational position of each shield before optimization, more consistent, and even better, results could be seen.

It is also important to consider that the results presented herein are for highly non-circumferential tumor volumes. Specifically, these were all cases where the ICMA used no more than three of the eight available channels because if more channels are needed, the tungsten rod is not inserted. That is, in treatment if the tumor is not of this geometrical category, all benefits of a shield are lost. However, even for tumor geometries more circumferential than this, the grooved applicators would still have a large amount of shielding to spare the surrounding healthy tissues. This also means that if this work had included larger, but still non-circumferential cases, an even greater disparity between the two applicators would have been seen, since no shielding would be

present in any form for the ICMA and sparing could only be achieved by manipulating the geometric placement of the source channels.

While the grooved type applicators are a clear step forward from the ICMA, it should be noted that they failed in most aspects to match the DMBT design.[12] This was to be expected because the DMBT was able to produce a far more directional dose distribution(s) which then could be easily translated and rotated as needed. While the grooved type applicators represented a small step back in regards to tumor coverage, they are superior to the DMBT in some aspects. The most important of these is that these applicators are static in nature (i.e., no moving parts during treatment). While this limits the capacity for high CTV conformality, it means easier implementation in clinic. The DMBT system, while highly effective, requires specialized robotics for moving the applicator which makes treatment setup more difficult. Also, the extremely high number of potential dwell positions for the DMBT makes dose optimization and calculation a more demanding process. However, the grooved applicators have far fewer dwell positions and therefore dose can be calculated as fast as any other standard multi-channel brachytherapy applicator.

Overall, the implementation of this sort of applicator in clinic would be fairly manageable. Another point of consideration is the uncertainty in dwell positions for these devices. While DMBT requires the source position to be very well known and accurately placed in order to get the desired dose distribution, the new applicators' translational symmetry makes this less important. Although there are still uncertainties in the source

position of ±1 mm,[27,28] this shouldn't affect the plans any more than other commercially available applicators.

Although the tungsten shields in these applicators have a considerably larger diameter than the ICMA's tungsten rod (i.e., 16-mm vs. 8-mm), the total applicator size is the same at 20-mm diameter. This means that these applicators should be comparable to the ICMA for both ease of placement and patient comfort. Moreover, this would mean that minimal additional training would be required for learning how to use these applicators. However, the shielding, which make the applicator designs so advantageous, does create one major hindrance, which is the need for new dose calculation software. Currently, almost all clinically used dose planning software assume TG-43 dose distributions in water. Under these circumstances, it would be impossible to implement any shielded applicator. However, due to the rotational and nearly translational symmetry of the designs, it is a straightforward task to calculate and optimize dose once given the channel locations. Also, a new technique which may be applicable to these shielded applicators, called tufts, has been developed recently for complex MC-based brachytherapy dose distributions using conventional TPS.[29,30] Furthermore, there has been more and more work done on programs capable of accounting for inhomogeneity in the surrounding materials, such as with the grid-based Boltzmann solvers.[31,32] In 2012, the Task Group 186 report strongly recommended using these sorts of programs for calculating brachytherapy doses and specifically mentioned the need to be able to account for shielded applicators.[33] Therefore, although it is not currently the case, wide spread use of these sorts of programs should be seen in the coming years.

A greater use of inhomogeneity calculations could also allow for an improvement upon the designs presented here. For a non-circumferential tumor requiring only a subset of the available channels, one potential option would be to block off the remaining channels with additional tungsten inserts. This would limit the spill to healthy tissues at practically no cost to the CTV coverage. This would be especially useful when using the shields with more numerous or deeper channels.

3.5 Conclusion

Intensity modulated brachytherapy is an evolving field, with many opportunities for advancement. The manipulation of the spatial dose distribution rather than just the geometrical positioning of dose is starting to be more widely considered and this investigation has explored a more extreme case of this concept than is currently used in clinic, with the source being physically placed into grooves within the shielding itself. In this work, the efficacy of such designs has been explored and determined to be very encouraging. With tumor volume becoming easier and more accurate to define, using 3D imaging technologies such as CT and MRI, a shift towards more "modulating" HDR brachytherapy applicators such as the ones put forth in this work are the next logical step in rectal cancer treatment.

3.6 Acknowledgements

The text of Chapter 3, in part or in full, is a reprint of the material as it appears in the following publication: Webster M.J., Devic S, Vuong T, Han D, Scanderbeg D, Choi D, Song B, Song WY . HDR Brachytherapy of Rectal Cancer Using a Novel Grooved-

Shielding Applicator Design. Med Phys 2013;40(9):091704-1-091704-10. The dissertation author was the primary researcher and author, and the co-authors listed in this publication directed and supervised the research which forms the basis for this chapter.

3.7 References

1. A. Bujold, T. Craig, D. Jaffray, L. A. Dawson, “Image-Guided Radiotherapy: Has It Influenced Patient Outcomes?,”Semin. Radiother. Oncol. 22, 50-61 (2011)

2. A. N. Viswanathan, and B. A. Erickson, "Three-Dimensional Imaging in Gynecologic Brachytherapy: A Survey of the American Brachytherapy Society,” Int. J. Radiat. Oncol. Biol. Phys. 76, 104-109 (2009).

3. B. D. Kavanagh , C. C. Pan, L. A. Dawson, S. K. Das, X. A. Li, R. K. Ten Haken, and M. Miften, “Radiation dose-volume effects in the stomach and small bowel,” Int. J. Radiat. Oncol. Biol. Phys. 7, S101–S107 (2010).

4. I. Yau, T. Vuong, A. Garant, T. Ducruet, P. Doran, S. Faria, S. Liberman, C. Richard, F. Letellier, P. Charlebois, R. Loungnarath, B. Stein, and S. Devic, “Risk of hypogonadism from scatter radiation during pelvic radiation in male patients with rectal cancer,” Int. J. Radiat. Oncol. Biol. Phys. 74, 1481-1486 (2009).

5. T. Vuong, C. Richard, T. Niazi, S. Liberman, F. Letellier, N. Morin, K. Hu, D. Anderson, and S. Devic, “High dose rate endorectal brachytherapy for patients with curable rectal cancer,” Sem. Col. Rect. Surg. 21, 115-119 (2010).

6. A. Sun Myint, T. Mukhopadhyay, V. S. Ramani, K. Perkins, A. J. Snee, F. Jelley, H. Wong, and C. D. Lee, “Can increasing the dose of radiation by HDR brachytherapy boost following pre operative chemoradiotherapy for advanced rectal cancer improve surgical outcomes?” Colorectal. Dis. 12, 30-36 (2010).

7. A. Sun Myint, C. D. Lee, A. J. Snee, K. Perkins, F. E. Jelley, and H. Wong, “High dose rate brachytherapy as a boost after preoperative chemoradiotherapy for more advanced rectal tumours – the Clatterbridge experience,” Clin. Oncol. 19, 711-719 (2007).

8. S. Devic, T. Vuong, B. Moftah, M. Evans, E. B. Podgorsak, E. Poon, and F. Verhaegen, “Image-guided high dose rate endorectal brachytherapy,” Med. Phys. 34, 4451-4458, (2007).

9. S. Devic, T Vuong, and B. Moftah, “Advantages of inflatable multichannel endorectal applicator in the neo-adjuvant treatment of patients with locally advanced rectal cancer with HDR brachytherapy,” J. Appl. Clin. Med. Phys. 6, 44-49 (2005).

10. E. Poon, B. Reniers, S. Devic, T. Vuong, and F. Verhaegen, “Dosimetric characterization of a novel intracavitary mold applicator for 192Ir high dose rate endorectal brachytherapy treatment,” Med. Phys. 33, 4515-4526 (2006).

11. E. Poon, J. F. Williamson, T. Vuong, and F. Verhaegen, “Patient-specific Monte Carlo dose calculations for high-dose rate endorectal brachytherapy with shielded intracavitary applicator,” Int. J Radiat. Oncol. Biol. Phys. 74, 1259-1266 (2008).

12. M. J. Webster, S. Devic, T. Vuong, D. Y. Han, J. C. Park, D. Scanderbeg, J. Lawson, B. Song, W. T. Watkins, T Pawlicki and W.Y. Song, “Dynamic modulated brachytherapy (DMBT) for rectal cancer.” Med. Phys. 40, 011718. (2013).

13. M. A. Ebert, “Possibilities for intensity-modulated brachytherapy: Technical limitations on the use of non-isotropic sources,” Phys. Med. Biol. 47, 2495-2509 (2002).

14. Varian Brachytherapy: Applicators and Accessories, Varian Medical Systems, (2011).

15. Applicator Guide 2008: Applicators and accessories for HDR and PDR brachytherapy, Nucletron, (2008).

16. G. M. Daskalov, E. Löffler, and J. F. Williamson, "Monte Carlo-aided dosimetry of a new high dose-rate brachytherapy source," Med. Phys. 25, 2200-2208 (1998).

17. S. Civjan, E. F. Huget, and L. B. DeSimon, “Potential applications of certain nickel-titanium (nitinol) alloys,” J. Dent. Res. 54, 89-96 (1977).

18. National Nuclear Data Center: http://www.nndc.bnl.gov/

19. Varian Brachytherapy: VariSource iX, iX(t) HDR Afterloaders, Varian Medical Systems, (2011).

20. T. Vuong, S. Devic, and E. Podgorsak, “Chapter 17: High-dose-rate preoperative endorectal brachytherapy for patients with rectal cancer,” Editors: B. G. Czito and C. G. Willett, Rectal Cancer: International Perspective on Multimodality Management (Current Clinical Oncology). Springer Science+Business Media, LLC (2010).

21. MCNP – A General Monte Carlo N-Particle Transport Code, Version 5: http://mcnp-green.lanl.gov/pdf_files/MCNP5_manual_VOL_I.pdf

22. J. Borg and D. W. O. Rogers, “Monte Carlo Calculations of Photon Spectra in Air from 192Ir Sources,” NRC Report PIRS-629r: http://www.irs.inms.nrc.ca/inms/irs/papers/PIRS629r/ pirs629r.html (1998).

23. V. Coen, E. Lartigau, C. Haie-MEder, P. Lambin, H. Marsiglia, E. Briot, and A. Gerbaulet, “The heterogeneity index (HI) : a new parameter to evaluate tumor local control and late morbidity in interstitial brachytherapy,” Radiother. Oncol. 39, 9-9 (1) (1996).

24. R. Nath, L. L. Anderson, G. Luxton, K. A. Weaver, J. F. Williamson, and A. S. Meigooni, “Dosimetry of interstitial brachytherapy sources: Recommendations of the AAPM Radiation Therapy Committee Task Group No. 43,” Med. Phys. 22, 209-234 (1995).

25. M. J. Rivard, B. M. Coursey, L. A. DeWard, W. F. Hanson, M. S. Huq, G. S. Ibbott, M. G. Mitch, R. Nath, and J. F. Williamson, “Update of AAPM task group No. 43 report. A revised AAPM protocol for brachytherapy dose calculations,” Med. Phys. 31, 633-674 (2004).

26. A.A. Martinez, G. Gustafson, J. Gonzalez, E. Armour, C. Mitchell, G. Edmundson, W. Spencer, J. Stromberg, R. Huang, and F. Vicini, “Dose escalation using conformal high-dose-rate brachytherapy improves outcome in unfavorable prostate cancer,” Int. J. Radiat. Oncol. Biol. Phys. 53, 316–327 (2002).

27. G. Kertzscher, C. E. Andersen, F. A. Siebert, and S. K. Nielsen, “Identifying afterloading PDR and HDR brachytherapy errors using real-time fiber-coupled AL2O3 dosimetry and a novel statistical error decision criterion,” Radiother. Oncol. 100, 456-462 (2011).

28. B. Plamer, N. Davis, and L. DeWerd, “Kinematics of Varian Varisource high dose rate afterloading system when subjected to obstruction,” University of Wisconsin Medical Radiation Research Center Report.

29. M. J. Rivard, C. S. Melhus, D. Granero, J. Perez-Calatayud, and F. Ballester, "An approach to using conventional brachytherapy software for clinical treatment planning of complex, Monte Carlo-based brachytherapy dose distributions," Med. Phys. 36, 1968-1975 2009.

30. Yun Yang, Christopher S. Melhus, Shirin Sioshansi, and Mark J. Rivard, "Treatment planning of a skin-sparing conical breast brachytherapy applicator using conventional brachytherapy software," Med. Phys. 38, 1519-1525 2011.

31. K. A. Gifford, J. L. Horton, Jr., T. A. Wareing, G. Failla, and F. Mourtada,“Comparison of a finite-element multigroup discrete-ordinates code with Monte Carlo for radiotherapy calculations,” Phys. Med. Biol. 51, 2253–2265 (2006).

32. O. N. Vassiliev, T. A.Wareing, J. McGhee, G. Failla, M. R. Salehpour, and F. Mourtada, "Validation of a new grid-based Boltzmann equation solver for dose calculation in radiotherapy with photon beams," Phys.Med. Biol. 55, 581–598 (2010).

33. L. Beaulieu, A. Carlsson Tedgren, J. F. Carrier, S. D. Davis, F. Mourtada, M. J. Rivard, R. M. Thomson, F. Verhaegen, T. A. Wareing, and J. F. Williamson, "Report of the Task Group 186 on model-based dose calculation methods in brachytherapy beyond the TG-43 formalism: Current status and recommendations for clinical implementation," Med. Phys. 39, 6208–6236 (2012).

Chapter 4 Analysis of Potential Applicators for intensity Modulated Brachytherapy for Accelerated Partial Breast Irradiation

4.1 Introduction

During the last decade, accelerated partial breast irradiation has rapidly gained acceptance as a major treatment modality for clinical practice on a wide scale. It has slowly replaced traditional postoperative radiotherapy which consists of external-beam, whole-breast irradiation (WBI) delivered daily for 5-6 weeks. Recently, evidence has suggested that the main benefit of this technique is to reduce recurrence risk within the tissue surrounding the surgical cavity.[1,2] Therefore, evidence suggests, that for properly selected patients, WBI is unnecessary and APBI is acceptable.[3-12] Many techniques have been used for the implementation of APBI, including external beam teletherapy, multi-catheter interstitial implantation, single-channel MammoSite, and multi-catheter intracavitary brachytherapy.[13-30] External beam teletherapy is limited by its requirement to have dose traverse much of the patient, including delivering high dose to skin. Interstitial implantation allows for much better dose conformality. However, this technique requires highly trained physicians with specialized technical skills. MammoSite intracavitary brachytherapy has been widely implemented, and is technically easy to perform, but provides little opportunity for dose sculpting. The spherically symmetric distribution from the source is a major disadvantage. Recently, several devices have been developed to merge the versatile dose conformality of interstitial treatments

with the convenience and ease of single-entry devices. These are multi-catheter intracavitary applicators and include Contura and the Strut-Adjusted Volume Implant (SAVI). To date, these devices have shown much promise for APBI treatment.[31-33]

While these newer treatment modalities have been fairly successful and been widely accepted for APBI treatment in clinic, the benefits versus WBI have remained controversial.[34,35] While the reports which exposed the potential drawbacks of intracavitary APBI applicators failed to distinguish between the types of applicators studied and did not account for proper patient selection, they do raise a realistic concern about the efficacy of SAVI and similar applicators. Despite the quality of multi-catheter designs, there is still a non-negligible amount of dose received by healthy tissues, especially the skin, ribs, lungs, and heart. This has been shown to be especially important for dose to the heart. The risk of a major coronary event increases linearly with the mean dose to the heart by 7.4% per gray with no threshold.[36] In addition, 5-year follow up studies have reported 13.4% local tumor recurrence as well as 9.4% of patients with fair/poor cosmetic outcomes.[37] In addition, 23% of patients have reported skin late toxicity and 45% reported subcutaneous late toxicity.[38]

All of these factors lead to the need for an applicator with better dose-sculpting capabilities. In order to achieve this, this study explores the abilities of two classes of new potential applicators. The first set of applicators was designed as an extension of SAVI's multi-catheter system. Currently, there are three SAVI designs available for different lumpectomy sizes. These include a central catheter plus 6, 8, or 10 peripheral channels which form an eggbeater like shape (6+1, 8+1, and 10+1 catheters,

respectively). There are two possible ways to expand upon this setup. The first is to simply add more channels along the periphery for more dwell positions which can be used for treatment planning. Within the current SAVI designs, the more channels the applicator has, the larger the applicator is and therefore the larger the cavity it is intended for. That is, the 6-strut design is only intended for smaller cavities and the 8-strut design is only intended for larger cavities. However, smaller tumor volumes may benefit from more struts since smaller cavities often present more difficult treatment geometries. For all cavity sizes, the addition of more peripheral catheters may prove very useful. The logical extreme of this is to reduce the number of peripheral channels to unity and allow that channel to rotate, thus effectively creating infinite dwell positions. The second way to potentially improve the abilities of a multi catheter system would be to add additional catheter layers. Currently SAVI has a central channel and multiple channels on the boundary of the lumpectomy volume. Conversely, Contura has a central channel and 4 additional channels located slightly off center, but still several centimeters from the lumpectomy edge. Neither device explores the possibility of catheters placed at varying depths from the lumpectomy edge. Therefore, several designs with multi-depth catheters will be explored for their potential use in future APBI treatment.

The addition of more catheters will undoubtedly add to the degrees of freedom in the dose-modulation abilities of intracavitary APBI applicators, allowing for greater control in dose delivery. However, regardless of the number and position of the catheters used, there is still an inherent limitation of this type of design which comes from the isotropic nature of the source at each dwell position. Having numerous catheters only aids

in the treatment planning by allowing for the geometric modulation of the dwell positions. It is therefore necessary to explore new applicator designs capable of intensity modulated brachytherapy (IMBT). In the last few years, there have been a number of intracavitary high-dose-rate (HDR) applicators proposed for different cancer sites, including colorectal and cervical, which utilize shielding to modulate the dose profile.[39-41] These applicators have shown very promising results for potentially being the next generation of HDR brachytherapy devices. They are all based on the idea of having a directional beam profile at each dwell position which can be aimed as needed. This allows for a level of dose modulation completely unachievable with isotropic open source systems. To assess the applicability of IMBT to APBI treatments a set of shielded applicators have been designed and simulated.

4.2 Materials and Methods

A. Isotropic dwell position modulation

A.1 Applicator design

A series of applicators, extending the concept of the SAVI design, were developed. These applicators were created to examine the potential benefits of adding more isotropic dwell positions within the PTV cavity. For these new designs, there are effectively two main degrees of freedom; the depth of each strut and the quantity of struts at each depth. The first set of applicators considered retained the basic SAVI design, but added more struts around the edge of the PTV. Specifically, designs with a central channel plus 3, 4, 6, 8, 10, 12, 15, 20, 25, 30, 36, 72, and 360 channels were considered. Designs with fewer channels than the current SAVI devices were used to determine the

relative efficiency of the current designs and to ensure that fewer channels would not be just as useful.

From a practical standpoint, designs with more than approximately ten channels may prove very difficult to manufacture and use in clinic. Therefore, to gain the same effect as adding additional peripheral channels to the system, it would be more practical to have a single strut that can be rotated within the cavity. This forces an unavoidable deviation from the SAVI design. Since SAVI uses the struts themselves to expand the cavity, invagination of tissue between the struts can occur. The tissue penetrating between the struts would make a rotating design very difficult to implement and likely very uncomfortable for the patient. Instead, a balloon, such as the type used for the MammoSite applicator is considered as the means of expanding the cavity and allowing the strut(s) to move freely. In addition, accurately modeling the geometry of tissue invagination is very difficult for an arbitrary number of struts. Therefore, for all the designs mentioned above, ellipsoidal cavities, similar to one that an inflated balloon would create, were used in dose planning, as described later in this section.

Using a balloon for the cavity expansion allows for the struts to move freely without affecting the patient geometry. Likewise, replacing all the struts at a given depth with a single rotating strut allows for the added benefit of being able to easily add other struts at different depths. The effect of both these ideas is that additional dwell positions may be added at depths other than the center and the periphery of the cavity. This possibility was explored by adding a second depth of dwell positions to the standard 8+1 catheter design. Three methods of doing this, shown in Figure 4-1, were considered. The

first is derived from the simple expansion of a single catheter stopping at an intermediate depth. That is, it still spans the length of the cavity and at all points the ratio of the depth of the peripheral channel away from the central channel to the depth of this second channel from the central channel is constant. For this study, the ratios of depths used were 0.75, 0.5 and 0.25. The remaining designs require the presence of a second strut, dedicated to shallower dwell positions. The first of these looked at having an additional strut that keeps the distance from the geometric center of the cavity at a constant. That is, it is a scaled version of the larger strut. This allows for a greater number of dwell positions at a given distance from the edge of the cavity. The final design is a hybrid of the other two. It is based on the idea of having a second strut with an endpoint preceding the outer struts. This may be more practical than the previous design because it would share the same initial point of curvature as the outer catheter, but still allows for more centralized dwell positions. For this design, endpoints at half and three-fourths the depth of the cavity were considered.

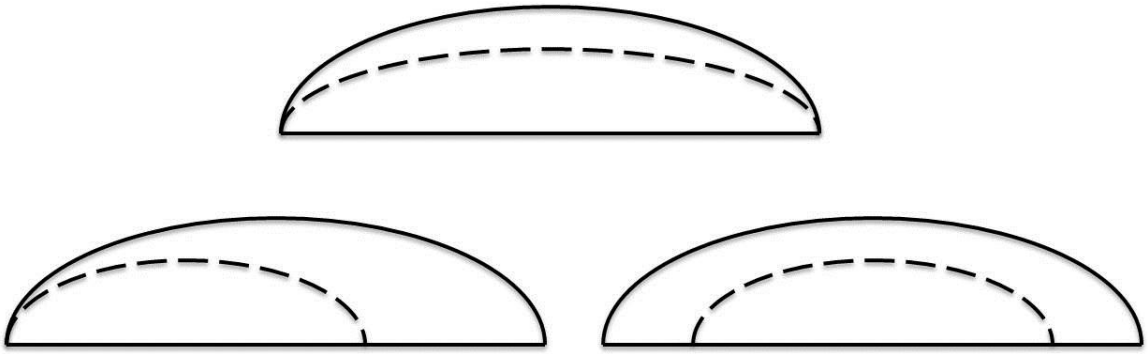

Figure 4-1. Proposed methods of adding an addition catheter depth to a SAVI-like design. The additional strut can expand in the same way (top) have a different end point (bottom left) or be centered (bottom, right) relative to the peripheral catheter

To test the absolute limit of geometric modulation for intracavitary ABPI brachytherapy, a multi-depth fully rotational system was simulated. This designed mimicked a single rotating catheter which could be set at any depth. In the simulations, 10 depths were used with 360 points of rotation at each depth.

A.2 Phantom geometries

To test the new isotropic dwell position applicators, simulated, idealized, phantom geometries were used. As previously mentioned, changing the number of struts significantly changes the geometry of the system and so a balloon is necessary for accurately comparing these types of applicators. As a result, available patient geometries from SAVI treated cases could not be used for these simulations. Instead, idealized geometries were used. An example can be seen in Figure 4-2. For these, the PTV was treated as an ellipsoidal shell, 1 cm thick at all points, unless otherwise specified. A 10 mm diameter cylinder was removed from one end to simulate the entrance point of the applicators.

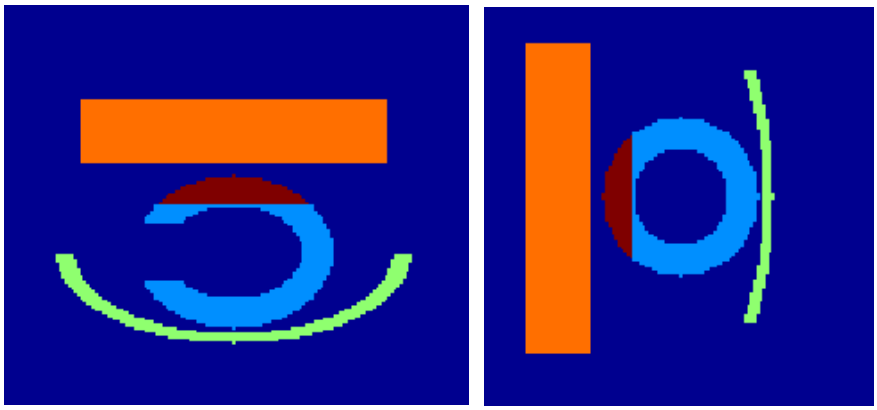

Figure 4-2. Example of phantom geometries used showing the PTV(light blue), high risk chest wall (red), lungs (orange), and skin (green).

To account for the variety in tumor size seen in clinic, the semi-minor and semi-major axes of the ellipsoid were varied for a total of 9 tumor sizes. The semi-major axis was defined as the radius of the cavity (i.e., the inner edge of the PTV) in the direction parallel to the central catheter. The semi-minor axis refers to the radius of the cavity perpendicular to the direction of the applicator. The semi-minor access ranged from 10 to 20 mm in increments of 5 mm and the semi-major axis was set to 1, 1.25, or 1.5 times the length of the semi-minor axis. Therefore, the maximum semi-major axis considered was 30 mm. Within each tumor size, 10 shapes were considered to simulate difficult patient geometries, such as the chest wall impinging on the PTV and causing a deviation from the uniform 1 cm rind. Using a Cartesian coordinate system, where the z-direction is along the semi-major axis, tissue was excluded if it exceeded a certain distance off the z-axis in the x-direction. See Figure 4-2 for an example. This distance was set equal to the semi-minor axis length plus 0, 2, 4, 6, 8 or 10 mm. The last of these cases does not remove anything from the 10 mm rind and is a perfect elliptical shell. The high-risk (HR) chest wall was defined as the area of the PTV removed by the shaping criteria. This means that for the last case, there is no HR chest wall.

The HR lung tissue was set as a cuboid starting 3 mm from the outer edge of the HR chest wall and PTV system, extending 20 mm in the x-direction. In the y- and z-directions the length was set to 10 cm. The y- and z-coordinates of the center of the HR lung tissue was set to match the center of the PTV. That is, it was symmetric with relation to the PTV. Finally, the HR skin was simulated as a portion of an ellipsoidal shell, 3 mm thick. The center of the inner edge was set to be 1 mm from the outer edge of the PTV in

the negative x-direction such that it was positioned exactly opposite from the HR lung tissue and chest wall. It was given a semi-major axis of 10 cm and a semi-minor axis which was 1 mm greater than the semi-major axis of the PTV.

B. Intensity modulated applicators

B.1 Shield designs

Two classes of IMBT applicators were developed to test the capabilities of shielded applicators for use in APBI. The first of these effectively adds a shielding component to the existing SAVI design. This was done by replacing the isotropic dose distributions of each dwell position with an anisotropic, shielded, dose distribution. To determine the optimal shield design, 6 shield designs were considered. All the shields simulated were 1 cm long cylinders and made of high-density tungsten (18.5 g/cm^3). Three sizes of shields were simulated. These were given 1, 2, and 3 mm radii. Anything larger than that would most likely be too large to enter the cavity and move along the struts. For each of these sizes, a design was simulated with an ^{192}Ir source located at the center of the shield with opening in the tungsten on one side to create the anisotropic dose distributions. The openings ran the length of the shield and were 2 mm thick, extending from the source to the edge of the shield. For the larger radii shields, other locations for the source were considered. For the 2 mm diameter shield, an additional design with the source located 1 mm off-center in the radial direction, putting it halfway between the center of the shield and the edge. For the 3 mm diameter shield, two more designs were simulated, one with the source 1 mm from the center and one with the source 2 mm from the center. These three additional, off-centered, designs were created to minimize the

amount of dose spilling to the contralateral side of the shields. However, this comes at the cost of reducing the shielding to the sides of the shield.

An additional highly unrealistic shield design was also simulated. This design was created by taking an open source distribution and reducing the magnitude of dose by 90% to all areas that did not fall inside an 18 degree conical window while keeping the dose within that cone unchanged.

The second class of shielded applicators investigated in this study departs entirely from the designs of the current APBI brachytherapy applicators. These designs were long-cylindrical shields, made of tungsten alloy, that are to be placed in the center of the cavity. Each cylinder was made to be 1 cm in diameter to match the typical size of the surgical opening left after a lumpectomy. There were seven designs of the type considered in this investigation. The first three designs each had eight equally spaced channels running along the length of the shield. The next set of three matched this design with the addition of a central channel running through the center of the shield. This central channel was implemented to allow for greater dose control to the PTV at the distal end of the cavity, where dose modulation is the most difficult. The benefit of being able to add an extra dwell position capable to delivering dose to this region comes at the cost of losing some shielding throughout the rest of the shield. To further improve the dose to this region, the 9-channel designs had a conical section, 1 cm in depth, removed from the shield at this end. This allows for more dosage to reach the far end of the PTV while reducing the likelihood of overdosing the nearby tissues. For both the 8-channel and 9-channel sets three sub-designs were created. Similar to the SAVI-like shielded designs,

the sub-designs were created to test the tradeoffs of putting the source deeper into the shield, thus trading shielding for collimation. To do this, in each case, outer channels placed at depths of 1, 2, and 3 mm were considered. An additional shielded design with 8 channels was also considered. Design had 8 channels, each 1 mm from the shield edge, but instead of being a cylinder, it had a 1 cm long ellipsoidal cap to it, allowing the channels to converge at the end of the shield. A schematic of this design, referred to as the ‘bullet applicator’ can is shown in Figure 4-3.

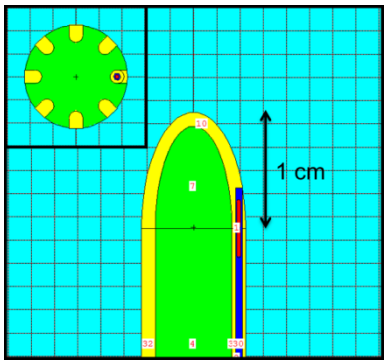

Figure 4-3. A schematic of the cross-section of the 'bullet' applicator.

B.2 Patient Dataset

To test these shielded applicators, patient data from UCSD was used. The geometries from 36 patients, previously treated using the SAVI device at UCSD, were optimized upon. While the use of a balloon for cavitation makes the most sense for the cylindrical, and perhaps the SAVI-like, shields the desire to test the systems on real patient data outweighed this issue. Therefore, plans optimized using the new shielded applicators could be directly compared to the treatment plans delivered using SAVI. For each patient, the plan used for comparison was that of the first fraction within a 3 fraction

plan. Each fraction was delivered with a 3.4 Gy prescription. All plans included dose calculations to the PTV, chest wall, skin, and lungs.

B.3 Reduced cavity size

Using a centrally located shielded applicator has a disadvantage compared to a strutted applicator since the dwell positions are located far from the PTV edge. This results in the shielded applicators being unable to take advantage of the high dose gradient near the source in limiting the dose further away. While this reduces hotspots, it also increases dose to healthy tissues. Therefore, treating while not expanding the cavity may prove beneficial. This is especially important since the purpose of expanding the cavity for isotropic source applicators is partly to allow for dose fall off across the cavity. However, a shielded applicator would have far less need for this and could do without the balloon or struts. To explore this possibility, two phantom geometries were simulated. The first mimics the geometries from the previous sections for the isotropic source designs with a 1.5 cm semi major axis and 2 cm semi-major axis. The second geometry resembles the first, but replaces the ellipsoidal PTV with a cylindrical one with hemispherical caps, while keeping the distances between the PTV and the remaining structures constant. See Figure 4-4.

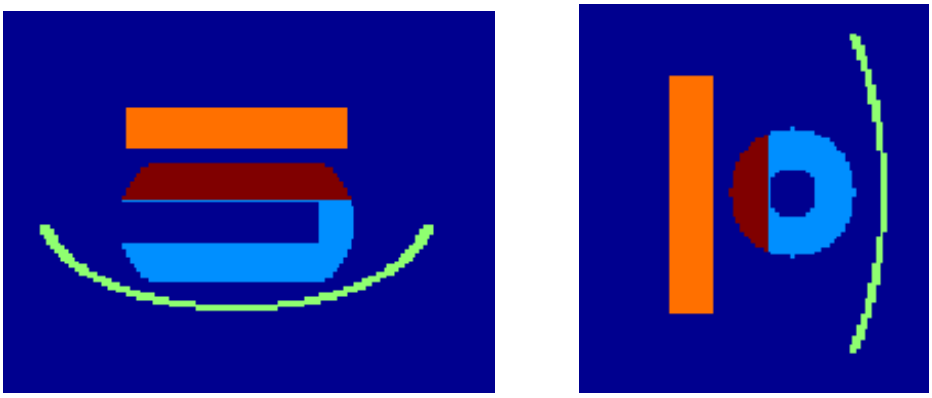

Figure 4-4. Ideal phantom geometries with no cavity expansion used.

C. MCNP5 dose calculations

Every applicator mentioned thus far was simulated using an MCNP Monte Carlo code, version 2.6.0,[42] All components of the devices which would be present during treatment were created using the set of built-in macro-bodies. For each simulation, the specifics of the dose calculations and voxel geometry are the same as from the previous DMBT work.[39] For each decay event simulated, on average 2.363 gamma emissions were generated.[43] Bremsstrahlung X-rays, electron-induced X-rays, knock-on electrons and secondary electrons were used for photon interactions. Other interactions used were incoherent scattering, coherent scattering (Rayleigh scattering), fluorescence emission, Compton scattering, capture, and pair production. In order to achieve better simulation efficiency, a lower energy cutoff of 10 keV for electron transport simulations was enforced. All space outside of the applicator was treated as water. All simulations were run through the San Diego Supercomputer Center, using 512 CPU cores, each simulating 100,000 particles. Due to the rotational symmetry of the applicators, it was only necessary to simulate one dwell position for each design.

D. Plan comparison Indices

To assess the plan qualities of each design, dose to the PTV, chest wall, skin and lungs were considered. For the PTV, the maximum dose, V90, V100, V150, and V200 were calculated. Vχ represents the volume, in cm^3, of the PTV receiving at least χ percent of the prescription dose. Finally, the dose heterogeneity index (DHI) was calculated. The DHI is defined by the following formula:

$$DHI = \frac{V100 - V150}{V100}. \quad (4.1)$$

For each of the healthy tissues, the maximum dose, $V_{Gy}0.5$, $V_{Gy}1$, $V_{Gy}1.5$, and $V_{Gy}2$, were calculated. Here, $V_{Gy}\chi$ refers to the total volume, in cm^3, receiving χ Gy. Statistically significant differences between plans across all patient data were determined using the two-tailed pair t-test.

E. Dose optimization

All plans calculated were done so using an in-house coded gradient projection convex optimization algorithm. A quadratic objective function was used to minimize the dose to the OARs while keeping the CTV dose as uniform as possible. Except for a non-negativity condition on the dwell times, no dose constraints were imposed. A rigorous explanation of the optimization process used is presented in the DMBT work.[39] For all applicators a lateral dwell position resolution of 5-mm was used. All plans were set to have a 3.4 Gy prescription.

4.3 Results

A. Additional peripheral channels

For all tumor sizes and shapes simulated, the effective maximum dosimetric quality plateaued for systems with 8 or more peripheral channels. Furthermore, after about the 4th peripheral channel was added, even in the most extreme cases, there was little benefit seen from adding more outer channels. The DVH for the PTV and HR chest wall can be seen in Figure 4-5. As can be clearly seen, there is virtually no difference in dose coverage between optimizing on 8 and 18 channels. Not shown are the DVH curves for the HR lung tissue and skin. These were omitted because effectively no difference was seen in the dose distribution to them for any of the channel quantities used. Also, the systems with even more channels are not shown in this figure, but yield nearly identical results, even when 360 rotational dwell positions were used. This result comes from the fact that in all cases, the central channel was used for a baseline dose to the PTV and then, in optimization, the outer channels were used to refine the dose distribution. However, it appears that the dose sculpting is not sensitive enough to the precise location of the outer channels to see a major change in the plan quality. In all cases, the outer channels away from the chest wall were used the most and ones close to the chest wall were effectively unused. Therefore, channels approximately every 45 degrees yielded the same ability to modify the dose distribution as channels more closely spaced since the major dose optimizing ability came mostly from gross channel location away from the chest wall.

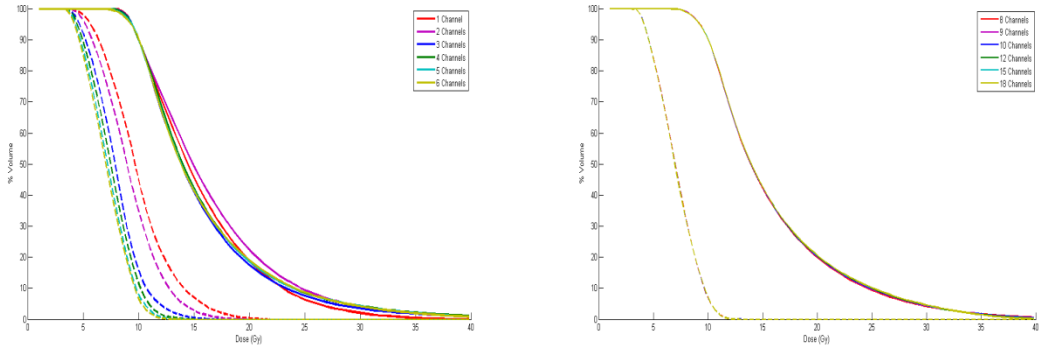

Figure 4-5. DVHs for ideal geometries of the PTV (solid line) and high risk chest wall (dashed line) for SAVI like applicators. The designs had a central catheter with 1 (red), 2 (magenta), 3 (blue), 4 (green), 5 (teal), and 6 (yellow) peripheral catheters (left) and with 8 (red), 9 (magenta), 10 (blue), 12 (green), 15 (teal), and 18 (yellow) peripheral catheters (right)

B. Additional channel depths

Allowing more depths of channels between the central catheter and the edge of the PTV resulted in only negligible improvements in the simulated plan qualities. Regardless of which of the three designs was used, the result was to create a marginal improvement in the PTV coverage with no significant change in the healthy tissues. In each case, the V150 saw a drop of no more than 2% and the V200 dropped by no more than 5% for any of the geometries simulated. Again, the largest benefits were seen for the smaller, more asymmetrical geometries used. Analysis of the dwell times at each dwell position showed little usage of the intermediate channels in the dose optimization. The designs with the channels closer to the center showed the best results, but still lacked any significant improvements.

In the extreme case where ten channel depths were used for 360 rotational steps per depth, there was still minimal improvement. Compared to the applicators with only

peripheral channels, this extreme situation preformed nearly identically to the applicators with just a high number of rotational points.

C. Shielded strut applicators

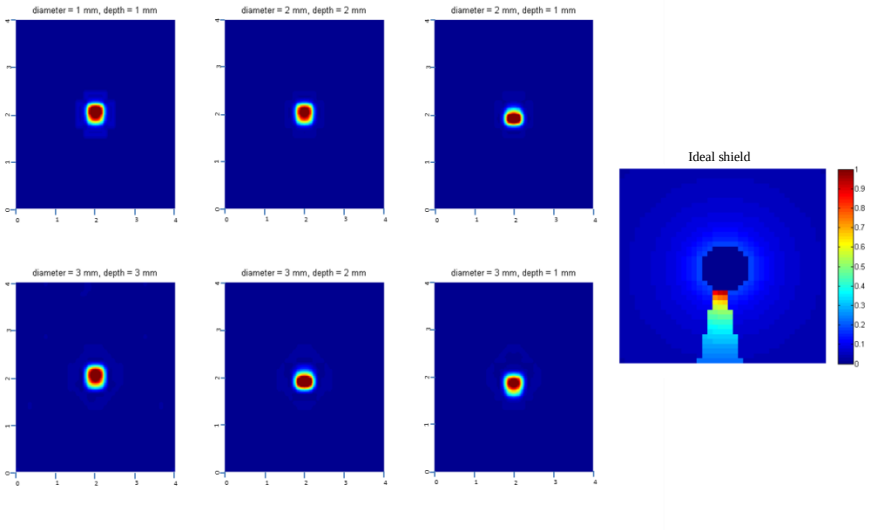

Figure 4-6. Resulting relative dose distributions for the strut-based shield designs. Distances are in centimeters.

The resulting dose distributions from the shielded strut-based applicators can be seen in Figure 4-6. The anisotropy of the smaller shields is minimal and the directionality from these shields is not extreme. However, it still allows for greater potential dose modulation than purely isotropic sources. The shielded applicators placed in the same dwell positions as the SAVI applicator had mixed results. These applicators were able to reduce the maximum dose to the PTV and reduce dose to the HR chest wall. However, all other plan parameters increased. For all cases, the maximum dose to the PTV decreased by approximately 50% and the chest wall saw decreases of 20-50% for all dose levels measured. In contrast, the V150 and V200 values both increased dramatically as did the

doses to the HR lung tissue and skin, the HR skin being the worst. In addition, for the low dose values, $V_{Gy}0.5$ and $V_{Gy}1$ for the lungs and $V_{Gy}0.5$ for the skin, the shielded applicators did slightly better than SAVI. However, as the minimum dose criteria increases, the results switched to highly favor SAVI. The values of selected parameters can be seen in Table 4-1. Between the different applicators, the ones with the least shielded did the best. The 1 mm diameter shield was among the best in all metrics for the simulated shields. Conversely, the 3 mm diameter shields consistently did the worst, regardless of the depth of the source within the shield. The most dramatic effect was with the dose to the skin, which increased approximately 20% with for each additional cm of shielding.

Table 4-1. Dosimetric plan indices for shielded peripheral strut-based applicators. The ideal shield had an 18 degree canonical opening with 10% spill elsewhere. The SAVI design had no shielding.

Shield Description		Plan Indices							
Diameter (mm)	Source Depth (mm)	D_{max}	CW_{max}	$Lung_{max}$	$Skin_{max}$	V90	V100	V150	V200
1	1	43.81	7.90	3.39	5.51	95.09	90.85	56.89	30.15
2	2	35.95	8.63	3.78	6.17	94.61	91.04	62.52	36.25
	1	40.73	8.28	3.74	7.05	94.45	91.18	65.01	39.96
3	3	51.49	10.25	5.34	8.65	94.49	91.57	68.23	44.44
	2	48.49	8.31	3.61	7.96	94.68	91.62	67.14	43.89
	1	49.74	8.84	3.86	8.55	94.26	91.60	70.39	49.53
Ideal shield		12.99	5.60	3.24	9.11	96.78	91.31	47.57	14.68
SAVI		90.29	11.89	2.74	3.30	97.06	91.37	45.80	22.90

With regards to the source depth within the shield, results varied greatly. For the 2 mm diameter shield, the design with the centered source had better PTV coverage and HR skin sparing, but did worse for sparing the lungs and chest wall when compared to the design with the off-center source. For the 3 cm diameter design, the best results all came for the shield with the source 1 mm off-center. This was true for both PTV coverage and normal tissue sparing, although

the differences for many of the metrics were negligible. Of the remaining two designs, the results were the opposite as with the 2 mm diameter shields in that the shield with the centrally located source did better normal tissue sparing, but worse for PTV coverage.

The final, idealized, system with the conical dose distribution was able to achieve significantly better results than any of the other realistic applicators. Furthermore, it fully outperformed SAVI, with the exception of the skin dose.

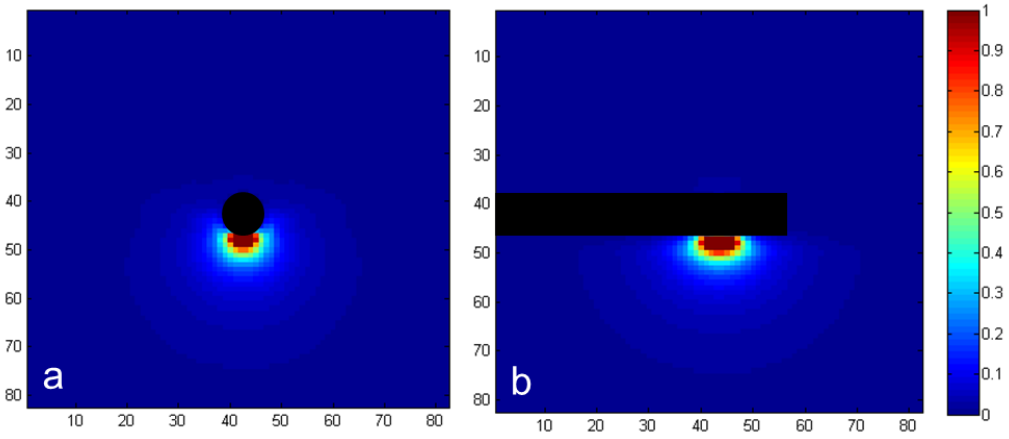

Figure 4-7. In-plane (a) and sagittal views of the dose distributions formed by the 8-channel, 3-mm deep shielded applicator

Table 4-2. Dosimetric plan indices for the large rod shaped applicators. The 'bullet' design had 8 channels coming to a point with an ellipsoidal cap. The channels were 1 mm deep for this design. The SAVI design had no shielding.

Shield Description		Plan Indices						
Channels	Source Depth (mm)	D_{max}	CW_{max}	$Lung_{max}$	$Skin_{max}$	V90	V150	V200
8	1	18.74	5.25	2.66	3.94	95.58	49.06	22.27
	2	19.16	5.24	2.67	3.90	95.52	48.82	21.75
	3	18.58	5.64	2.84	4.16	96.28	46.32	19.80
9	1	17.29	5.05	2.62	3.84	96.05	46.83	20.48
	2	17.00	4.99	2.55	3.72	96.04	46.89	20.43
	3	18.18	5.08	2.67	3.78	96.06	45.66	18.88
	Bullet	15.84	4.96	2.57	3.84	96.22	46.58	20.18
	SAVI	90.29	11.89	2.74	3.30	97.06	45.82	22.93

D. Large shielded applicators

The larger cylindrical applicators gave the best results of all the designs tested. The resulting dosimetric data can be found in Table 4-2. A typical dose distribution for one of the dwell positions of the cylindrical applicators can be seen in Figure 4-7. In all cases, the maximum dose to the PTV was significantly reduced by approximately 80% compared to SAVI, 90Gy versus ~18Gy. V150 and V200 were not statistically significantly affected. Meanwhile the dose to the chest wall was reduced by 40-60% for all dosimetric parameters compared to SAVI. In addition, the maximum dose to the lungs was within 10% of the dose from SAVI, with some shield designs doing slightly better and others doing slightly worse, but not the difference was not statistically significant for any of these. Therefore, the dose to the lung can be considered comparable. However, the dose to the skin was increased by 15-25% and was statistically significantly different. It is worth noting however, that the $V_{Gy}0.5$ of the skin was reduced using the shielded applicators. This indicates that less of the skin received significant amounts of radiation, but the areas that which did receive radiation, got larger amounts.

Of the purely cylindrical applicators, the 9-channel designs outperformed or matched the 8-channel designs in all dosimetric criteria. For practically all the comparison criteria, the 9-channel system did 5-10% better than their 8-channel counterparts. In addition, for both the 8-channel and 9-channel systems, the best results were seen for the shields where the outer channels had a depth of 2 mm. Most of the comparison criteria were approximately 5% better using these designs. The only noteworthy exception is that the maximum dose to the PTV was greatest for the 8-

channel system with the 2 mm deep channel. Of the remaining two depths, the shallower channels produced consistently better results by approximately 3% compared to the deeper channels. Overall, the best of these simple applicators was the 9-channel, 2 mm deep system.

The final design simulated with the ellipsoidal-cap "bullet" shaped applicator. This applicator produced the lowest maximum dose to the PTV at only 15.8 Gy on average. In addition, the dose to the chest wall was the second lowest of all the applicators, being beaten by only the 9-channel, 2 mm deep system. However, with regards to skin dose, the bullet design gave results similar to all the purely cylindrically shaped shielded applicators.

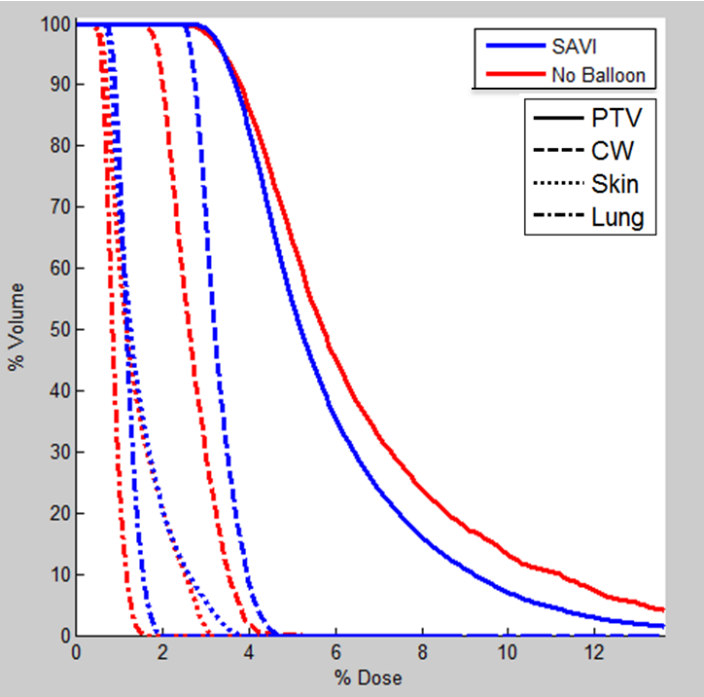

Figure 4-8. A DVH comparing SAVI (blue) in a typical filled cavity against a bullet design shielded applicator with no cavity expansion (red).

E. Unexpanded cavity

Removal of the balloon to not expand the cavity resulted in significantly reduced dose to all the healthy tissues in the system for the ideal geometry. The DVH comparing the SAVI applicator to the "bullet" design with no cavity expansion is shown in Figure 4-8. As can be clearly seen, the dose to the chest wall and lungs dropped significantly while the high-dose region to the skin also was greatly reduced. The maximum dose delivered to the HR chest wall was 3% lower than SAVI and the dose to the maximum dose to the skin and lungs each were 18% lower than the SAVI doses. Furthermore, the approximately 20% decrease in dose to these regions was fairly consistent for all dose levels down to the minimum dose received by the phantom structures. Conversely, the dose to the PTV was significantly increased when the balloon was removed. The V150 was 20% higher than for SAVI while the V200 was 35% higher.

4.4 Discussion

A. Capabilities of isotropic dwell positions

Several possibilities for increased dose modulation, through the addition of more dwell positions, from isotropic sources have been explored. It has become clear through the simulations of these applicators that the use of geometric source modulation has reached its maximum effective potential. In the simulations conducted, neither adding more channel depths nor more channels at a given depth, most importantly, on the periphery of the system, allowed for significant improvements to the dose distributions to the critical structures. This results largely from mainly rotationally symmetric nature of the PTV. As a result, much of the dose, for all cases, came from the central dwell

positions. Furthermore, the existing dose sculpting all came from the outermost dwell positions. For the geometries tested, the implementation of more catheter depths proved irrelevant.

The addition of more channels on the periphery of the cavity failed to add any notable dosimetric benefits after the 8th channel was added. This may have been a result of the geometries used. In the most extreme cases of modulating the PTV shape, the tissue removed from the volume spanned a 60 degree angle. This matches closely with the fact that once the peripheral channels were placed more closely than 60 degrees the dose sculpting was maximized. At this point, the applicator would have enough degrees of freedom to easily add dose fairly uniformly to the remainder of the PTV while avoiding this region. Therefore, it may be the case that more complex geometries would benefit more from the additional channels.

Similarly, the ineffectiveness of the other strut could be a consequence of the practically uniform depth of the PTV. That is, since the PTV extended 1 cm to almost all places, these middle-located catheters could contribute very little in comparison to the central catheter. A more gentle change in the PTV volume, one which skews the general shape of it, may be able to benefit from these added channels. However, geometries matching this description, as well as the one for the ones potentially benefitting from adding more peripheral channels, are very uncommon in clinical practice. Typically the asymmetry of the PTV is a consequence of the chest wall or skin impinging on the volume. These scenarios closely match the geometries used for this study.

B. Shielded strut-based designs

For clinically plans, treated with the SAVI applicator, replacing the isotropic sources with partially shielded anisotropic sources proved ineffectual. Furthermore, the results proved detrimental for several criteria. This result likely has two major factors contributing to it. The first of these is that the source-to-PTV edge distance is increased with the addition of the shield. For the isotropic sources in the SAVI applicator, located directly against the PTV edge, the ability to take advantage of the high gradient dose fall off of the source is maximized. As the source is placed further from the edge, especially at these small distances, the dose drop-off becomes less significant. This results in more dose extending past the PTV to the normal tissues. This suggests that additional shield designs, with the source located at the edge of the shield may prove useful. These could take the form of simply placing a shield contralaterally to the source, reducing back-spill. This would have the added benefit of being easier to manufacture and implement.

The second cause of the dosimetric degradation from the shielded strut-based applicators is the limited dwell positions. While isotropic dwell sources reach a maximum ability after about eight channels, this isn't the case for shielded applicators. By reducing the lateral spill of the shields, the ability to deliver dose to angles between the strut positions was compromised. This is especially true for the PTV tissue which penetrated between the catheters. Therefore, these same shield designs may perform better if given more dwell positions to optimize upon.

C. Strut-less shields

Of all the systems simulated, these showed the most promise. At 1-cm in diameter, these shields gave significantly more intensity modulation than the much small strut-based shields. This allowed for finer dose modulation, leading to encouraging results. This was especially true for the structures closest to the shields, the PTV and chest wall. The absence of similar results for the other structures is related to the source-to-structure distance. Without channels located at the periphery of the system, it is impossible to take advantage of the dose fall off near the source. As a result, the dose penetrates further into the skin and lungs. One simple way to work around this problem would be to add a SAVI-like component to the shielded applicators. That is, have struts, which could be partially shielded, with the ability to extend away from the shield as part of the system. This would complicate the system and possibly require the shield diameter to be reduced to allow for the addition of these struts.

Another way to increase the benefit of the high dose gradient near the source is to not expand the cavity, thus placing the applicator as close to possible to the PTV. The results of simulating such a system were very encouraging. The dose to the healthy tissues was significantly reduced, even beyond that of the SAVI applicator, while the PTV was given much high V150 and V200 values. However, these numbers are partially misleading. In the geometries considered, the PTV was reduced in overall size, but the 1-cm rind was kept constant. Therefore, overall volume of the PTV was considerably smaller when the cavity was not expanded. Therefore, a higher percentage of the volume receive a certain dose does not necessarily mean more total volume of the structure

received that given dose. However, it is still clear by looking at the maximum dose to the PTV from the two applicator designs that the PTV is still receiving a more intense hotspot. This likely comes from the high degree of collimation created by the shield. This results in the tissue of the PTV which is adjacent to the shield, but in between channels being very difficult to deliver dose to without causing much higher doses to be received by the adjacent tissues which are directly next to the opening.

There are two ways to work around this issue. The first would be to partially expand the cavity, to an intermediate level. This would allow for the PTV to receive a more homogenous dose while keeping the dose to the normal tissues relatively low. The other method to avoid these hotspots would be to increase the capabilities of the shield, either by adding more channels or reducing the number of channels, but then allowing the shield to rotate. The first option would compromise some of the dose anisotropy for each channel, but give more channels to work with. The second option would see a benefit of more shielding, but at the cost of making the system more complicated and harder to implement.

4.5 Conclusion

Based on these findings, it is clear that any device based on open radiation source modulation could not be improved much further. Therefore, it is necessary to consider shielded designs to create better treatment plans. The basic designs considered thus far using tungsten shielding have given some noteworthy results. While results are unfavorable for strut-based shielded applicators, there is still much potential for this type of applicators and refined designs should be tested before the idea is considered a dead-

end. However, tungsten rod applicators showed a great deal of promise to be the next generation in APBI brachytherapy technologies. It has been shown that basic designs are capable of reducing dose to the chest wall and improve PTV coverage. Adjusting these designs and the use of cavity expansion can provide even better results and merits much consideration for future work.

4.6 Acknowledgements

The text of Chapter 4, in part or in full, is being prepared for submission to the Journal of Medical Physics. The dissertation author was the primary researcher and author, and the co-authors listed in this publication directed and supervised the research which forms the basis for this chapter.

4.7 References

1. Fowble, B. Ipsilateral breast tumor recurrence following breast-conserving surgery for early stage invasive cancer. Acta. Onco. 1(Suppl 13):9 –17; 1999.

2. Fowble, Barbara, Lawrence J. Solin, Delray J. Schultz, James Rubenstein, and Robert L. Goodman. "Breast recurrence following conservative surgery and radiation: patterns of failure, prognosis, and pathologic findings from mastectomy specimens with implications for treatment." International Journal of Radiation Oncology* Biology* Physics 19, no. 4 (1990): 833-842.

3. Fisher, Bernard, Stewart Anderson, John Bryant, Richard G. Margolese, Melvin Deutsch, Edwin R. Fisher, Jong-Hyeon Jeong, and Norman Wolmark. "Twenty-year follow-up of a randomized trial comparing total mastectomy, lumpectomy, and lumpectomy plus irradiation for the treatment of invasive breast cancer."New England Journal of Medicine 347, no. 16 (2002): 1233-1241.

4. Veronesi, U., E. Marubini, L. Mariani, V. Galimberti, A. Luini, P. Veronesi, B. Salvadori, and R. Zucali. "Radiotherapy after breast-conserving surgery in small breast carcinoma: long-term results of a randomized trial." Annals of Oncology12, no. 7 (2001): 997-1003.

5. Clark, R. M., T. Whelan, M. Levine, R. Roberts, A. Willan, P. McCulloch, M. Lipa, R. H. Wilkinson, and L. J. Mahoney. "Randomized clinical trial of breast irradiation following lumpectomy and axillary dissection for node-negative breast cancer: an update." Journal of the National Cancer Institute 88, no. 22 (1996): 1659-1664.

6. Holli, Kaija, Rauni Saaristo, Jorma Isola, Heikki Joensuu, and Matti Hakama. "Lumpectomy with or without postoperative radiotherapy for breast cancer with favourable prognostic features: results of a randomized study." British journal of cancer 84, no. 2 (2001): 164.

7. Liljegren, Göran, Lars Holmberg, Jonas Bergh, Anders Lindgren, L. Tabar, Hans Nordgren, and Hans-Olov Adami. "10-Year results after sector resection with or without postoperative radiotherapy for stage I breast cancer: a randomized trial."Journal of Clinical Oncology 17, no. 8 (1999): 2326-2326.

8. Veronesi, Umberto, Natale Cascinelli, Luigi Mariani, Marco Greco, Roberto Saccozzi, Alberto Luini, Marisel Aguilar, and Ettore Marubini. "Twenty-year follow-up of a randomized study comparing breast-conserving surgery with radical mastectomy for early breast cancer." New England Journal of Medicine347, no. 16 (2002): 1227-1232.

9. Morrow M. Rational local therapy for breast cancer. N Engl J Med 2002;347:1270–1.

10. Smith, Tanya E., Daesung Lee, Bruce C. Turner, Darryl Carter, and Bruce G. Haffty. "True recurrence vs. new primary ipsilateral breast tumor relapse: an analysis of clinical and pathologic differences and their implications in natural history, prognoses, and therapeutic management." International Journal of Radiation Oncology* Biology* Physics 48, no. 5 (2000): 1281-1289.

11. Fisher, Edwin R., James Dignam, Elizabeth Tan-Chiu, Joseph Costantino, Bernard Fisher, Soonmyung Paik, and Norman Wolmark. "Pathologic findings from the National Surgical Adjuvant Breast Project (NSABP) eight-year update of Protocol B-17." Cancer 86, no. 3 (1999): 429-438.

12. Faverly, D. R., Lambert Burgers, Peter Bult, and Roland Holland. "Three dimensional imaging of mammary ductal carcinoma in situ: clinical implications." In Seminars in diagnostic pathology, vol. 11, no. 3, pp. 193-198. 1994.

13. Vicini, Frank, Kathy Baglan, Larry Kestin, Peter Chen, Gregory Edmundson, and Alvaro Martinez. "The emerging role of brachytherapy in the management of patients with breast cancer." In Seminars in radiation oncology, vol. 12, no. 1, pp. 31-39. WB Saunders, 2002.

14. Kuske Jr RR. Breast brachytherapy. Hematol Oncol Clin North Am 1999;13:543–58.

15. Vicini, Frank A., Kathy L. Baglan, Larry L. Kestin, Chris Mitchell, Peter Y. Chen, Robert C. Frazier, Greg Edmundson Neal S. Goldstein, Pamela Benitez, Raywin R. Huang and Alvaro martinez. "Accelerated treatment of breast cancer." Journal of clinical oncology 19, no. 7 (2001): 1993-2001.

16. Baglan, Kathy L., Alvaro A. Martinez, Robert C. Frazier, Vijay R. Kini, Larry L. Kestin, Peter Y. Chen, Greg Edmundson, Elizabeth Mele, David Jaffray, and Frank A. Vicini. "The use of high-dose-rate brachytherapy alone after lumpectomy in patients with early-stage breast cancer treated with breast-conserving therapy." International Journal of Radiation Oncology* Biology* Physics 50, no. 4 (2001): 1003-1011.

17. Kuske, R. R., Martin, E., Hanson, W., Arthur, D., Rabinovitch, R., White, J., Wilenzick, R. M., Harris, I., Tailor, R. and Davis, D. Quality assurance and reproducibility on RTOG 95-17: a Phase II trial of brachytherapy alone for select breast cancers. Personal communication. 2001.

18. Wazer, David E., Lisa Berle, Roger Graham, Maureen Chung, Janice Rothschild, Theresa Graves, Blake Cady, Kenneth Ulin, Robin Ruthazer, and Thomas A. DiPetrillo. "Preliminary results of a phase I/II study of HDR brachytherapy alone for T1/T2 breast cancer." International Journal of Radiation Oncology* Biology* Physics 53, no. 4 (2002): 889-897.

19. King, Tari A., John S. Bolton, Robert R. Kuske, George M. Fuhrman, Troy G. Scroggins Jr, and Xiao Zhang Jiang. "Long-term results of wide-field brachytherapy as the sole method of radiation therapy after segmental mastectomy for T< sub> is, 1, 2</sub> breast cancer." The American journal of surgery 180, no. 4 (2000): 299-304.

20. Keisch, Martin, Frank Vicini, Robert R. Kuske, Mary Hebert, Julia White, Coral Quiet, Doug Arthur, Troy Scroggins, and Oscar Streeter. "Initial clinical experience with the MammoSite breast brachytherapy applicator in women with early-stage breast cancer treated with breast-conserving therapy." International Journal of Radiation Oncology* Biology* Physics 55, no. 2 (2003): 289-293.

21. Jeruss, Jacqueline S., Frank A. Vicini, Peter D. Beitsch, Bruce G. Haffty, Coral A. Quiet, Victor J. Zannis, Angela J. Keleher, Delia M. Garcia, Howard C. Snider, Mark A. Gittleman, Eric Whitacre, Pat W. Whitworth, Richard E. Fine, Stacey Arrambide and Henry M. Kuerer. "Initial outcomes for patients treated on the American Society of Breast Surgeons MammoSite clinical trial for ductal carcinoma-in-situ of the breast." Annals of surgical oncology 13, no. 7 (2006): 967-976.

22. Niehoff, Peter, Csaba Polgár, Horst Ostertag, Tibor Major, Zoltán Sulyok, Bernhard Kimmig, and György Kovács. "Clinical experience with the MammoSite< sup>®</sup> radiation therapy system for brachytherapy of breast cancer: Results

from an international phase II trial." Radiotherapy and oncology 79, no. 3 (2006): 316-320.

23. Vicini, Frank, Peter D. Beitsch, Coral A. Quiet, Angela J. Keleher, Delia Garcia, Howard C. Snider, Mark A. Gittleman, Victor J. Zannis, Henry M. Kuerer, and Maureen Lyden. "Three-year analysis of treatment efficacy, cosmesis, and toxicity by the American Society of Breast Surgeons MammoSite Breast Brachytherapy Registry Trial in patients treated with accelerated partial breast irradiation (APBI)." Cancer 112, no. 4 (2008): 758-766.

24. Baglan, Kathy L., Michael B. Sharpe, David Jaffray, Robert C. Frazier, Julie Fayad, Larry L. Kestin, Vincent Remouchamps, Alvaro A. Martinez, John Wong, and Frank A. Vicini. "Accelerated partial breast irradiation using 3D conformal radiation therapy (3D-CRT)." International Journal of Radiation Oncology* Biology* Physics 55, no. 2 (2003): 302-311.

25. Formenti, Silvia C., Barry Rosenstein, Kristin A. Skinner, and Gabor Jozsef. "T1 Stage Breast Cancer: Adjuvant Hypofractionated Conformal Radiation Therapy to Tumor Bed in Selected Postmenopausal Breast Cancer Patients—Pilot Feasibility Study 1." Radiology 222, no. 1 (2002): 171-178.

26. Vicini, Frank A., Peter Chen, Michelle Wallace, Christina Mitchell, Yasmin Hasan, Inga Grills, Larry Kestin Scott Schell, Neal S. Goldstein, Jonathan Kunzman, Sam Gilbert, Alvaro Martinez. "Interim cosmetic results and toxicity using 3D conformal external beam radiotherapy to deliver accelerated partial breast irradiation in patients with early-stage breast cancer treated with breast-conserving therapy." International Journal of Radiation Oncology* Biology* Physics 69, no. 4 (2007): 1124-1130.

27. Zannis, Victor J., Lise C. Walker, Belinda Barclay-White, and Coral A. Quiet. "Postoperative ultrasound-guided percutaneous placement of a new breast brachytherapy balloon catheter." The American journal of surgery 186, no. 4 (2003): 383-385.

28. Dowlatshahi, Kambiz, Howard C. Snider, Mark A. Gittleman, Cam Nguyen, Phillip M. Vigneri, and Robert Lee Franklin. "Early experience with balloon brachytherapy for breast cancer." Archives of Surgery 139, no. 6 (2004): 603-608.

29. Richards, Gregory M., Anthony M. Berson, John Rescigno, Seema Sanghavi, Beth Siegel, Deborah Axelrod, Stephanie Bernik, Vincent Scarpinato, and Christopher Mills. "Acute toxicity of high-dose-rate intracavitary brachytherapy with the MammoSite applicator in patients with early-stage breast cancer."Annals of surgical oncology 11, no. 8 (2004): 739-746.

30. Zannis, Victor, Peter Beitsch, Frank Vicini, Coral Quiet, Angela Keleher, Delia Garcia, Howard Snider Mark Gittleman, Henry Kuerer, Eric Whitacre, Patrick

Whitworth, Richard Fine, Bruce Haffty, Alan Stolier, and John Mabie. " Descriptions and outcomes of insertion techniques of a breast brachytherapy balloon catheter in 1403 patients enrolled in the American Society of Breast Surgeons MammoSite breast brachytherapy registry trial." The American journal of surgery 190, no. 4 (2005): 530-538.

31. Scanderbeg, D.J., Yashar, C., Rice, R., and Pawlicki, T. Clinical implementation of a new HDR brachytherapy device for partial breast irradiation. Radiation and Oncology 2009;90:36-42

32. Lu, S.M., Scanderbeg, D.J., Barna, P., Yashar, W., and Yashar, C. Evaluation of two intracavitary high-dose-rate brachytherapy devices for irradiating additional and irregularly shaped volumes of breast tissue. Medical Dosimetry, 2012;37:9-14

33. Arthur, D.W., Vicini, F.A., Todor, D.A., Julian, T.B., Cuttino, L.W., and Mukhopadhyay, N.D., Contura multi-lumen balloon breast brachytherapy catheter: comparative dosimetric findings of a phase 4 trial. Rad. Onc. 2013;86(2):264-9

34. Smith, G.L, Xu, Y., Buchholz, T.A., Giordano, S.H., Jiang, J., Shis, YA.,T., Smith, B.D., Association between treatment with brachytherapy vs whole-breast irradiation and subsequent mastectomy, complications, and survival among older women with invasive breast cancer. JAMA, 2012;17:1827-1837.

35. Bartelink, H., Bourgier, C., Elkhuizen, P., Has partial breast irradiation by IORT or brachytherapy been prematurely introduced into the clinic? Radiation and Oncology, 2012;104:139-142.

36. Darby, Sarah C., Marianne Ewertz, Paul McGale, Anna M. Bennet, Ulla Blom-Goldman, Dorthe Brønnum, Candace Correa David Cutter, Giovanna Gagliardi Bruna Gigante, Maj-Britt Jensen, Andrew Nisbet, Richard Peto, Kazem Rahimi, Carolyn Taylor, D.Phil., and Per Hall. "Risk of ischemic heart disease in women after radiotherapy for breast cancer." New England Journal of Medicine 368, no. 11 (2013): 987-998.

37. Vicini, F., Beitsch, P., Quiet, C., Gittleman, M., Zannis, V., Fine, R., ... & Lyden, M. (2011). Five-year analysis of treatment efficacy and cosmesis by the American Society of Breast Surgeons MammoSite Breast Brachytherapy Registry Trial in patients treated with accelerated partial breast irradiation. International Journal of Radiation Oncology* Biology* Physics, 79(3), 808-817.

38. Wazer, D. E., Kaufman, S., Cuttino, L., DiPetrillo, T., & Arthur, D. W. (2006). Accelerated partial breast irradiation: an analysis of variables associated with late toxicity and long-term cosmetic outcome after high-dose-rate interstitial brachytherapy. International Journal of Radiation Oncology* Biology* Physics,64(2), 489-495.

39. M. J. Webster, S. Devic, T. Vuong, D. Y. Han, J. C. Park, D. Scanderbeg, J. Lawson, B. Song, W. T. Watkins, T Pawlicki and W.Y. Song, "Dynamic modulated brachytherapy (DMBT) for rectal cancer." Med. Phys. 40, 011718. (2013).

40. Webster, M. J., Devic, S., Vuong, T., Han, D. Y., Scanderbeg, D., Choi, D., ... & Song, W. Y. (2013). HDR brachytherapy of rectal cancer using a novel grooved-shielding applicator design. Medical physics, 40(9), 091704.

41. Han D, Webster M.J., Scanderbeg D, Mell L, Yashar C, Mundt AJ, Choi D, Song B, Devic S, Song WY . Dynamic Modulated Brachytherapy (DMBT) for Cervical Cancer (I): A Multi-Groove Tandem Design. Int J Radiat Oncol Biol Phys 2013 Submitted

42. MCNP – A General Monte Carlo N-Particle Transport Code, Version 5: http://mcnp-green.lanl.gov/pdf_files/MCNP5_manual_VOL_I.pdf

43. J. Borg and D. W. O. Rogers, "Monte Carlo Calculations of Photon Spectra in Air from 192Ir Sources," NRC Report PIRS-629r: http://www.irs.inms.nrc.ca/inms /irs/papers/PIRS629r/ pirs629r.html (1998).

Chapter 5 Conclusions and Future Work

This dissertation presents multiple novel applicator designs for improved dosimetric quality in brachytherapy treatment. It has been shown that the use of geometric modulation of isotropic sources has reached a plateau and new innovations must be developed to improve the field. This has been accomplished by implementing tungsten-alloy shielding to create highly anisotropic dose distributions which can be used to accurately direct dose. Monte Carlo and in-house optimization methods were used to account for the shields in calculating dose distributions.

In Chapter 2 the capabilities of dynamic modulated brachytherapy was investigated for applications in the treatment of rectal carcinomas. It was shown that a shield, used to create a highly collimated dose profile, if rotated and translated intelligently is capable of delivering unparalleled treatments compared to any known clinical applicator. Due to the complexity of the system, the consequences of potential errors were evaluated. It was determined that, errors of any reasonable magnitude in the system would lead to negligible detriments to the plan quality.

In Chapter 3 a set of static grooved applicators were presented as another option for the treatment of rectal carcinomas. These devices were developed as alternatives to the DMBT system in order to reduce the complexity of treatments to allow for easier clinical implementation. It was shown that these applicators, while failing to match the extraordinary abilities of DMBT, were still significantly better than the current applicators in use and therefore would be very reasonable for use in future treatments.

In Chapter 4 the potential of intensity modulated brachytherapy for the treatment of breast cancers was analyzed. First, it was shown that there is no further room for improvement in APBI by using only isotropic sources within a lumpectomy cavity. Next, several intensity modulated brachytherapy applicator designs were proposed to get around this issue. The strut-based IMBT applicators designed failed to provide significant improvements over the SAVI design. However, the tungsten rod applicators yielded encouraging results, showing an ability to provide better PTV coverage and chest wall sparing. The absence of cavity expansion allowed for better healthy tissue sparing at the cost of losing PTV coverage quality.

Future work includes improvements upon the applicators developed and reported in this work. This is especially true for the APBI applicators, given the difficult nature of the location. Several design adjustments have been proposed in this dissertation, which warrant further consideration. In addition the concepts applied in this work for rectal and breast cancer treatments have a great deal of promise for other tumor sites. These include cervix, vaginal, skin, and esophageal cancers.

Once optimal designs have been developed, the next steps are to build the shielded applicators and begin testing. This process includes the building of the shields, robotic applicators, and any additional components needed to apply them. These then must be thoroughly tested for quality assurance and dose accuracy.

The last couple decades have witnessed a rapid evolution in brachytherapy as technologies and radiobiology continually improve. DMBT and IMBT applicators are a very promising candidate for the next leap forward in cancer treatment.